General Disclaimer

One or more of the Following Statements may affect this Document

- This document has been reproduced from the best copy furnished by the organizational source. It is being released in the interest of making available as much information as possible.

- This document may contain data, which exceeds the sheet parameters. It was furnished in this condition by the organizational source and is the best copy available.

- This document may contain tone-on-tone or color graphs, charts and/or pictures, which have been reproduced in black and white.

- This document is paginated as submitted by the original source.

- Portions of this document are not fully legible due to the historical nature of some of the material. However, it is the best reproduction available from the original submission.

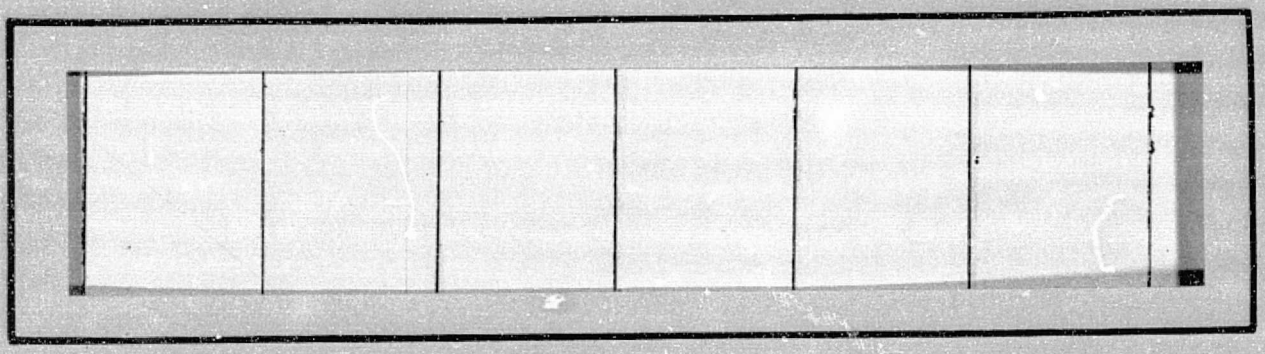

Axiomatix

Marina del Rey • California

INTEGRATED SOURCE AND CHANNEL ENCODED DIGITAL COMMUNICATION SYSTEM DESIGN STUDY

FINAL REPORT

Contract No. NAS 9-13467
Exhibit E

Prepared for

NASA Lyndon B. Johnson Space Center
Houston, Texas 77058

Prepared by

Sergei Udalov
Gaylord K. Huth

Axiomatix
13900 Panay Way, Suite 110M
Marina del Rey, California 90291

Axiomatix Report No. R7704-1
April 13, 1977

TABLE OF CONTENTS

LIST OF TABLES

LIST OF FIGURES

INTEGRATED SOURCE AND CHANNEL ENCODED DIGITAL COMMUNICATION SYSTEM DESIGN STUDY

SUMMARY

The analysis of the forward link signal structure for the Shuttle Orbiter Ku-band communication system has been carried out, based on the assumptions of a 3.03 Mcps PN code. It is shown that acquisition requirements for the forward link can be met at the acquisition threshold C/N_0 value of about 60 dB-Hz, which corresponds to a bit error rate (BER) of about 10^{-2}. It is also shown that the tracking threshold for the forward link is at about 57 dB-Hz. The analysis of the bent-pipe concept for the Orbiter is carried out, along with the comparative analysis of the empirical data. The complexity of the analytical approach warrants further investigation to reconcile the empirical and theoretical results. Techniques for incorporating a text and graphics capability into the forward link data stream are considered and a baseline configuration is described.

1.0 INTRODUCTION AND OVERVIEW

This report presents the results of several analytical tasks pertaining to the design of the Ku-band communication link of the Space Shuttle. The tasks performed fall into the following three categories:

(1) Forward link signal design and performance considerations;
(2) Bent-pipe mode implementation considerations; and
(3) Text and graphics implementation considerations.

Section 2.0 of this report deals with the first topic. Appendixes A, B, C, and D provide the supporting analyses. The bent-pipe mode implementation considerations are presented in Section 3.0, and the supporting analysis is given in Appendix E. The subject of text and graphics implementation is addressed in Section 4.0.

Contributions to this report were made by Drs. A. Waddah Alem, Marvin K. Simon, and Charles L. Weber.

2.0 KU-BAND FORWARD LINK SIGNAL DESIGN AND PERFORMANCE CONSIDERATIONS

2.1 Link Parameters

2.1.1 Data Rates and Acquisition Threshold

The forward link carries the data from the ground, via TDRS, to the Orbiter. The salient parameters of this link are summarized in Table 1. The primary operating mode is Mode 1, which employs a 216 kbps Bi-ϕ-L encoded data stream composed of (1) 72 kbps operational data, (2) 128 kbps scientific and instrument data, and (3) 16 kbps overhead. Because these data streams are time-division-multiplexed (TDM), a demultiplexer is employed at the Orbiter. The demultiplexer separates the 72 kbps data stream and applies it to the Network Signal Processor (NSP), which is not a part of the Ku-band equipment. The recovered 128 kbps stream may be routed either to an attached payload or to other equipment onboard the Orbiter.

In Mode 2, a selectable data configuration is available. Because no TDM is used, the demultiplexer is bypassed and any one of the data streams (32 kbps, 72 kbps, 96 kbps, or 216 kbps) is applied directly to the NSP.

In both modes, the forward link data spectrum is widened by superimposing a PN code on the data-modulated carrier. For reasons described in section 2.1.2, the clock rate of the code is approximately 3.03 Mcps and the code length is 1023 chips.

The performance of the forward link can be estimated by considering the C/N_0 values available at the receiver output during the worst-case condition. The worst-case condition will exist when the TDRS EIRP is at its lowest point, i.e., 36.6 dBw, and the Orbiter's antenna has not fully acquired (i.e., centered on) the TDRS. As shown in Part A of Table 2, the worst-case condition may occur when the positioning of the antenna is performed by the General Purpose Computer (GPC) and the TDRS is at the edge of the 3 dB beamwidth of the antenna. The C/N_0 at this point is 60.4 dB-Hz.

However, as indicated in Part B of Table 2, the lowest acceptable link performance corresponds to C/N_0 of 60.2 dB-Hz, a value which, within the assumptions stated, will provide a bit error rate (BER) of 10^{-2}. Consequently, one has to assume that the acquisition threshold of the forward link is at 60.2 dB-Hz and that all of the acquisition subunits must perform

Table 1. Forward Link Data Parameters

Channel Number	Mode 1		Mode 2	
	Rates	Modulation Type	Rates	Modulation Type
Single Channel Only	216 kbps (Composite, see Comments)	Bi-phase on carrier. Data format Bi-ϕ-L	32 kbps or 72 kbps or 96 kbps or 216 kbps	Bi-phase on carrier.
Comments	1. 216 kbps is composed of: 72 kbps OPS data 128 kbps scientific and instrument data 16 kbps overhead All three are time-division-multiplexed (TDM). 2. PN code superimposed on carrier to reduce spectral density.		1. PN code superimposed on carrier to reduce spectral density.	

NOTES:

1. Orbiter receives forward link data on carrier frequency of f_{RX} = 13.775 GHz.
2. PN code clock = 3.028 Mcps, code length = 1023 chips (see text).

Table 2. Calculation of C/N_0 for Worst Case TDRS Acquisition and for Lowest Acceptable* Forward Link Performance

Part A - TDRS Acquisition

Signal Calculation

TDRS EIRP	+ 36.6 dBW
Path Loss (Maximum)	-208.5 dB
Polarization Loss	- 0.3 dB
Antenna Gain	+ 38.9 dB
C (exclusive of antenna pointing loss, APL)	-133.3 dBW

Noise Density Calculation

Boltzman Constant	-228.6 dBW/°K/Hz
System Noise Temperature (T_s = 1563°K)	+ 31.9 dB-°K
N_0	-196.7 dBW/Hz

Therefore,

$$C/N_0 \text{ (scan)} = -133.3 \text{ dBW} - 0.6 \text{ dB (APL)} - (-196.7 \text{ dBW/Hz}) = 62.8 \text{ dB-Hz}$$

$$C/N_0 \text{ (GPC design)} = -133.3 \text{ dBW} - 3.0 \text{ dB (APL)} - (-196.7 \text{ dBW/Hz}) = 60.4 \text{ dB-Hz}$$

Part B - Lowest Acceptable Link Performance

E_b/N_0 for BER = 10^{-2} (From standard BER curve)	+ 4.4 dB
Correlation and Sync Loss	+ 2.5 dB
Bit Rate Bandwidth (10 log 216 kbps)	+53.3 dB-Hz
Required C/N_0	60.2 dB-Hz

*Lowest acceptable link performance defined in Part B of this table corresponds to a minimum satisfactory delta-modulated voice channel operation.

their functions satisfactorily at this C/N_0 value. Furthermore, it must be noted that, because this threshold refers to C/N_0 at the receiver input (i.e., antenna output), use of data rates below 216 kbps, although improving BER, will not affect the acquisition performance.

2.1.2 PN Code Rate Considerations

To limit the field strength of the signal transmitted by the TDRS and impinging on the earth's surface, the spectral density of the forward link signal is reduced by addition of a PN code to the data-modulated carrier. As stated in the initial version of the Procurement Specification, the code rate of about 11.23 Mcps and of length 2047 chips [1] was requested. Thus, it was expected that the spectrum of the 216 kbps Manchester encoded data would be spread to a bandwidth (first null) of about 11.7 MHz. At the receiver, following the despreading process, this widened spectrum would be collapsed to the data spectrum width.

In an ideal case, i.e., the case of no doppler shift and no carrier drift in the TDRS forward link carrier, the bandwidth of the post-correlation IF filter would be approximately 4 x 216 kbps or 864 kHz. However, <u>without compensation</u>, the frequency uncertainties of the forward link signal are as follows:

Carrier frequency uncertainty: ±500 kHz
Carrier doppler uncertainty: ±500 kHz

The combined effect of the uncertainties, plus the requirement to accommodate the 216 kbps Manchester data stream, set the post-correlation IF bandwidth requirements, for an uncompensated signal, at about 2.8 MHz. The corresponding doppler shift in the clock rate of the received PN code was estimated at ±400 Hz.

The most recent developments in the Ku-band communication program indicated, however, a requirement for reducing the PN code rate to a value which is compatible with the "standard" TDRS users. These users have the code rate related to the carrier frequency by the following relationship:

$$r_c = \frac{31 \times f_c}{96 \times 1469}, \qquad (1)$$

where r_c is the code rate and f_c is the carrier frequency. Substituting the forward link carrier frequency of 13,775 MHz (13.775 GHz) into (1), one obtains the new code rate:

$$r_c = \frac{31 \times 13{,}775\ (\text{MHz})}{96 \times 1469} = 3.028\ \text{Mcps}\ . \qquad (2)$$

Another modification which was introduced along with the reduction of the code clock frequency was that of reducing the code length from 2047 chips to 1023 chips. The purpose of this change was to shorten the acquisition time of the PN code.

2.1.3 Frequency Compensation and Residual Frequency Uncertainty

In the preceding paragraph, it was shown that, to accommodate the frequency uncertainties of the received TDRS carrier, the post-correlation bandwidth had to be about 2.8 MHz. Note, however, that with the reduced code rate, the spectrum of the PN signal and the bandwidth required to process the despread signal become very close in their values, i.e., about 3.0 MHz versus 2.8 MHz. Furthermore, because the detection of the code synchronization is based on a significant change of signal level in the 2.8 MHz bandwidth due to the collapse of the spread signal, the miniscule change of signal bandwidth presents a significant problem to the code acquisition process. Specifically, as is shown below, unless the doppler correction is also employed, the PN acquisition may become extremely difficult with the reduced code rate. The reason for this difficulty is that the bandwidth of the 3.028 Mcps PN signal is only slightly wider than the 2.8 MHz bandwidth of the post-correlation IF amplifier. Note again that the 2.8 MHz bandwidth is required to accommodate the 216 kbps Manchester data (≈400 kHz BW) riding on a ±1 MHz doppler-plus-carrier frequency uncertainty.

Figure 1 shows the simplified block diagram for a PN code search implementation. Briefly, the device shown operates in the following manner: The frequency of the code clock is changed from its nominal value of 3.03 MHz and thus the phase of the locally generated code is stepped past the phase of the incoming code. The step increment is assumed to be $\tau/2$, i.e., one-half chip width. The actual rate of stepping, or the search rate, is determined by the code doppler, but does not exceed the lowpass filter bandwidth, B_v. The stop search command is generated when the DC value at the LPF output exceeds a predetermined threshold. This increase in DC value is the result of code phases stepping into synchronism.*

*A more detailed description of the PN code acquisition process is given in section 2.2.2 and in Appendix A.

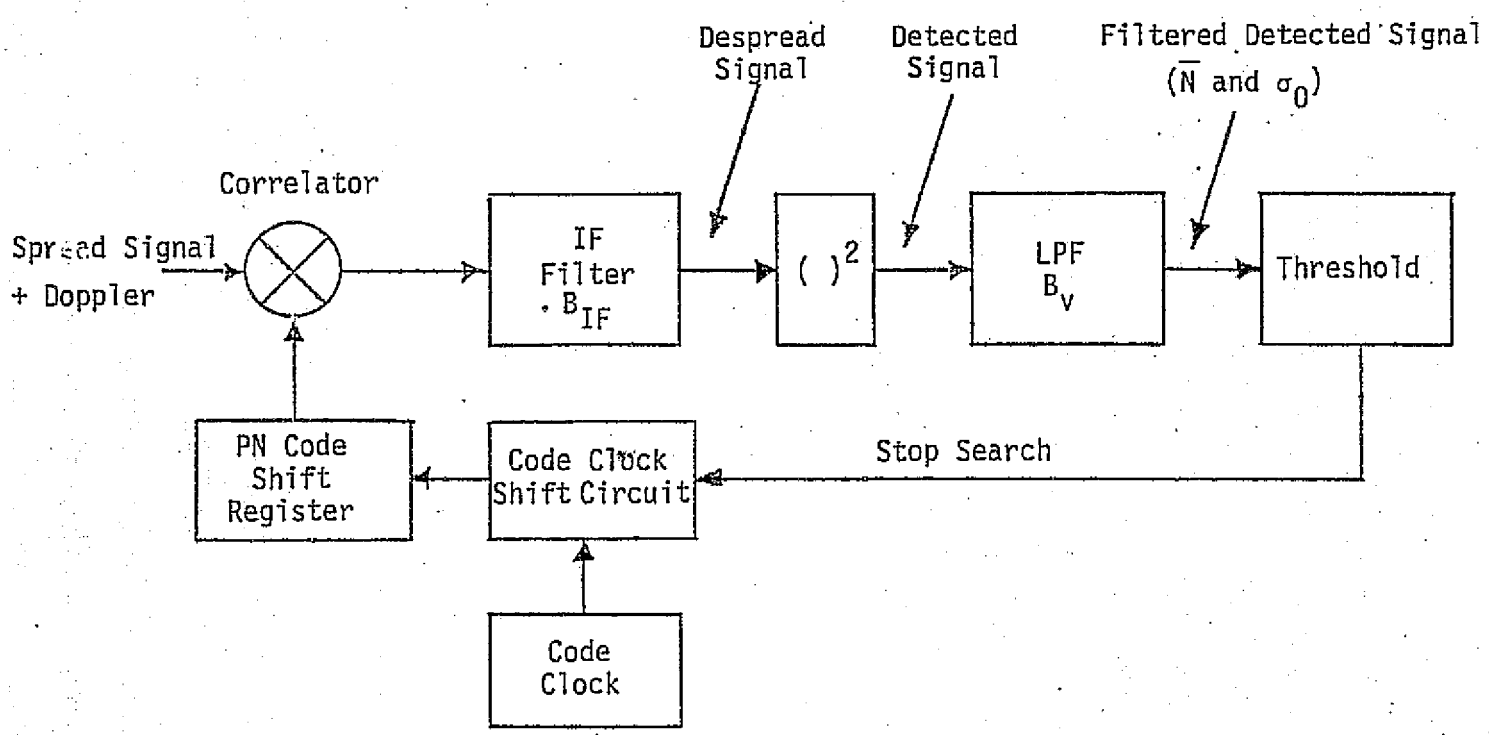

Figure 1. Simplified Block Diagram for PN Code Search Implementation

For a numerical example, let us consider the PN acquisition at the aforementioned C/N_0 of 60.2 dB-Hz. First, we compute the SNR at the output of the 2.8 MHz IF filter when the input is the 3.03 Mcps PN spectrum shifted by the 1 MHz carrier offset. Thus,

$$\begin{aligned} S/N \text{ (Spread)} &= C/N_0, \text{ dB-Hz} - L_s \text{ (spectrum loss)}, \text{ dB} \\ &\quad - 10 \log_{10} (2.8 \times 10^6), \text{ dB-Hz} \\ &= 60.2 \text{ dB-Hz} - 2.5 \text{ dB}^* - 64.5 \text{ dB-Hz} \\ &= -6.8 \text{ dB} \quad \text{or} \quad 0.209 \text{ numeric.} \end{aligned} \tag{3}$$

The SNR for the despread will be determined also by (3) except that the value of L_s will be for the correlated signal rather than the spread signal. Table 3 shows the values of SNR (despread) versus the correlation loss L_s (correlated). Note that, for 2.5 dB correlation loss, a value which is characteristics of a code search pause at either $+\tau/4$ or $-\tau/4$, the PN synchronization detection is totally impossible. The reason is obvious—there is no difference in output signal for the spread and despread (correlated) conditions!

Table 3. Despread Signal Magnitude vs. Correlation Loss for the Case of No Frequency Correction

L_s, Correlation Loss dB	SNR (despread) dB	Numeric	ΔS (spread-despread) numeric
2.5	-6.8	0.209	0 (see Note)
2.0	-6.3	0.234	0.025
1.5	-5.8	0.263	0.054
1.0	-5.3	0.295	0.086

NOTE: With $\Delta S = 0$, the PN correlation is not possible, regardless of the time spent!

*The 2.5 dB loss value is for the case of a maximum frequency-shifted (±1 MHz) 3 Mcps PN signal passed through a 2.8 MHz IF filter.

The solution to this problem, proposed by Axiomatix and adopted by NASA, was to reduce the combined carrier drift and doppler uncertainty to about ±7500 Hz by compensation at TDRS. Such compensation reduces the overall frequency instability of the forward link to the instability (drifts) of the Shuttle Ku-band receiver local oscillators. In view of the frequency compensation available, the remaining carrier uncertainty at the Shuttle receiver can be estimated as:

Incoming Carrier Frequency	± 7.5 kHz
First and Second LO (5×10^{-6})	± 70.0 kHz
Costas Loop VCO (1×10^{-3})	± 55.0 kHz
	±132.5 kHz

A conservative assumption used in the analysis in this report is that the residual carrier uncertainty ($\pm\Delta f_0$) amounts to about ±150 kHz. With this assumption, the post-correlation bandwidth requirement is reduced to

$$\begin{aligned} B_{IF}(\text{post-correlation}) &= 2(|\Delta f_0| + 2 \times \text{Data Rate}) \\ &= 2(150\times10^3 + 2 \times 216\times10^3) \\ &= 1.164 \times 10^6 \text{ Hz or about 1.2 MHz.} \end{aligned} \tag{4}$$

With this reduced bandwidth requirement, the despread S/N at $C/N_0 = 60.2$ dB-Hz and $L_s = 2.5$ dB becomes

$$\begin{aligned} \text{S/N (despread)} &= 60.2 \text{ dB-Hz} - 2.5 \text{ dB} - 10 \log (1.164 \times 10^6) \\ &= -3 \text{ dB or } 0.501 \text{ numeric.} \end{aligned}$$

Note that this numeric value is significantly different from the 0.209 value obtained in (3) for the S/N (spread). The PN acquisition process thus becomes feasible at C/N_0 of 60.2 dB-Hz and correlation loss of 2.5 dB. Section 2.2.2 and Appendix A provide a detailed description of the PN acquisition process under these conditions.

It must also be noted that the frequency compensation combined with code rate reduction also provide a significant reduction in the code clock doppler uncertainty. Thus, prorating the ±7500 uncertainty at the Ku-band carrier to a 3.03 MHz clock frequency, we get

$$\Delta r_c = (\pm 7500) \frac{3.03}{13,775} = \pm 1.63 \text{ Hz} \leq \pm 2 \text{ Hz} . \tag{5}$$

Compared to the ±400 Hz code rate uncertainty of the uncompensated signal, the ±2 Hz value is negligible. However, the uncertainty due to code clock VCO at the Shuttle receiver remains now a determining factor. Normally, a voltage controlled crystal oscillator (VCXO) is used for a code clock source. The stability of such a device may be, typically, $\pm 3 \times 10^{-5}$.

For a 3 MHz code, this implies instability of about ±90 Hz. A conservative value of ±100 Hz is used throughout this report.

Table 4 presents the summary of salient parameters assumed for the analysis of the forward link performance.

Table 4. Salient Parameter Assumptions for Shuttle Ku-Band Receiver Channel

Parameter Description	Value*	Remarks
PN Code Rate	3.028 Mcps	Reduced from 11.232 Mcps
PN Code Length	1023 chips	Reduced from 2047 chips
Incoming carrier doppler and drift uncertainty	(±7.5 kHz)	Corrected at TDRS. Without correction: ±1.0 MHz
Residual received carrier uncertainty	±150 kHz	Receiver oscillator(s) drift contribution
Incoming code clock doppler uncertainty	(≤ 2 Hz)	Coherent with carrier. Corrected at TDRS. Without correction: ±400 Hz
Residual code clock oscillator uncertainty	±100 Hz	Reduced from ±300 Hz for 11.223 mcs code rate

*Values in brackets () have negligible effect on threshold calculations.

Using these parameters, we proceed with the estimation of the acquisition threshold performance of the forward link.

2.2 Acquisition Performance

2.2.1 Spatial Acquisition of TDRS

The alignment of the antenna directivity patterns along a common line-of-sight (LOS) is the first step for establishing the TDRS/Shuttle Ku-band communication link. The alignment of the TDRS antenna is aided by the "wide beam" horn radiator mounted on the Shuttle antenna. The alignment of the TDRS antenna, however, must be performed by scanning across the residual uncertainty volume which may be as wide as a 20° cone. For best scan efficiency, a spiral pattern is used to search out the uncertainty volume. Furthermore, in order not to limit the rate at which the uncertainty volume is scanned, the energy detection is used to declare TDRS intercept [2]. The energy detected in this case is that of the spread spectrum signal entering the main lobe of the Shuttle antenna pattern.

Referring to the block diagram of Figure 2, the spatial acquisition and detection unit* works at the second IF and uses a portion of the sum-channel (Σ) signal. The spread PN signal is passed through a 3 MHz bandpass filter and applied ① to a square-law detector. The output of the square-law detector ② is, in turn, applied to a lowpass filter and a threshold estimator. The function of the lowpass filter is to reduce the magnitude of the fluctuating component of the detected noise. The function of the threshold estimator is to provide a well-smoothed value of the DC component of the detected noise. This DC component is then scaled and applied ④ to the threshold circuit to provide the reference for the "signal present" condition. The threshold estimator circuit is essentially a lowpass filter whose bandwidth is at least several orders of magnitude narrower than B_V. Consequently, the detection of the signal ③ in the main beam of the antenna depends on the ability of the B_V filter to respond to the DC level change at the output of the square-law detector, such change being due to the antenna beam scanning across the TDRS signal. The actual value of B_V is therefore a compromise between the detection reliability and the antenna scan rate.

---

*In Hughes (Ku-band system subcontractor) documents [3,4], this unit is referred to as the independent spatial acquisition detection (ISAD) unit.

*Hughes documents refer to this circuit as Independent Spacial Acquisition Detector (ISAD).

**Az and El Δ-information time-multiplexed.

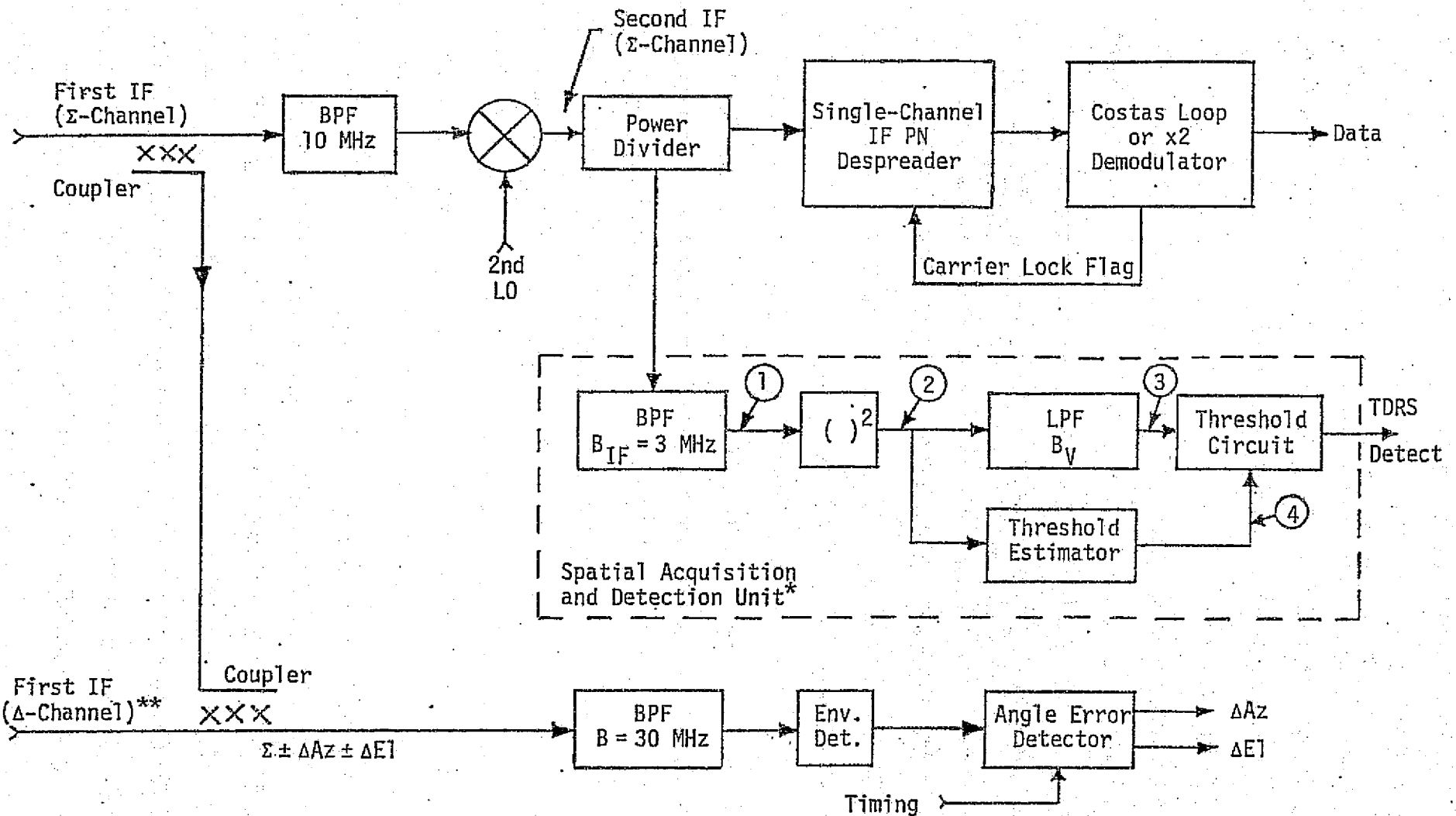

Figure 2. Signal Processing Portion of Shuttle Ku-Band Receiver - Simplified Block Diagram

For a constant scan frequency* spiral search pattern, the relationship between the minimum antenna dwell time and the scan frequency is given by [2]:

$$t_{dm} = \frac{\beta}{(2\pi)\,\theta_m\, f_s} \tag{6}$$

where t_{dm} = minimum antenna dwell time over 3 dB beamwidth (sec)

β = antenna 3 dB beamwidth (deg)

f_s = scan frequency (Hz)

θ_m = maximum half-cone scan limit (deg).

It must be noted that, with a constant scan frequency search, the t_{dm} occurs at the outer limit of the scan volume boundary defined by θ_m. The time required to spiral out to the maximum scan limit, i.e., area search time, is

$$T_m = \frac{\theta_m}{(\Delta\theta)\, f_s} \tag{7}$$

where T_m = search time

$\Delta\theta$ = angular advance of antenna beam per revolution (deg/rev).

Making use of the relationship

$$f_s = \frac{\dot{\phi}}{360^\circ}, \tag{8}$$

where $\dot{\phi}$ is the gimbal rate in deg/sec, one can rewrite (6) and (7) as

$$t_{dm} = \frac{360\,\beta}{(2\pi)\,\theta_m\,\dot{\phi}}, \tag{9a}$$

$$T_m = \frac{360}{(\Delta\theta)}\,\frac{m}{\dot{\phi}}. \tag{9b}$$

Using (9a) and (9b), one can determine t_{dm} and T_m as the functions of gimbal rate $\dot{\phi}$. Also, assuming that $B_v \approx 1/t_{dm}$, one can establish the interdependence between B_v and $\dot{\phi}$.

---

*This type of scan requires minimum implementation complexity.

Figure 3 shows T_m, t_{dm}, and B_v as functions of the gimbal rate $\dot{\phi}$, for the specific case which assumes:

$$\theta_m = 10° \text{ (20° cone)}$$

$$\beta = 1.6°$$

$$\Delta\theta = 0.72° \text{ (0.6 dB pointing loss during search)}.$$

From the data in Figure 3, it is evident that, with a constant frequency spiral scan, the maximum uncertainty area defined by the 20° cone ($\theta_m = 10°$) can be searched in about 50 seconds if the nominal 102°/sec gimbal rate is assumed [3, Table 3.4-1]. With 90°/sec gimbal rate, the area search time is about 55 seconds. The corresponding values of B_v are 11 Hz and 10 Hz and, as is shown in section 2.2.1.3 of Appendix A, these relatively low bandwidths may not be required. It therefore appears that the area search time is limited primarily by the gimbal rates, rather than the requirements for narrow B_v. Such limitation, as shown by the data in Figure 3, is in the 50 to 55 sec region, less than 1/3 of the specified [1] 180-second limit. Table 5 summarizes the forward link requirements.

Table 5. TDRS Signal Acquisition Requirements Summary (Forward Link)

Conical angle uncertainty (maximum)	8°	20°
Maximum search time	1 min	3 min
TDRS signal level	-126.9 dBm/m^2 (EIRP = 36.6 dBW)	
Probability of acquisition (P_D)	0.99	
False alarm probability (P_{fa})	10^{-6}	

The fact that all the parameters specified in Table 5 are also met at C/N_0 of 60.2 dB-Hz is demonstrated in section 2.2.1 of Appendix A.

After the spatial detector circuit provides a signal, thus indicating that the TDRS is within the mainlobe of the antenna, the antenna is returned to the angular position at which detection has occurred and

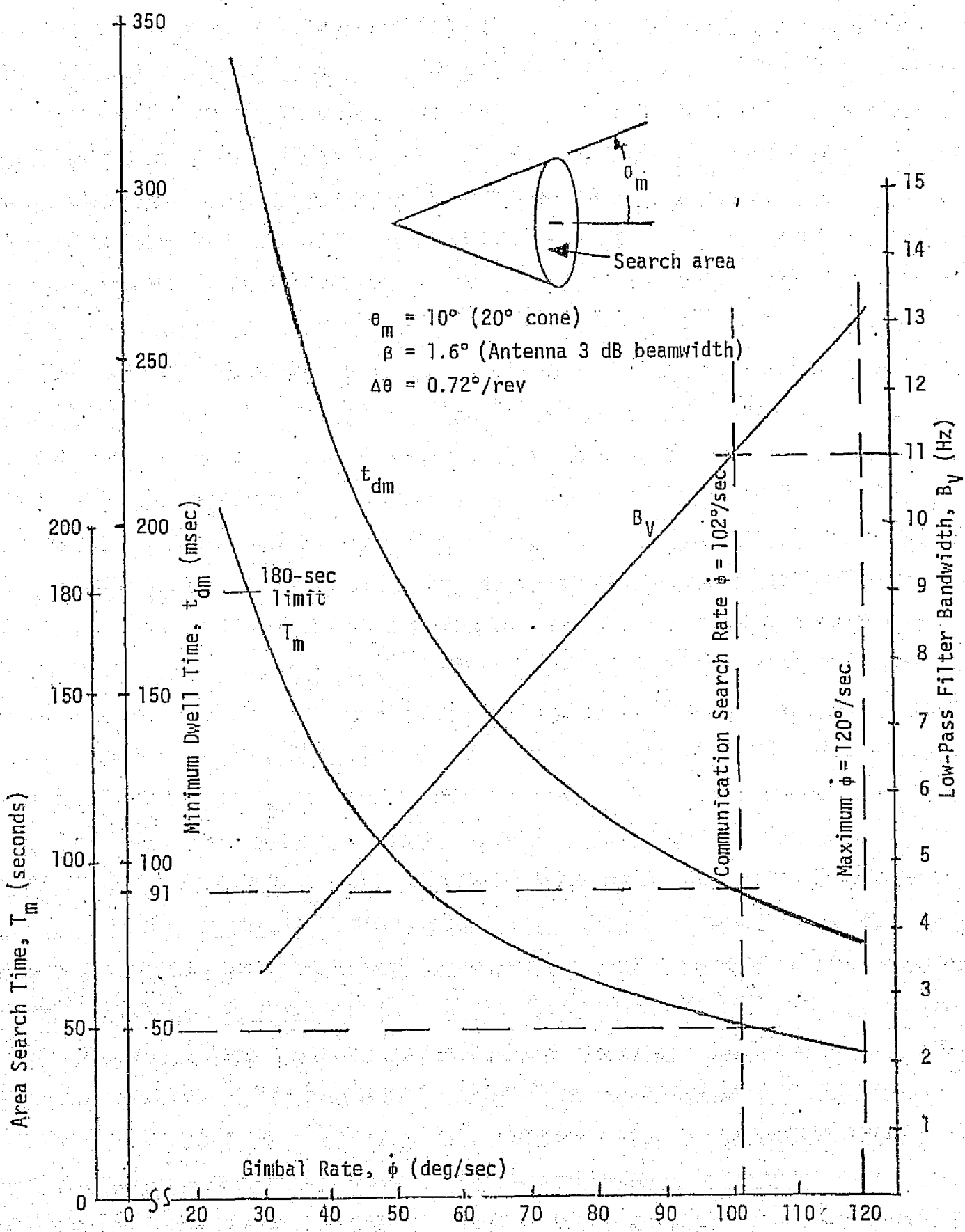

Figure 3: Area Search Time, Minimum Dwell Time, and Low-Pass Filter Bandwidth as Functions of Gimbal Rate (constant frequency spiral scan)

the miniscan program is initiated [5]. During the miniscan, the antenna beam is moved in a spiral pattern around the initial "signal detect" position and thus it is reasonable to assume that the TDRS signal provided to the receiver is no worse than that at which the initial space detection has occurred. Consequently, one can also assume that the next step, i.e., the PN code search and acquisition, takes place with at least the same C/N_0 ($\geq$ 60.2 dB-Hz) as the spatial detection.

2.2.2 PN Code Search and Acquisition

The purpose of the code search and acquisition stage of the signal acquisition procedure is to align the phases of the incoming and locally generated PN codes. The alignment is achieved by shifting the phase of the locally generated code until coincidence of the two codes is detected and the shifting is terminated. If the termination of the code phase shift is due to a true coincidence, the PN code tracking begins and the remainder of the acquisition sequence, i.e., carrier lock, bit and frame synchronization, is carried out.

Figure 4 shows the simplified block diagram for the PN code search implementation. The logic flow diagram for the PN code search, as well as for the acquisition and tracking phases, is given in Figure 5. Referring to Figure 4, the code search is performed as follows.

The frequency of the code clock applied to the PN register is changed so as to cause the phases of the incoming and locally generated codes to slip past each other. The change in code clock frequency is such that, even for the worst case of code clock drift (assumed at 100 Hz, see Table 4), the relative code phase slippage does not exceed 1/2 chip in the post-detection bandwidth B_v. Note that B_v is the bandwidth of one of the lowpass filters (LPF) which are placed at the output of the square-law envelope detector [4].

Consequently, as shown in Figure 4, the output of the correlator is passed through the post-correlation IF filter of bandwidth B_{IF}, is square-law detected, and is applied to lowpass filters B_v and b_v, as well as to the threshold estimator. As the code phase difference approaches 1/4 chip width, the output of the B_v filter exceeds the threshold Th_1. Crossing of threshold Th_1 results in a 10 msec pulse at the output of the one-shot multivibrator (MV). This pulse inhibits the code search process for 10 msec.

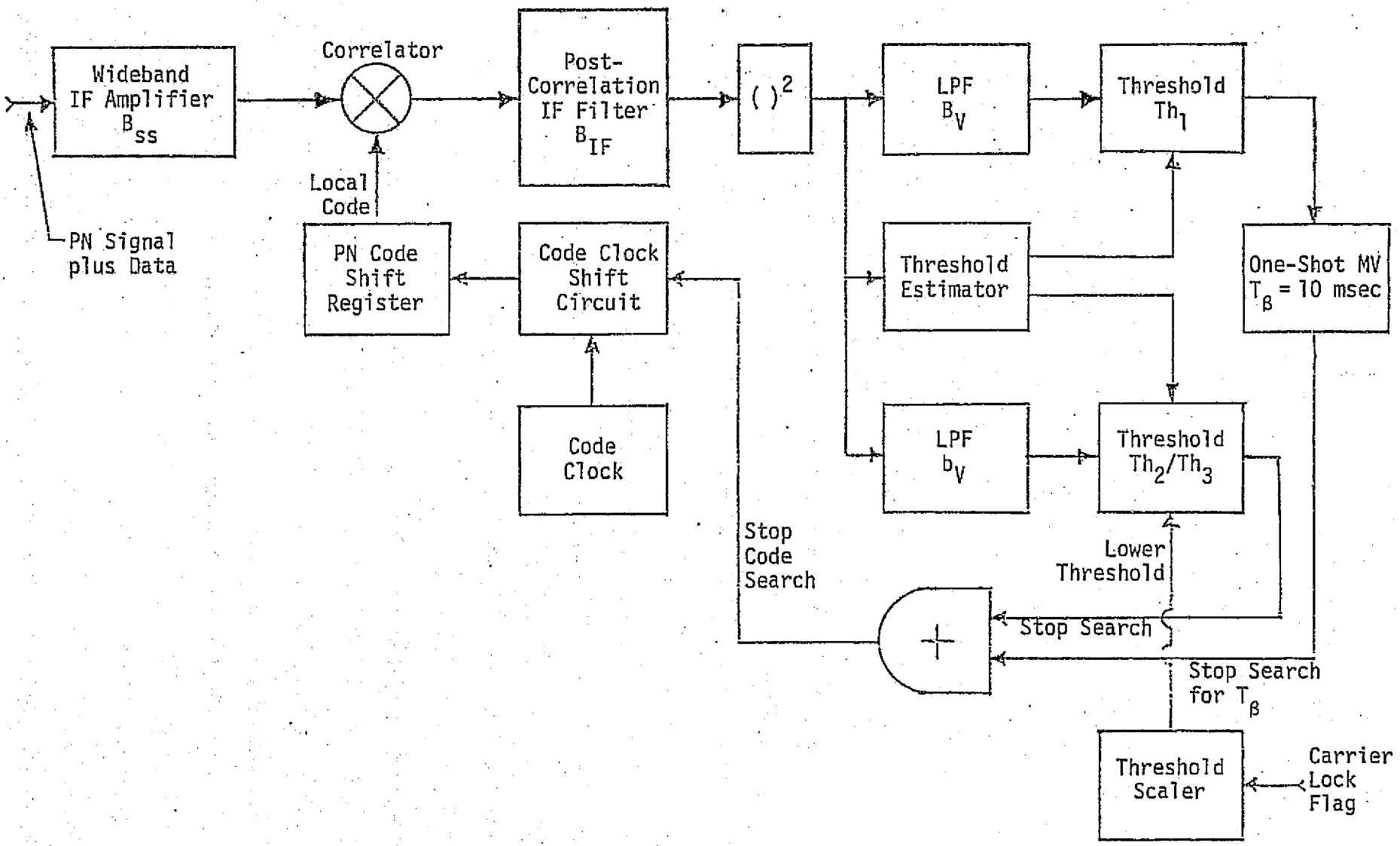

Figure 4. Simplified Block Diagram for PN Code Search Implementation (Single-Channel Version)

If the crossing of Th_1 is due to partial correlation, which is the beginning phase of the full correlation, the code tracking loop (shown in Figure 8) pulls into code synchronism.* The pull-in causes the output of b_v to exceed the secondary threshold Th_2, and the search is terminated. The subsequent acquisition of the carrier causes the secondary threshold to be lowered to Th_3, a value which prevents the code search from reoccurring unless the C/N_0 drops below a predetermined tracking threshold value.

On the other hand, if the crossing of Th_1 is due to a noise pulse, i.e., due to a false alarm, Th_2 is not exceeded after 10 msec, and the code search is resumed upon expiration of the 10 msec interval. Therefore, each false alarm triggering halts the search process for only 10 msec. The logic flow diagram of Figure 5 shows both the true and false alarm paths.

Because of the importance of B_v and b_v to the acquisition performance, a detailed quantitative analysis has been carried out (see Appendix A, sections 2.2.2.2 and 2.2.2.3) relating these bandwidths to the statistics of the PN acquisition process. Of particular importance is the relationship between B_v and the 0.99 probability of code synchronization time $T_{ss}(0.99)$ at the system acquisition threshold of $C/N_0 = 60.2$ dB-Hz. This relationship is shown in Figure 6.

From Figure 6, it is evident that a broad minimum for $T_{ss}(0.99)$ values lies in the region of B_v from 1500 Hz to 2500 Hz. It must be emphasized, however, that the plot shown pertains only to the set of conditions indicated and $C/N_0 = 60.2$ dB-Hz. Other sets of conditions would results in different relationships between B_v and T_{ss}.

It must also be pointed out that the plot in Figure 6 is based on a threshold setting commensurate with <u>two</u> samples contributing to the cumulative probability of PN synchronization detection per pass of 0.99. Furthermore, the acquisition times indicated are below the 10 sec value given by the equipment specification [1]. The PN code acquisition time of 8 seconds would therefore be a reasonable value to assume as a revised goal. Requiring PN code acquisition times of less than 8 seconds is not warranted, however, in view of the fact that practically no threshold tolerance (or margin) is available at C/N_0 of 60.2 dB-Hz.

---

*Pull-in behavior of the code tracking loop is given in Appendix D. It is shown there that a 10 msec assumption is adequate.

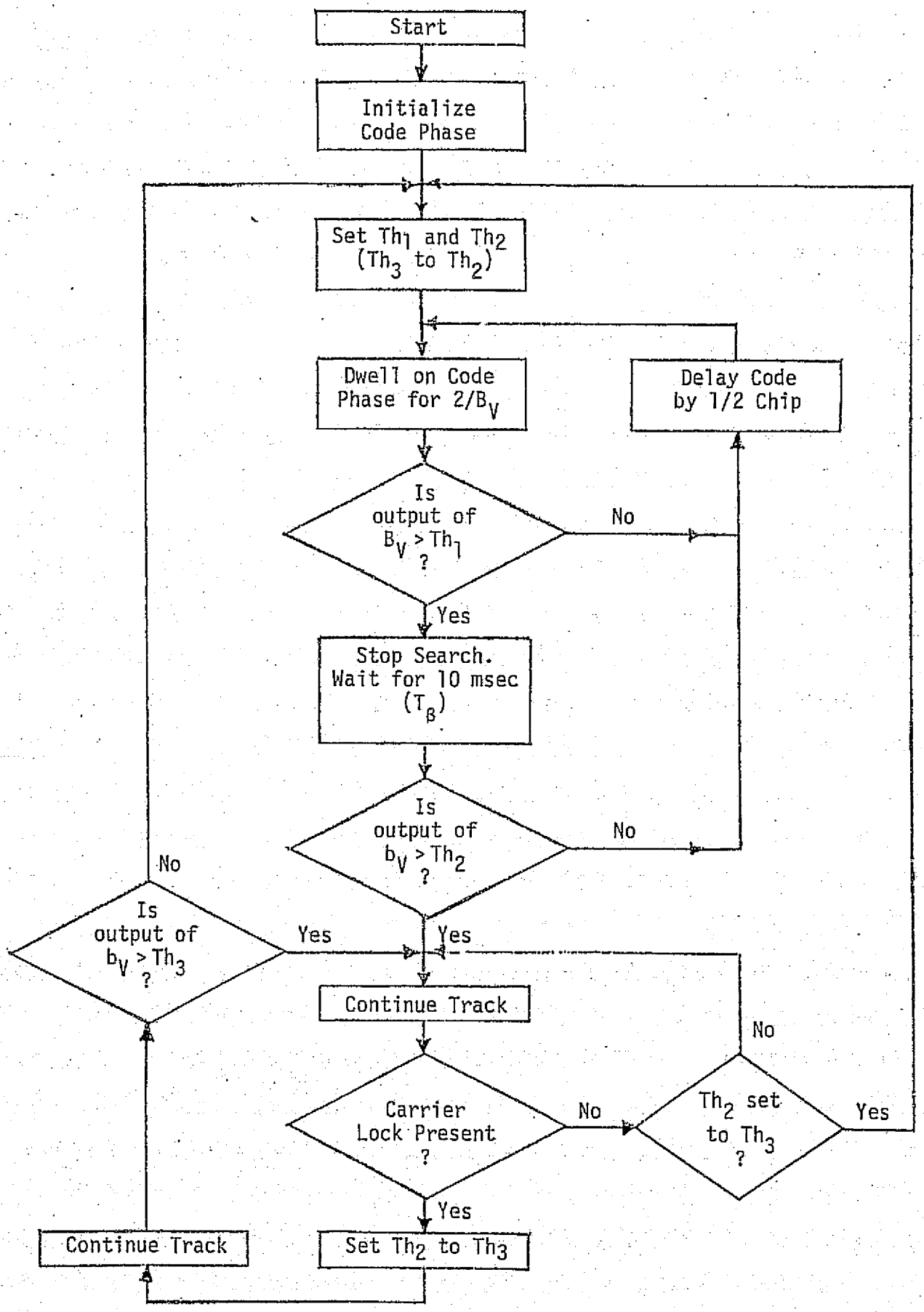

Figure 5. Logic Flow Diagram for PN Code Search, Acquisition and Track

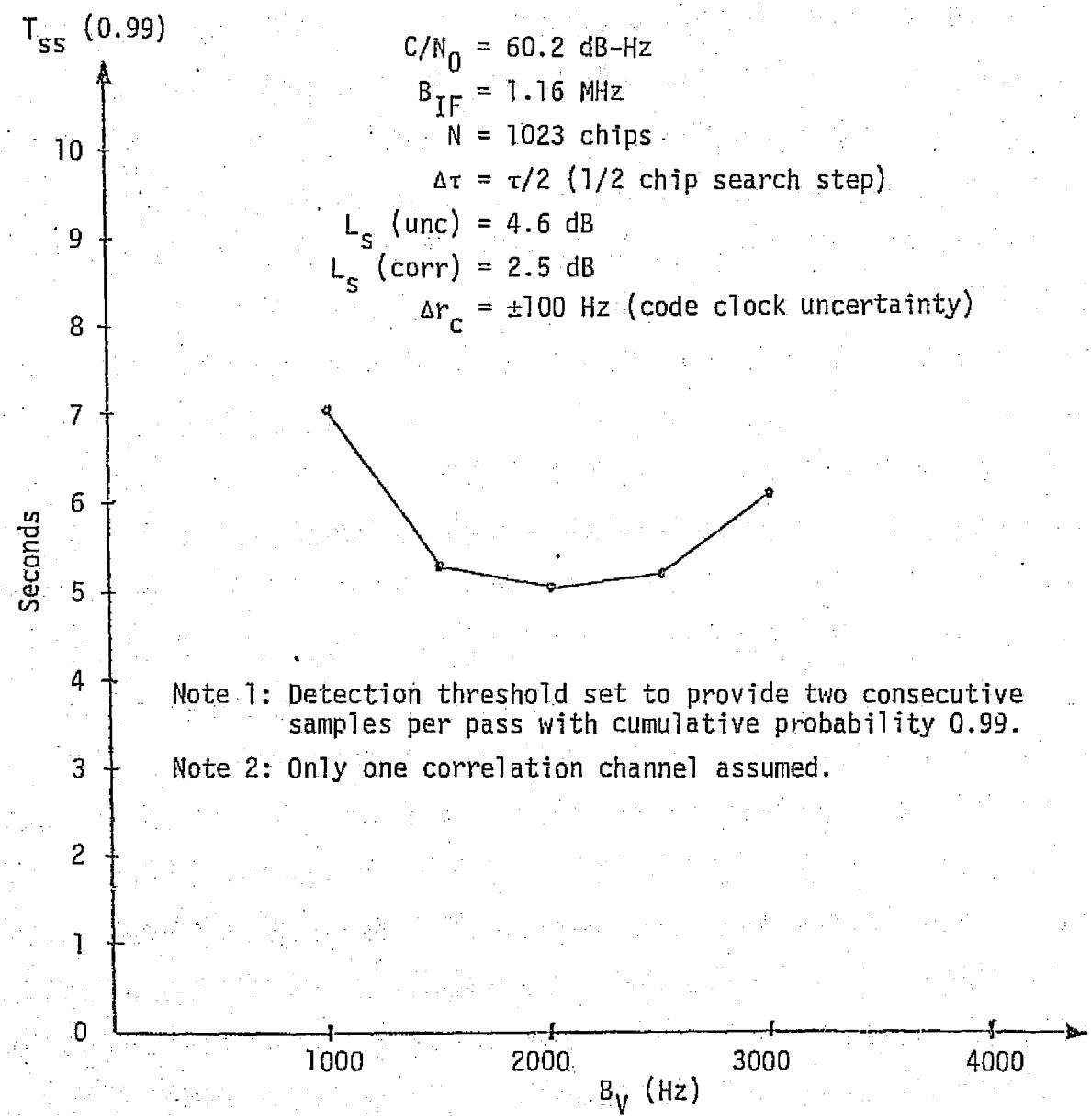

Figure 6. PN Code Search Time Versus Post-Detection LPF Bandwidth B_V

Furthermore, because of acquisition time optimization at C/N_0 of 60.2 dB-Hz, there may not be a marked decrease in acquisition time as the C/N_0 increases. This is due to an assumption that threshold Th_1 is set for constant false alarm rate with respect to the level of the uncorrelated signal plus noise. Therefore, unless other threshold setting criteria are used, the acquisition time will not decrease appreciably with increased C/N_0.

2.2.3 Carrier Acquisition

Following completion of the PN code search, carrier acquisition takes place. For carrier acquisition, the Costas loop demodulator VCO frequency is swept over the residual carrier uncertainty range which, for the case under consideration, is ±150 kHz. Thus, the total range over which the VCO is swept is about 300 kHz.

The time to acquire the carrier and the probability of acquisition are determined by the loop one-sided noise bandwidth B_L and the signal-to-noise ratio in the loop, i.e., SNR_L.

As shown in section 2.2.3 of Appendix A, with $B_L = 2500$ Hz, reliable carrier acquisition ($P_{acq} \geq 0.99$) can occur at $C/N_0 = 60.2$ dB-Hz, within a time interval less than one second. It is also shown there that, because of a relatively high SNR_L (> 10 dB), trade-offs can be carried out between B_L, acquisition phase error, and carrier acquisition time.

2.2.4 Bit and Frame Synchronization

The performance of the bit and frame synchronization subunits is difficult to predict analytically; therefore, empirically derived data must be relied upon. Of specific interest is the bit synchronizer performance described in [6]. According to [6], mean acquisition times of less than 0.7 sec are obtained at E_b/N_0 values as low as 0 dB. Referring to the data rate of 216 kbps, the corresponding C/N_0 is

$$\begin{aligned} C/N_0(\text{dB-Hz}) &= 10 \log (216 \times 10^3) - 0 \text{ dB} \\ &= 53.3 \text{ dB-Hz}. \end{aligned} \tag{10}$$

This means that bit synchronization acquisition time of 1 sec at C/N_0 of 60.2 dB-Hz can be easily achieved with at least a 6 dB margin.

No exact data on frame synchronization time is available, except for a statement in [6], most likely based on empirical data, that average frame synchronization time is less than 10 msec. Because it is also stated in [6] that total time for bit and frame acquisition is approximately 0.5 sec at 0 dB of E_b/N_0, we conclude that 1.0 sec combined bit and frame synchronization at C/N_0 = 60.2 dB-Hz is quite realistic and does not impose unnecessary complexity requirements on the Ku-band equipment design.

2.3 Tracking Performance

In the preceding section, acquisition performance of the various subunits was considered at C/N_0 of about 60 dB-Hz. It was shown that reasonable acquisition performance can be obtained at the nominal C/N_0 value of 60.2 dB-Hz. Tracking performance of the receiver subunits will now be considered.

2.3.1 Angle Tracking Performance and Threshold

Angle tracking threshold can be defined as that value of C/N_0 at which the angle tracking loops break lock or at which the angle noise in these loops becomes sufficiently high so as to significantly degrade the BER performance. Thus, by examining the behavior of the rms angle tracking error as a function of C/N_0, tracking as well as threshold performance of the angle tracking loops can be defined. Although there are two tracking loops in the system under consideration, one for the AZ axis and one for the EL axis, examination of the angle tracking error in either one of these loops is indicative of the angle tracking threshold performance.

An expression for the square of the angle tracking error can be obtained by modifying the equation on page 3-37 of [3] into a more directly usable form:

$$\sigma_a^2 = \frac{4\beta^2 B_s A}{K_m^2\left(\frac{C}{N_0 D}\right)} \times \frac{1 + \frac{B_{IF}(\Delta)}{2(C/N_0 L_t)}}{1 - \frac{2B_s}{(C/N_0 D)}} \qquad (11)$$

where σ_a = rms value of angle tracking error

β = antenna 3 dB beamwidth

B_s = angle servo loop noise bandwidth

K_m = antenna tracking slope coefficient

A = coupling factor for the monopulse channel

D = effective increase in thermal noise N_0 due to coupling of noise from Δ channel

$B_{IF}(\Delta)$ = IF bandwidth of the angle tracking channel

C/N_0 = carrier-to-noise ratio (dB-Hz) at receiver input.

The angle tracking performance can be estimated using the parameters proposed by the Ku-band equipment contractor [3, p. 3-37]. These parameters are as follows:

$\beta = 1.6°$

$B_s = 1.0$ Hz

$K_m = 0.5$ (worst case)

A = 2 dB or 1.585 numeric

D = 2.1 dB or 1.622 numeric

and $B_{IF}(\Delta) = 30$ MHz.

Substituting the values indicated into equation (11), one obtains the relationship between σ_a and C/N_0. Figure 7 shows this relationship. From Figure 7, it is evident that, if the criterion for the threshold is $\sigma_a \leq 0.2°$ [1], the tracking threshold, based on the thermal noise alone is at about 54 dB.

The pointing loss at $C/N_0 = 60.2$ dB-Hz (acquisition threshold) can be estimated by first computing the corresponding value of σ_a and then substituting this value into the following equation:

$$M\ (dB) = \frac{12\,\sigma_a^2}{\beta^2} \tag{12}$$

where M is pointing loss in dB and β is antenna 3 dB beamwidth in degrees. Thus,

$$M\ (dB) = \frac{(12)(0.002)}{(1.6)^2} = 0.01\ dB. \tag{13}$$

This loss is negligible compared to RF and servo bias error, which may be expected in the system. An estimated pointing loss due to these bias

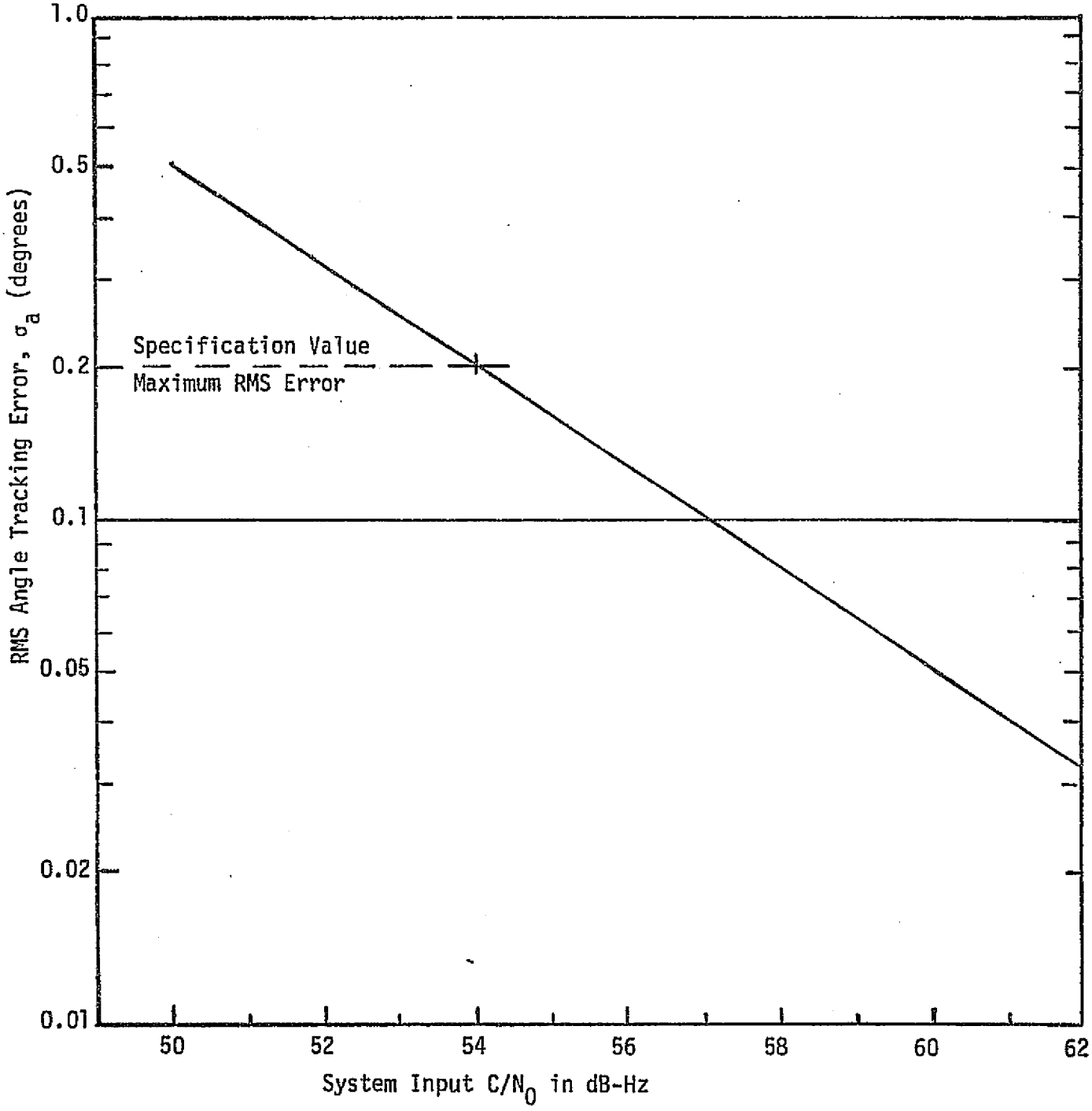

Figure 7. RMS Angle Tracking Error Versus C/N_0

errors is about 0.14 dB [3] and is well within the 0.3 dB pointing loss specification [1]. One therefore concludes that the thermal noise is not a limitation for the angle tracking subsystem if one takes into account the unavoidable bias errors.

2.3.2 PN Tracking

Upon acquisition of the PN code, the tracking loop takes over. The loop then maintains the synchronism between the phases of the incoming and locally generated codes. Figure 8 shows the block diagram of the delay lock (DLL) PN code tracking loop. With this loop, the tracking error is generated by comparing the outputs of the A-correlator (local code advanced by τ_d*) and the D-correlator (local code delayed by τ_d). A difference in the amplitudes of the two outputs is used to control the frequency, and hence the phase, of the local PN code clock.

As shown in Figure 8, the outputs of the A and D correlators are bandpass filtered and then square-law detected. The outputs of the square-law detectors are then passed through zonal filters which pass only the DC-centered components to the difference circuit. The output of the differencer is then applied to the loop filter and finally to the control circuit terminal of the code clock VCO. This closed loop configuration results in an equivalent noise loop bandwidth (one-sided) of B_L.

An alternate implementation for a PN code tracking loop is shown in Figure 9. This implementation is known as a tau-jitter loop. As shown in Figure 9, only one IF channel is used for the tracking function. This channel, which is fed by the output of the T-correlator, is time-shared by the advanced and delayed versions of the code correlation signals. The advance and delay are performed at the jitter frequency whose period is T_d. The magnitudes of these delays are τ_d. An obvious advantage of the tau-jitter loop is the reduced number of IF channels required to implement the tracking functions; only one channel is required, as compared to two channels required by the delay lock loop. Furthermore, the advantage

---

*τ_d is the correlator spacing and is restricted to a range of $\tau_d \leq \Delta$, where Δ is the code chip length. In other sections of this report and particularly in Appendixes B, C, and D, τ_d is defined as Δ/N, where N is any number larger than unity.

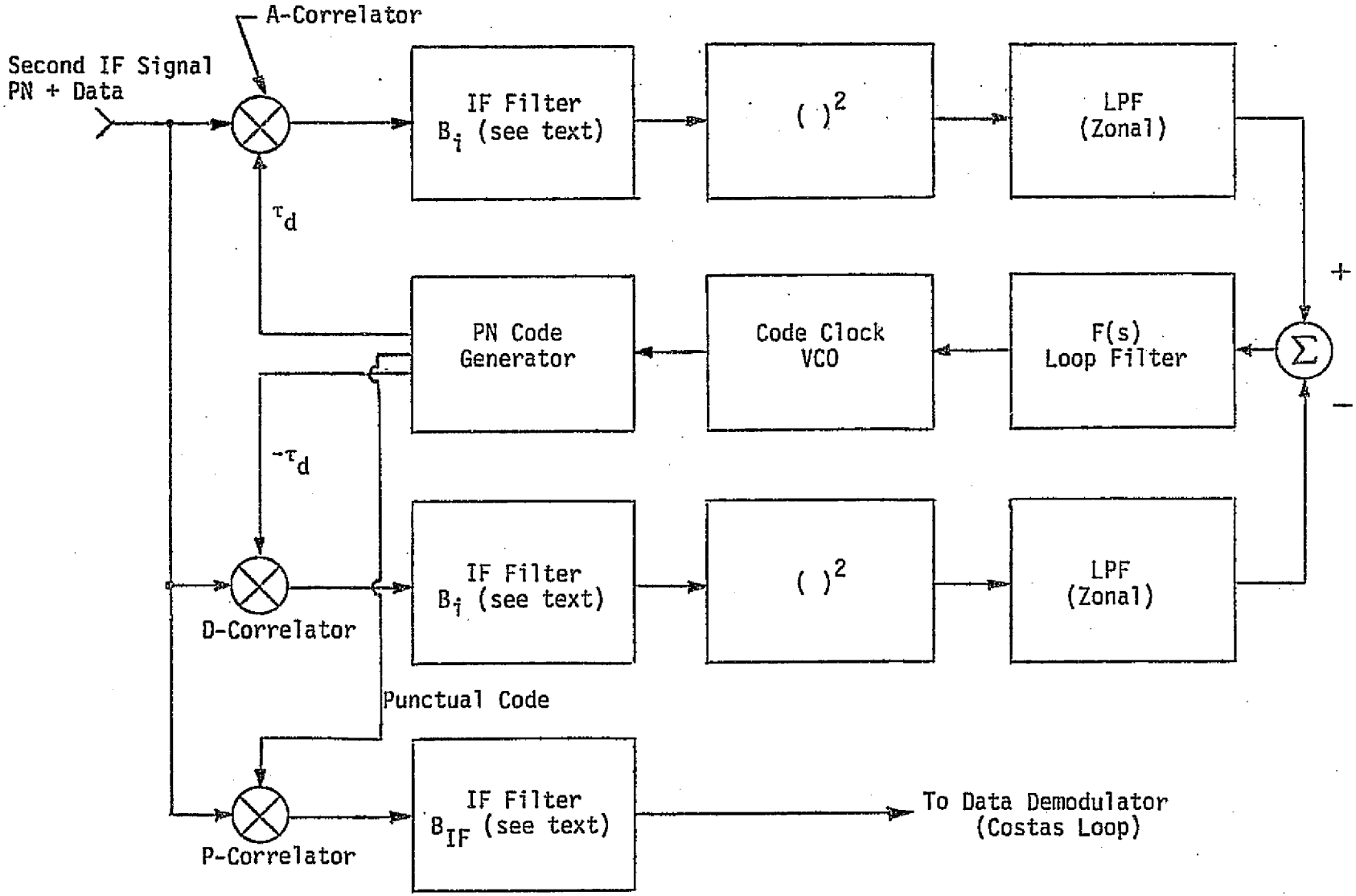

Figure 8. Delay Lock Type PN Code Tracking Loop (DLL)

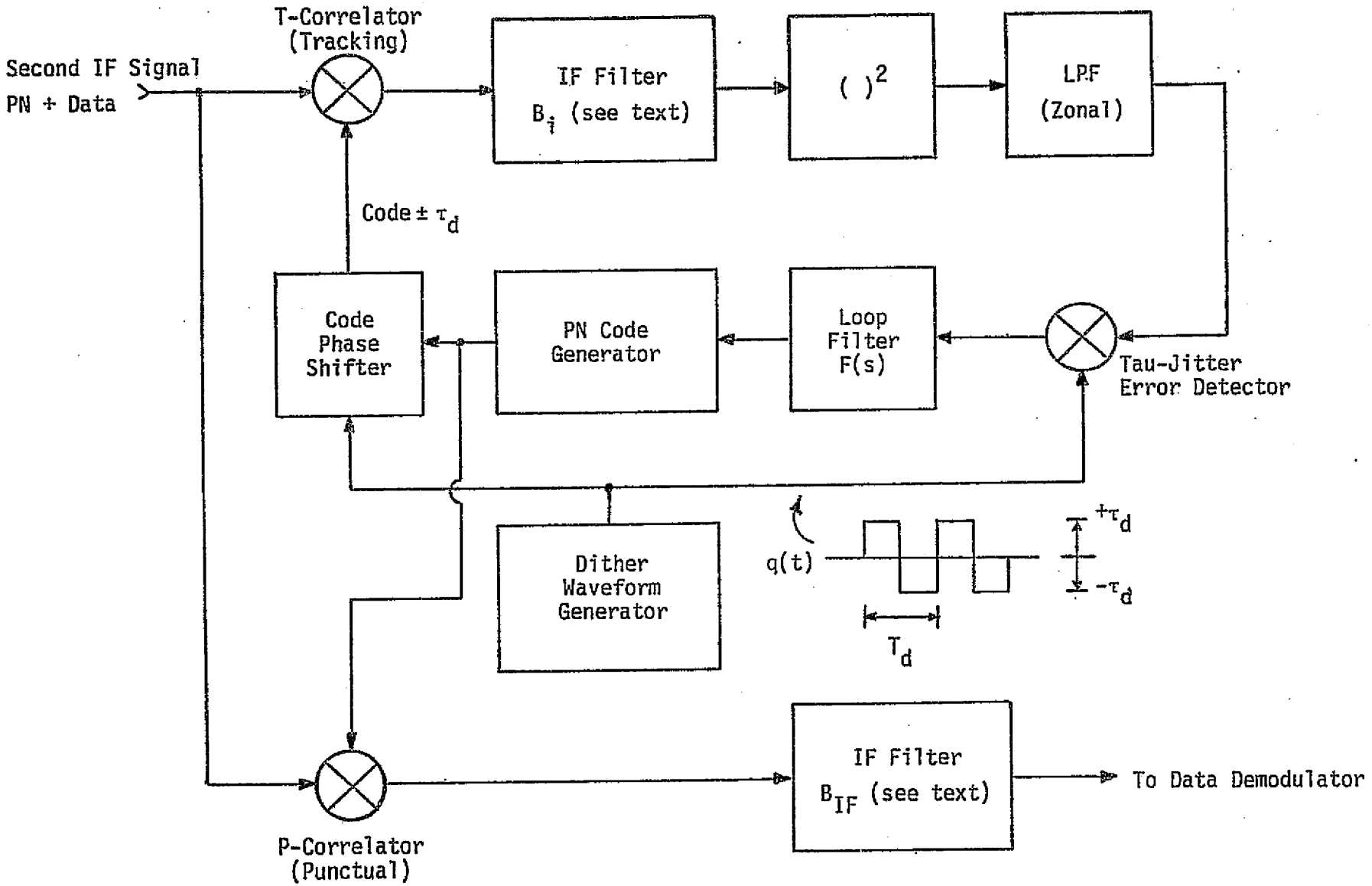

Figure 9. Tau-Jitter Type PN Code Tracking Loop (Tau-Jitter)

of time-sharing the same IF channel is that the distortions introduced by the channel (i.e., gain variations, bandpass, and phase nonlinearities) are common-moded out for the correlation samples.

The tracking performance of both the delay lock and tau-jitter loops are compared in detail in Appendixes B and C. The comparison is performed with respect to such parameters as loop noise bandwidth B_L, the tracking IF filter bandwidth B_i, correlator spacing τ_d (Δ/N), and carrier-to-noise ratio C/N_0. Figure 10 shows the rms tracking error for the two loops under consideration as a function of one-sided noise bandwidth B_L and C/N_0. From Figure 10, it is evident that, for any given value of B_L, the performance of the delay lock loop is from 2 to 2.5 dB better than that of the tau-jitter loop. A similar characteristic is indicated by Curves 1 and 2 of Figure 11, which shows the relationship between the normalized tracking error σ_T and the tracking loop bandwidth B_L.

Assuming the baseline value of $B_L = 300$ Hz, the normalized tracking error for the tau-jitter loop is about 1.97% or 0.0197. The effective signal loss at the output of the punctual correlator is [7]:

$$\begin{aligned} L_T &= 10 \log (1 - 1.6\, \sigma_T) \\ &= 10 \log [1 - (1.6)(0.0197)] \\ &= \underline{0.14}\ \text{dB} . \end{aligned} \tag{14}$$

The corresponding signal loss for a delay lock loop ($\sigma_T = 1.35\%$) is 0.09 dB. Thus, it appears that, from the standpoint of data recovery performance, the difference at $C/N_0 = 60.2$ dB-Hz is rather insignificant. At higher values of C/N_0, this difference will be even less.

Consequently, from the standpoint of data recovery performance, the use of a tau-jitter loop does not introduce significant degradation. The implementation complexity, however, is considerably reduced with use of the tau-jitter loop. It thus appears that, for the forward link, the tau-jitter loop is a potentially desirable candidate.

2.3.3 Carrier Tracking

The carrier tracking threshold is considered in section 2.3.3 of Appendix A. There it is shown that the threshold, as defined by 100 min mean time to unlock the carrier loop, is at about 57 dB-Hz.

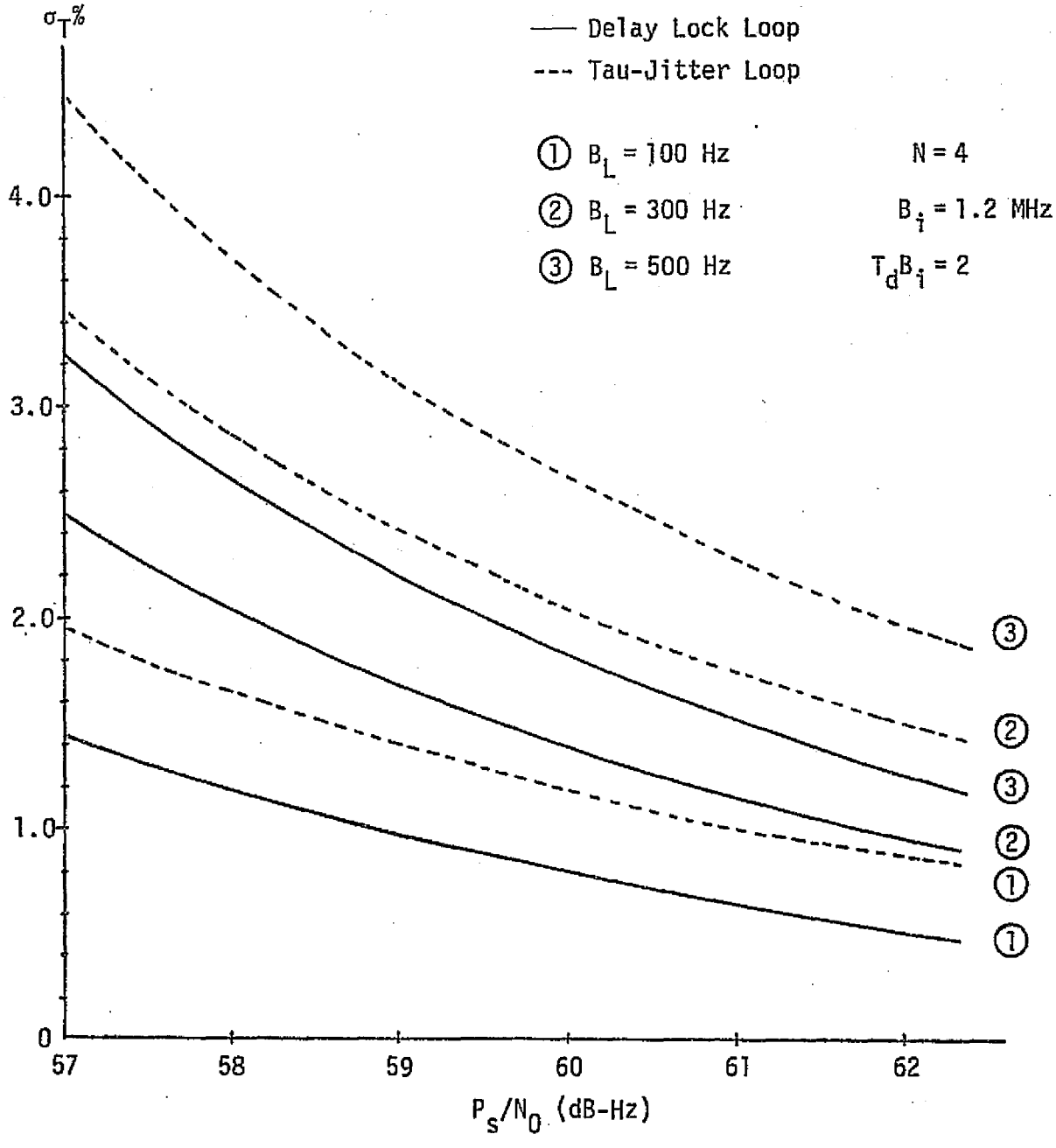

Figure 10. Percent Jitter Versus Signal-to-Noise Ratio (B_i = 1.2 MHz)

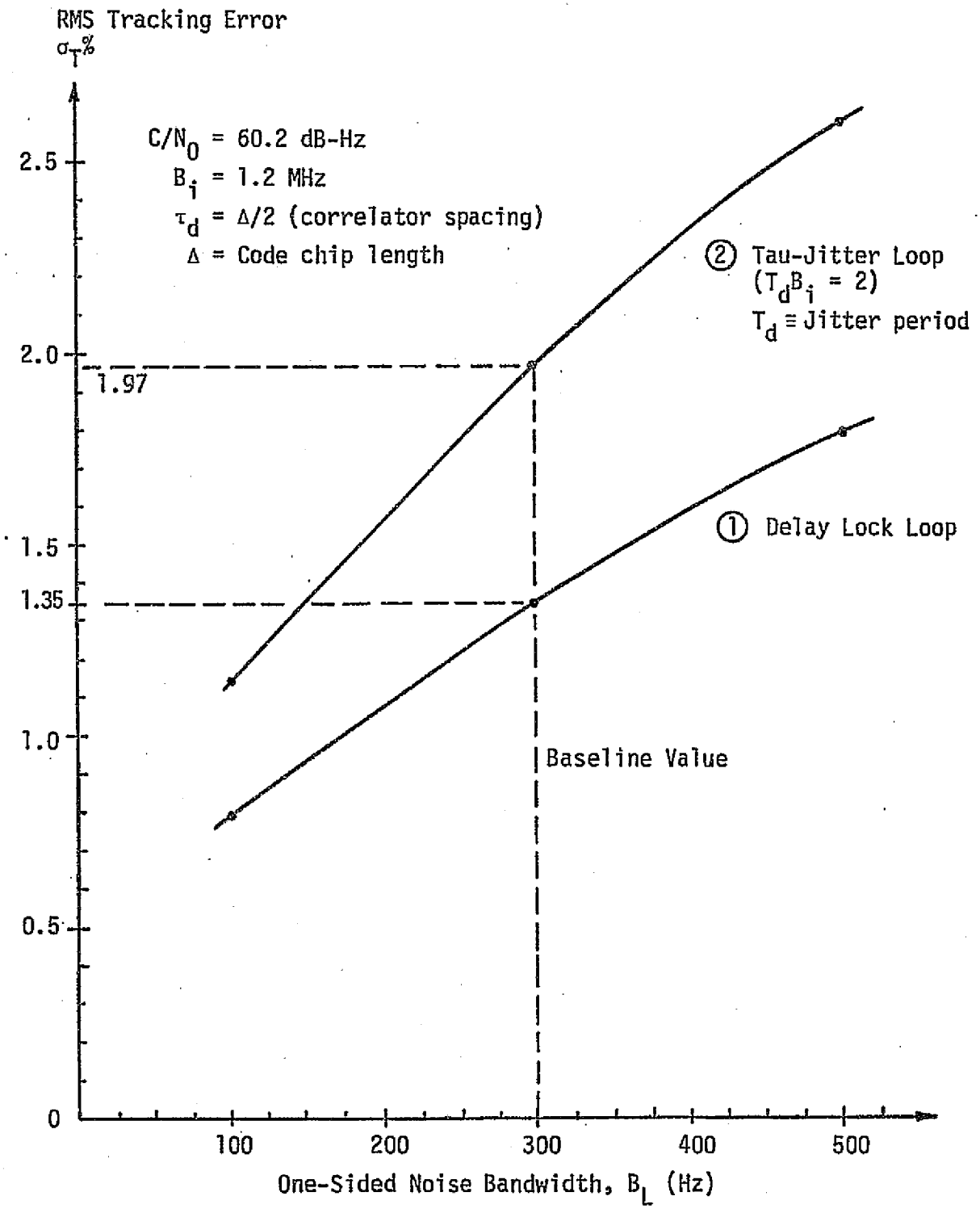

Figure 11. Tracking Error vs. Loop Noise Bandwidth for Delay Lock Loops and Tau-Jitter Loops at the Acquisition Threshold of C/N_0 = 60.2 dB-Hz

The degradation in signal due to carrier loop noise is only about 0.2 dB-Hz at this value of C/N_0 and it is negligible at 60.2 dB-Hz. Thus, one concludes that the carrier tracking loop is not a limiting subunit of the Ku-band receiver chain.

2.3.4 Bit Synchronizer Threshold

The bit synchronizer threshold, according to Table 5-5 in [6] is at about E_b/N_0 of -5 dB. For the 216 kbps forward link data rate, this corresponds to

$$\begin{aligned} C/N_0 &= 53.3 \text{ dB-Hz} - 5 \text{ dB} \\ &= 48.3 \text{ dB-Hz} . \end{aligned} \tag{15}$$

Thus, it appears that the bit synchronizer threshold is not a limitation on any of the other system subunits.

2.4 Summary of Acquisition and Tracking Threshold Performance for the Forward Link

The summary of the acquisition and tracking threshold performance estimates for the Shuttle Ku-band receiver is given in Table 6. From these estimates, it is evident that the requirement to acquire at C/N_0 of 60.2 dB does not violate any of the parameters included in the procurement specification [1]. Moreover, because the estimates in Table 6 are derived from a rather basic, simple system configuration, it is recommended that these estimates be used as guidelines for the Ku-band forward link performance. In this manner, any improvements in system configuration should result in a better performance.

Table 6. Summary of Acquisition and Tracking Threshold Performance for the Shuttle Ku-Band Communication Receiver Subunits (Forward Link)

Subunit	Acquisition		Tracking	
	Estimated Acquisition Time at C/N_0 = 60.2 dB-Hz	Aquisition Performance Limitation	Tracking Threshold C/N_0	Tracking Threshold Limitation or Driving Factor
Angle Search and Track	55 sec	Maximum gimbal rate of 120°/sec	54 dB-Hz	RMS angle track error of 0.2°
PN Code Search and Acquisition f_c = 3.03 Mcps N = 1023 bits	5-8 sec	1) SNR 2) Code clock uncertainty of 100 Hz due to receiver VCO	57 dB-Hz	Time to remain within lock for 100 minutes and P_{lock} = 0.99
Carrier Search and Lock	$\leq$ 0.5 sec	1) Probability of acquisition 0.9 or better 2) B_L of 2500 Hz	57 dB-Hz	Mean time to unlock of 100 minutes
Bit sync	1 sec	SNR	48.3 dB-Hz	SNR
Frame Sync	10 msec	SNR	Limited by bit sync threshold	SNR

3.0 BENT-PIPE IMPLEMENTATION CONSIDERATIONS

3.1 General Description

The bent-pipe mode for payloads allows transmission of data that is not in the standard NASA format. Thus, multiple formats and multiple modulator/demodulators can be used by the payloads. The design goal for the bent-pipe mode is to minimize the signal processing in the Orbiter for data that does not meet the standard NASA format. Therefore, no Orbiter control of command or telemetry for the bent-pipe data is proposed. Rather, the Orbiter will act as a relay which will either merely make a frequency translation at IF or perform RF demodulation and remodulation on a new carrier.

The block diagram for the Orbiter portion of the bent-pipe link is shown in Figure 12. Channel 1 is primarily an analog commercial TV channel with a bandwidth of 4.2 MHz. Alternately, however, Channel 1 may consist of one of the other data channels shown, namely, 4.5 MHz of analog data or up to 4 MHz of NRZ digital data.

The remaining channels are to be modulated onto an 8.5 MHz sine wave unbalanced QPSK subcarrier. The power split is 4:1. The 20% input is designated as Channel 3 and consists of a 192 kbps Bi-ϕ-L data channel from the network signal processor. The 80% input, Channel 2, is generally from the payload system and consists of up to 2 Mbps of data in the NRZ format. As shown in Figure 12, Channel 2 may also consist of information from recorder playbacks. Among the tests and analyses that have been performed are those in [8,9]. An analysis of the bent-pipe preprocessor is also included in Appendix E of this report.

3.2 Description of Test Results

Among the various candidate signal formats that are expected to be transmitted via nonstandard bent-pipe is a 16 kbps Bi-ϕ-L data stream on a 1.024 MHz subcarrier. This signal was tested and reported by Seyl and Smith [10]. A summary of the results of the tests is as follows:

A block diagram of the transmitter is shown in Figure 13. Figure 14 shows the block diagram for the receiver used in the tests. At the receiver, the post-detection filter for the 8.5 MHz subcarrier has a bandwidth of 7.6 MHz. The LPF for the analog TV channel is 4.2 MHz. The 16 kbps data

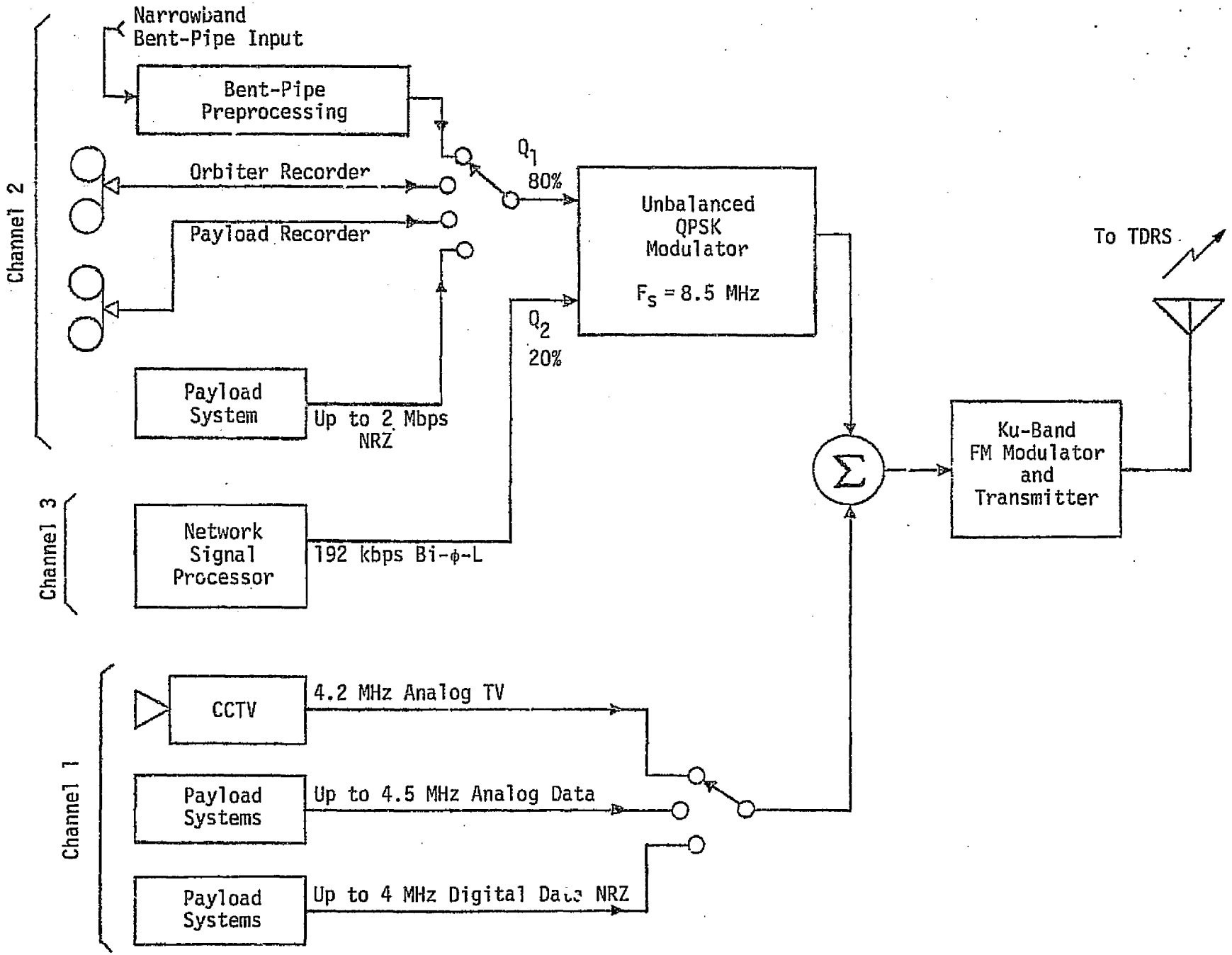

Figure 12. Orbiter Portion of the Bent-Pipe Link Implementation

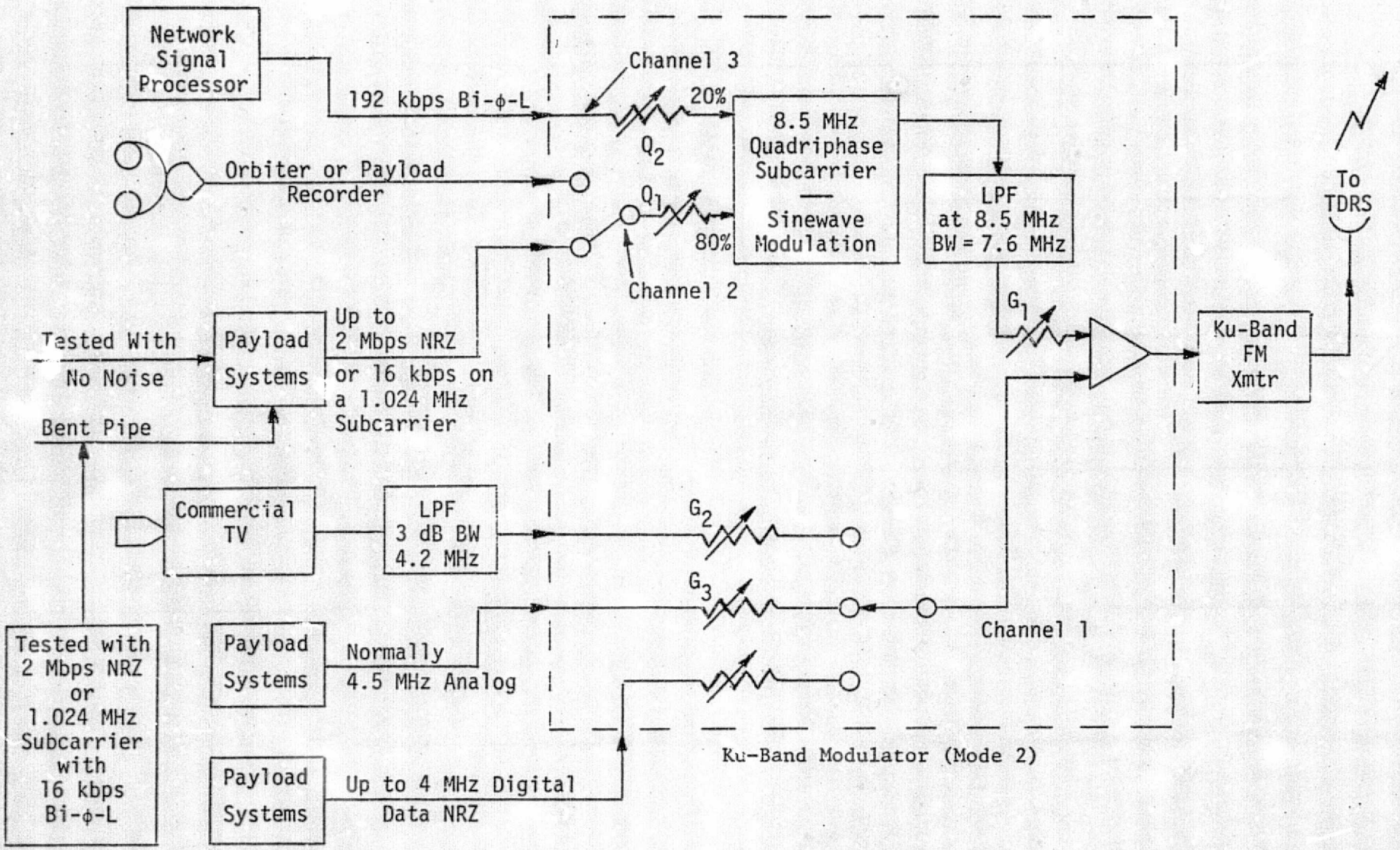

Figure 13. Orbiter System - Ku-Band Mode 2 FM Transmitter for Bent-Pipe Mode

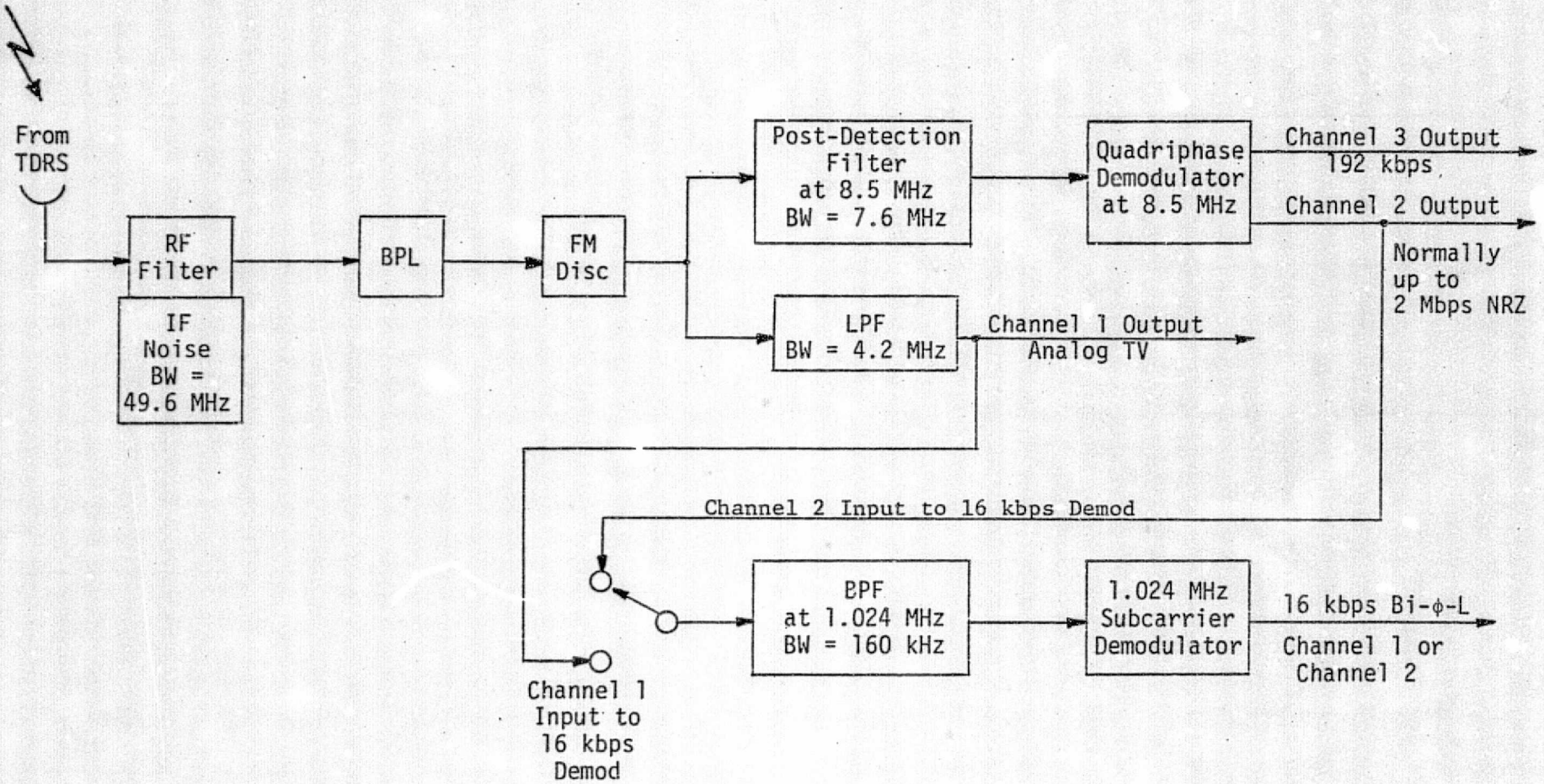

Figure 14. Ku-Band Mode 2 FM Receiver for Bent-Pipe Mode

signal on the 1.024 MHz subcarrier was also tested in Channel 1 as shown in Figure 14. The bandwidth of the prefilter for the 1.024 MHz subcarrier is set at 160 kHz.

For all tests, the FM deviations were set at the transmitter by adjusting the gains G_1, G_2, and G_3, each individually with the other signal inputs removed, as follows:

Gain	Channel	$\pm\Delta F$
G_1	8.5 MHz subcarrier	6 MHz
G_2	TV - Channel 1	11 MHz
G_3	16 kbps on 1.024 MHZ subcarrier in Channel 1	5 MHz

The total range of the instantaneous frequency deviation is $2\Delta F$ in each of the above cases.

The results of the tests are shown in Figures 15 and 16, and are summarized in Table 7. The signal formats of the tests A, B,..., K are described in Table 7, and the corresponding performance results are shown in Figures 15 and 16.

The bent-pipe test signal, namely, the 16 kbps on 1.024 MHz, was injected into Channels 1 and 2 without any external noise at the input. The actual signal will already have additive noise.

Also note that the addition of analog TV degrades all other channels between 2 and 3.5 dB.

3.3 Preprocessor Analysis Considerations

A preprocessor technique for accommodating narrowband bent-pipe payload data is presented in Figure 17. In this concept, the payload data can be in any modulation format and can be analog or digital, but its highest frequency must be less than 2 MHz. To guarantee this maximum frequency limitation, the input payload data is first lowpass filtered. The filtered payload data plus payload-Orbiter link noise is then hardlimited, making the resultant waveform appear as a pseudo-2 Mbps digital data stream which, for high signal-to-noise ratio, resembles the normal 2 Mbps NRZ data input for Modes 1 and 2 Ku-band communication. Thus, this concept allows for the normal Mode 2 operational data (192 kbps) and the 4.5 MHz analog

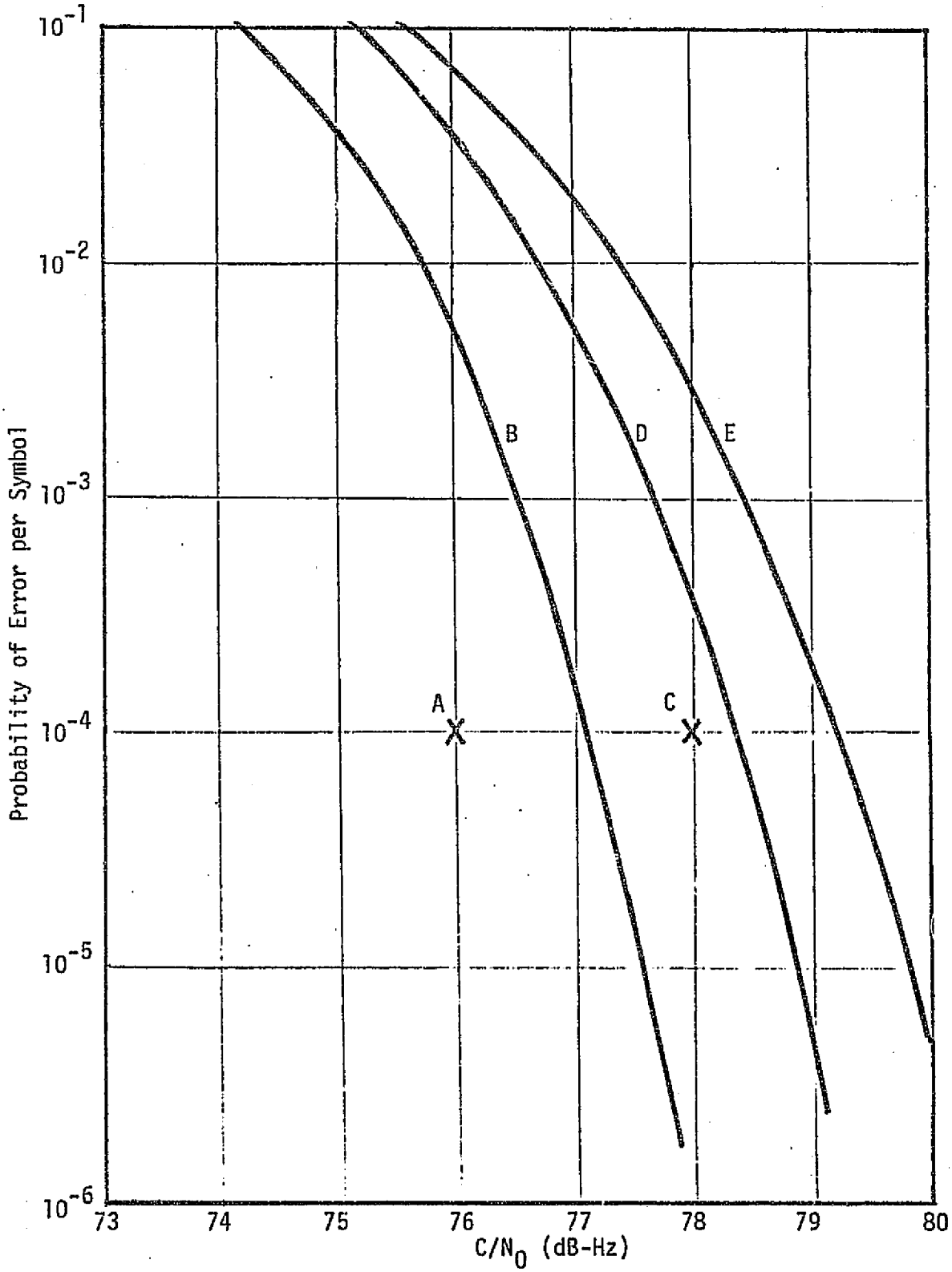

Figure 15. Probability of Error per Symbol Versus C/N_0 for Various Ku-Band Mode 2 Configurations

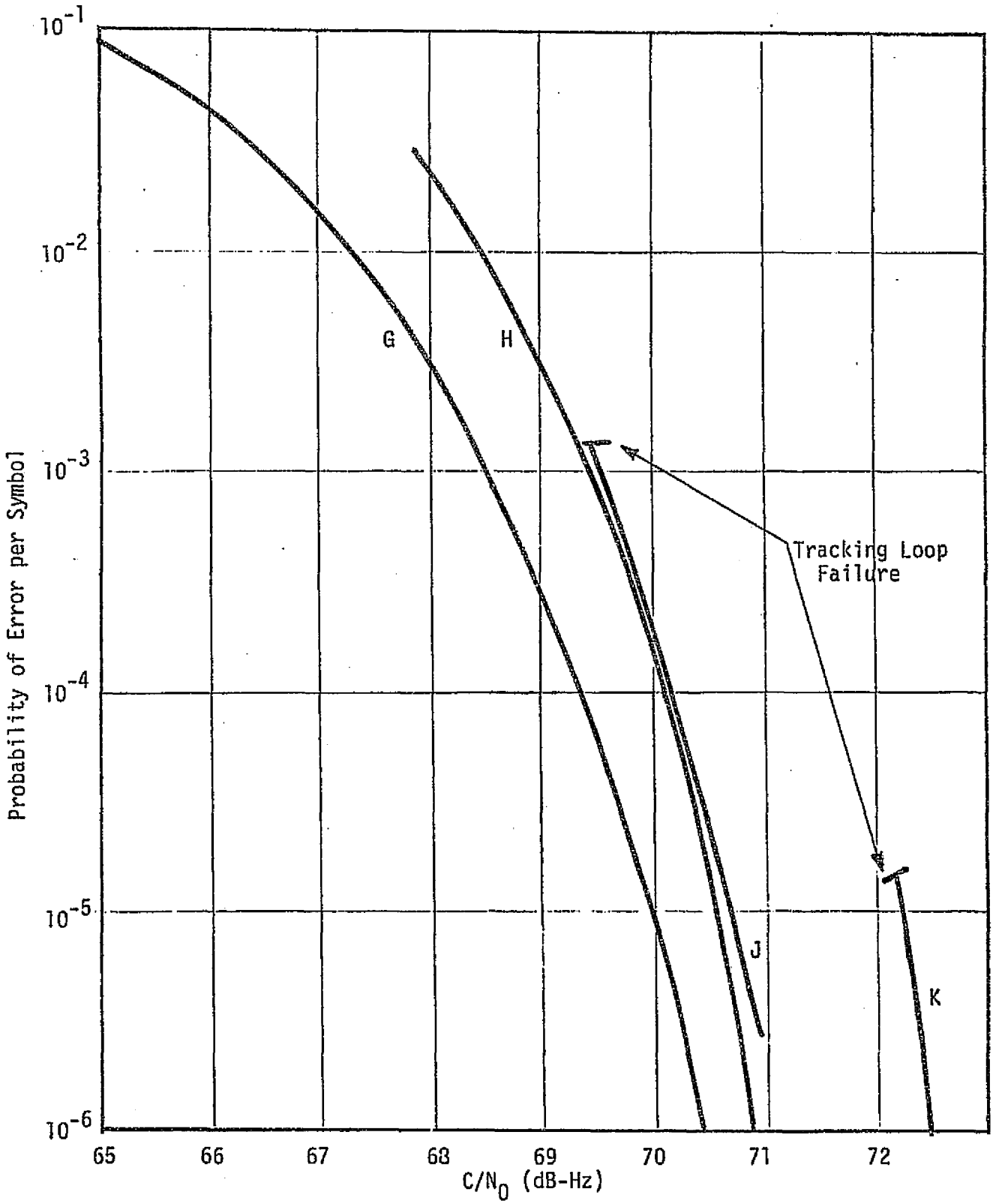

Figure 16. Probability of Error per Symbol Versus C/N_0 for Various Ku-Band Mode 2 Configurations

Table 7. Summary of Test Results

Test	P_e was Measured for:	Contents of Channel 1 (Baseband Channel)	Contents of Channel 2	Contents of Channel 3	Comments
A	192 kbps in Channel 3	0	2 Mbps NRZ	192 kbps Bi-ϕ-L	$P_e = 10^{-4}$ at $C/N_0 = 76$ dB-Hz
B	192 kbps in Channel 3	Commercial Analog TV	2 Mbps NRZ	192 kbps Bi-ϕ-L	Degradation in Channel 3 due to TV in Channel 3 is 2.3 dB
C	2 Mbps NRZ in Channel 2	0	2 Mbps NRZ	192 kbps Bi-ϕ-L	$P_e = 10^{-4}$ at $C/N_0 = 82$ dB-Hz
D	2 Mbps NRZ in Channel 2	16 kbps Bi-ϕ-L on 1.024 MHz S.C.	2 Mbps NRZ	192 kbps Bi-ϕ-L	Degradation of 2 Mbps in Channel 2 due to 16 kbps in Channel 1 = 0.8 dB
E	2 Mbps NRZ in Channel 2	Commercial Analog TV	2 Mbps NRZ	192 kbps Bi-ϕ-L	Degradation of 2 Mbps in Channel 2 due to TV in Channel 1 = 2.4 dB
G	16 kbps Bi-ϕ-L on 1.024 MHz S.C. in Channel 1	16 kbps Bi-ϕ-L on 1.024 MHz S.C.	2 Mbps NRZ	192 kbps Bi-ϕ-L	ΔF for 16 kbps in Channel 1 is 5 MHz
H	16 kbps Bi-ϕ-L on 1.024 MHz S.C. in Channel 2	0	16 kbps Bi-ϕ-L on 1.024 MHz S.C.	0	$\approx$ 1.5 dB degradation by changing 16 kbps to Channel 2 from Channel 1
J	16 kbps Bi-ϕ-L on 1.024 MHz S.C. in Channel 2	0	16 kbps Bi-ϕ-L on 1.024 MHz S.C.	192 kbps Bi-ϕ-L	Very little degradation by adding 192 kbps in Channel 3
K	16 kbps Bi-ϕ-L on 1.024 MHz S.C. in Channel 2	Commercial Analog TV	16 kbps Bi-ϕ-L on 1.024 MHz S.C.	192 kbps Bi-ϕ-L	More than 3 dB degradation by adding TV in Channel 1

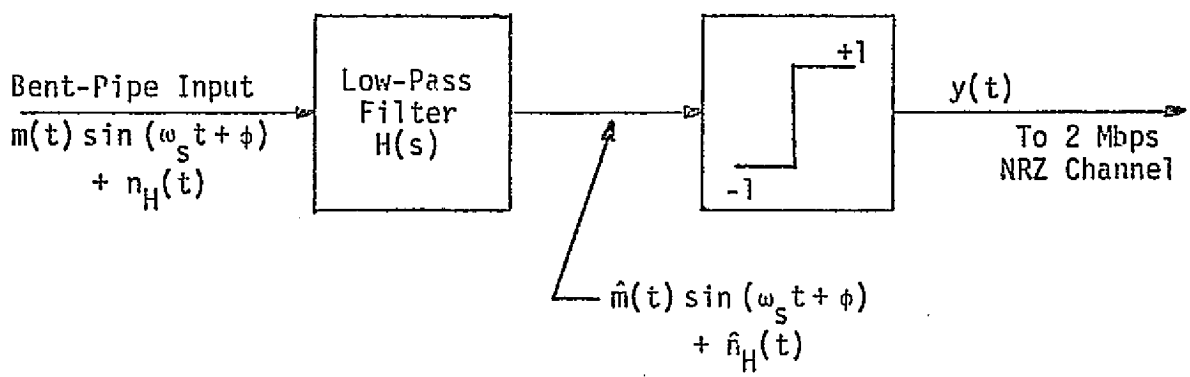

Figure 17. A Bent-Pipe Payload Data Preprocessor

data or the 4 Mbps digital data or the 4.5 MHz TV to be transmitted along with the bent-pipe payload data. Alternately, in Mode 1, the bent-pipe payload data can be transmitted along with the 192 kbps operational data and the 10-50 Mbps convolutionally coded digital data.

Previous designs of the FM Mode 2 and PM Mode 1 Ku-band return links have not considered the effects of a bent-pipe signal on the other two data channels nor the interfering effects of these channels on the preprocessed bent-pipe waveform. Before addressing these issues, one must first examine the nonlinear processing of the payload data plus noise which takes place in the bent-pipe preprocessor itself. In general, one would like to be able to statistically characterize the signal and noise components in the preprocessor output when its input is as unspecified as possible. As we shall see from the development given in Appendix E, this general task leads to mathematically intractable solutions. Fortunately, however, sufficient information is known about many of the payloads so that they can be characterized by specific data formats. Among the possible candidates are analog and various digital formats, including composite digital signals. One specific example which corresponds to NASA and DOD payloads is a 16 kbps Manchester coded telemetry data stream, bi-phase modulated on a 1.024 MHz subcarrier. This signal has been tested over a Mode 2 return link and the results of these tests reported in [10] and summarized in the preceding subsection.

In Appendix E, we focus our attention on characterizing the output signal and noise statistics of the bent-pipe preprocessor when the input signal is of the above form, namely, a low rate digital modulation on a subcarrier. Since the bent-pipe preprocessor output becomes modulated onto an 8.5 MHz unbalanced QPSK subcarrier, together with the 192 kbps Manchester coded operational data, one should then be able to modify previous analyses [11,12] of unbalanced QPSK demodulator performance to account for the presence of the noisy preprocessed bent-pipe signal as opposed to the noise-free 2 Mbps NRZ data stream which is normally transmitted on that channel. These modifications, along with the predictions of performance which follow from them, are the suggested subjects of further investigation.

4.0 TEXT AND GRAPHICS IMPLEMENTATION CONSIDERATIONS

4.1 Requirements

One of the requirements generated by NASA for the forward link is a potential capability to carry text and graphics information. The data rate designation for this link is 128 kbps, which is one of the data components comprising the composite 216 kbps rate. The baseline implementation configuration for this mode is a slow-scan, black-and-white TV compatible with the 128 kbps rate.

One of the requirements for the forward link text and graphics transmission is that of high fidelity reproduction of the original document. Consequently, when selecting bandwidth compression techniques, one should consider only those methods which result in either no distortion at all or only a minimal amount of distortion.

The type of information transmitted may typically involve, but may not necessarily be limited to: (1) photomaps, (2) printed maps, (3) sky imagery (star photos), (4) electronic schematics, and (5) mechanical assembly drawings.

Presently, four operating modes are being considered for the slow-scan TV text and graphics link. Table 8 summarizes the salient parameters of the four modes. It also provides an estimate for the time required to transmit an 8-in by 10-in document sheet. As shown in the table, Modes 1 and 3 provide a binary grey scale and Modes 2 and 4 provide a 64-level grey scale. The latter two modes are intended primarily for the transmission of multi-level sources, such as photomaps. The obvious penalty paid for using the multiple grey level capability is the increased transmission time.

Table 8. Image Resolution for an 8-in x 10-in Source

Mode	Spatial Resolution (Lines/Inch)	Grey Level Resolution (Bits/Sample)	Transmission Time (minutes)*
1	125	1	0.12
2	250	6	3.08
3	350	1	1.00
4	500	6	12.35

*Transmission time is based on 128 kbps forward link rate.

Binary grey scale modes (1 and 3) are considered to be suitable for transmission of information other than photomaps. The tradeoff within the binary grey scale modes is then line resolution versus transmission time. Acceptable performance with 350 lines/inch can be expected for printed maps, drawings and star imagery. However, with 120 lines/inch, only a printed (typed) text type of material can be transmitted with reasonable fidelity.

4.2 Implementation Considerations

One of the most likely candidates for encoding text and graphics data which consists of large sections of white is to use the Horlander-de-Coulon-Kunt (HCK) code. This code is specifically designed to skip the white places. A typical encoding scheme for binary grey level would then be as follows:

(1) The sampled line is divided in N picture elements (pel) blocks.

(2) If a block contains at least one black pel, an (N+1) bit word is transmitted, where the first bit is "1" and the next N bits represent the binary sequence of the block.

(3) If a block contains no black pels, there is no transmission and the next block is sampled.

The application of the HCK codes to multilevel graphics encoding can be performed in the following manner:

(1) The sampled scan line is divided into N-pel blocks. Each pels is encoded into m levels.

(2) If a block consists of all white picture elements, the encoder output is "0".

(3) All nonwhite blocks are encoded by (mN+1) bit code words, where the first "1" indicates a beginning of a nonwhite code word and "m" are the grey level code bits.

For the particular application at hand, a two-dimensional multi-level HCK encoding must be considered. With two-dimensional encoding, blocks of MxN pels are used. For an all-white block, a "0" is transmitted and, for a block of at least one nonwhite sample, a code word containing $[(M \times N \times m) + 1]$ bits is transmitted.

It must be noted that, for all types of the HCK encoding listed above, the compression ratio depends upon the total number of all-white blocks in the source document.

A conceptual block diagram for the forward link text and graphics decoder is shown in Figure 18. The input to the decoder is a serial 128 kbps data stream. Typically, the received data may consist of a one-bit preamble followed by 16 pixels (4 rows and 4 columns). If a simple, two-level encoding is used, a "1" preamble will indicate that the bits which follow represent the binary values of the corresponding pels. A "0" preamble, however, indicates that no additional data will be supplied and thus the decoder produces a string of either 16 zeros (if 0→white) or 16 ones (if 1→white). Note that the decoder also converts the data from block to line format usable by the display.

As shown in Figure 18, the inputs to the decoder are the serial data, the data clock and the frame sync. The state of the preamble bit is determined by the timing and control unit interrogating the buffered data stream. For a preamble of "1", the contents of the buffer are outputted to the memory unit. The data clock also advances the memory counters and the write command is supplied to the memory unit so that the buffered 16 bits are stored. For a preamble of "0", a set of 16 bits (either ones or zeros) is loaded into the memory. These bits, of course, are locally generated and they serve as white "fillers."

The operation of the 6 bit/pixel (multilevel greys) is similar except that a serial-to-parallel conversion takes place prior to loading the memory. Dotted arrows in Figure 18 show parallel data handling.

The format conversion for both the 1 bit/pixel and the 6 bit/pixel is performed within the decoder by the addressing logic.

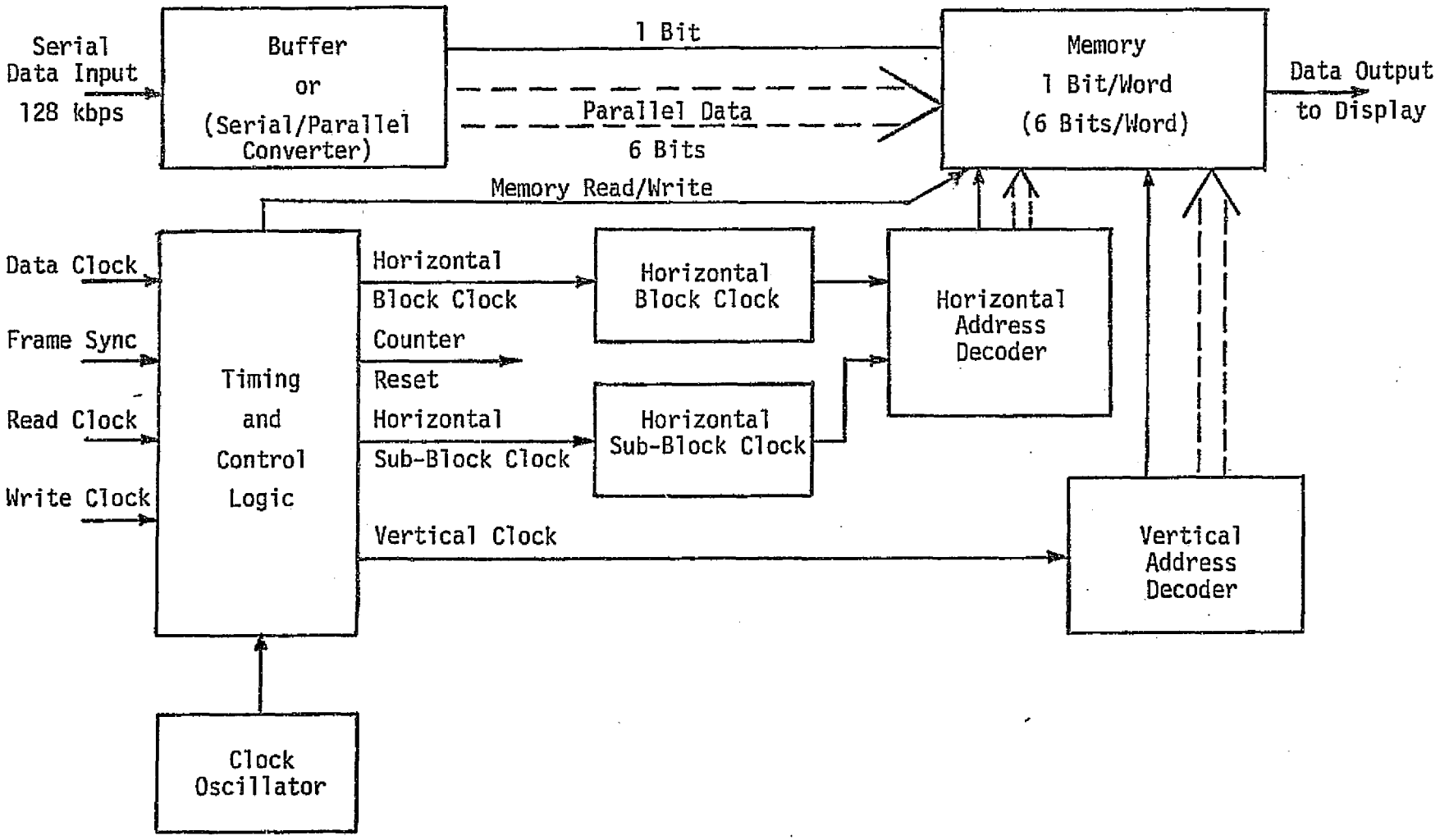

Figure 18. Conceptual Block Diagram for the Forward Link Text and Graphics Decoder
(Dotted Lines are for 6 bit/pixel encoding)

5.0 CONCLUSIONS AND RECOMMENDATIONS

The analysis of the forward link signal structure and performance predictions has been carried out and it is shown that the change to the new NASA-selected PN code rate of 3.03 Mcps (versus 11.23 Mcps originally specified [1]) does not degrade the performance of the forward link beyond the requirements stated in [1]. It is also shown that all of the acquisition requirements for the forward link can be met at the C/N_0 of 60.2 dB-Hz. The tracking threshold of the link is estimated at about 57 dB-Hz. PN tracking methods for the forward link have been investigated in detail and it appears that a tau-jitter loop, which is simple to implement, can be a good alternative for the delay lock loop (DLL) which is considered as a baseline device for PN code tracking.

The threshold analysis of the bent-pipe concept for the Orbiter has been carried out along with the comparative analysis of the empirical data. The complexity of the analytical approach, however, warrants further investigation to reconcile the empirical and theoretical results.

Techniques for incorporating text and graphics transmission capability into the forward link data stream have been considered and a baseline configuration is described.

The summarizing recommendation is that the results of the analyses presented in this report be considered in evaluating the approaches taken by the vendor(s) involved in the Ku-band system design.

REFERENCES

1. Procurement Specification MC409-0025, Ku-Band Integrated Radar and Communications Equipment, Vol. II, Space Division, Rockwell International, March 15, 1976.

2. S. Udalov, "Signal Detection and Angular Search Procedure for Shuttle Ku-Band Communication System," Axiomatix Report No. R7410-2 (under NASA Contract NAS 9-13467), October 2, 1974.

3. "Proposal for Ku-Band Integrated Radar and Communication Equipment for the Space Shuttle Orbiter Vehicle," Vol. II, Hughes Aircraft Company, Ref. No. D7768/SCG60176P, May 1976.

4. "Space Shuttle Ku-Band Integrated Rendezvous Radar/Communications System Study," Hughes Aircraft Company, Report D4148/SCG60041R, for NASA-JSC under Contract NAS 9-14595, March 1976.

5. "Ku-Band Integrated Radar and Communication Equipment for the Space Shuttle Orbiter Vehicle," Conceptual Design Review Booklet, Hughes Aircraft Company Ref. No. D7768/SCG66722V, January 18-20, 1977.

6. "Signal Design Study for Shuttle/TDRSS Ku-Band Uplink," Final Report, TRW Report No. 29210, CDRL No. 2, for NASA-JSC under Contract No. NAS 9-14842, August 1976.

7. G. A. DeCouvreur, "Effects of Random Synchronization Errors in PN and PSK Systems," IEEE Transactions , AES, January 1970, pp. 98-100.

8. "FM Mode 2 Return Link Evaluation Test Report," prepared by Lockheed Electronics Company for NASA-JSC, May 1976.

9. B. K. Levitt, J. R. Lesh, and J. C. Springett, "Shuttle/TDRSS Ku-Band Telemetry Study: Final Report," NASA-JPL Report 900-742.

10. J. Seyl and B. G. Smith, "Quick Look System Design Evaluation Tests of 16 kbps Channel Ku-Band FM Mode 2," NASA-JSC-EE7-76-435 Final Review.

11. M. K. Simon, "Tracking Performance of Unbalanced QPSK Demodulators," Axiomatix Report (to be published).

12. M. K. Simon, "Subcarrier Tracking Analysis for Three-Channel Orbiter Ku-Band Return Link," Axiomatix Report (to be published).

ACQUISITION AND TRACKING THRESHOLD ESTIMATES FOR THE FORWARD LINK OF THE SHUTTLE KU-BAND COMMUNICATIONS EQUIPMENT

by

Sergei Udalov

1.0 INTRODUCTION

The purpose of this appendix is to establish a set of parameters which can be used as a guideline for specifying the acquisition and tracking threshold performance of the Shuttle Ku-band communication receiver. As explained in the sections following, the acquisition threshold may be defined as that C/N_0 value* at which all of the receiver subunits can establish lock and the resulting performance is still compatible with some usable bit error rate (BER) at the system output. In comparison, the tracking thresholds may be defined as a set of C/N_0 values, lower than the acquisition threshold, at which the system performance either reaches an unacceptable level (excessive BER) or results in a high probability of losing lock (marginal time to unlock).

For the Shuttle Ku-band communication receiver, both the acquisition and tracking threshold performances are estimated for the subunits, which include spatial TDRS detector, PN despreader, data demodulator (Costas loop) and bit synchronizer. It is shown that, even at the "threshold" value of C/N_0 = 60.2 dB-Hz, all of the acquisition requirements specified for this equipment [1] can be met.

Section 2.0 contains all of the applicable performance estimates. Subsection 2.1 is devoted primarily to the assumptions and definitions used in carrying out the analyses. Subsections 2.2 and 2.3 consider the acquisition and tracking threshold performance, respectively. Conclusions and recommendations are presented in Section 3.0.

*Referred to antenna output terminal, i.e., receiver input.

2.0 PERFORMANCE ESTIMATION

2.1 ASSUMPTIONS AND DEFINITIONS

First, it is important to point out that the system model used for the analysis is a basic one and, consequently, the performance estimates provided in this report do not include trade-offs resulting from potential use of more sophisticated system models. For example, it is assumed that only one correlation channel is used to detect PN code sync. We also assume a "PN despread first" type of acquisition sequence.

Second, we must point out that the analysis is carried out for the PN code parameters which reflect the latest trend in NASA's forward link design philosophy. Specifically, the code rate of 3.028 mcs and the code length of 1023 chips are assumed. It is furthermore assumed that the doppler and the carrier uncertainties are reduced to within ±7.5 kHz at the TDRS and, consequently, any frequency uncertainties in excess of this value are due to the instabilities of the Shuttle's receiver oscillators.

Next, we present our definition of "thresholds" and the rationale for such definition. Specifically, in this report, the acquisition threshold performance is defined at the C/N_0 of 60.2 dB-Hz, which corresponds to a BER of 10^{-2} for 216 kbps data rate and a combined correlator and bit synchronizer loss of 2.5 dB.* The BER = 10^{-2} value is chosen here because it represents a system performance point useable for delta modulator-encoded voice communication.

Having defined the acquisition "threshold" in the above manner, the questions to answer are:

(a) Are the acquisition times and the corresponding statistical constraints within the values of the original specification?

(b) If different, what are their estimated values?

(c) How does the acquisition performance at C/N_0 = 60.2 dB-Hz relate to other pertinent system operating points, such as the 60.4 dB-Hz GPC designated condition and the 62.8 dB-Hz value commensurate with the TDRS search procedure?

---

*The assumed breakdown is 1.5 dB for correlator and 1.0 dB for bit synchronizer losses, respectively.

The characteristics of the tracking thresholds are more difficult to define because they involve not only the thermal noise performance, but also the dynamics of various Shuttle missions. The dynamics are of particular importance to the angle, the code, and the carrier tracking subunits of the communication equipments. Our estimates for the tracking thresholds are based, therefore, on the assumption of thermal noise only. Furthermore, wherever applicable, we use the definition of tracking threshold as that value of C/N_0 which would theoretically result in a mean time of 100 minutes to unlock a particular tracking function. The 100-minute interval is chosen as typical communication time with the same TDRS satellite.

Table 1 summarizes the salient system parameters assumed for the acquisition and tracking threshold analysis. Figure 1 shows the simplified block diagram of the Shuttle receiver portion which includes the spatial acquisition detection, PN despreader, data demodulator and angle track data detector.

2.2 ACQUISITION PERFORMANCE

2.2.1 Spatial Acquisition of TDRS

2.2.1.1 General Description

The alignment of the antenna directivity patterns along a common line-of-sight (LOS) is the first step for establishing the TDRS/Shuttle Ku-band communication link. The alignment of the TDRS antenna is aided by the "wide beam" horn radiator mounted on the Shuttle's antenna. The alignment of the TDRS antenna, however, must be performed by scanning across the residual uncertainty volume which may be as wide as a 20° cone. For best scan efficiency, a spiral pattern is used to search out the uncertainty volume. Furthermore, in order not to limit the rate at which the uncertainty volume is scanned, the energy detection is used to declare TDRS intercept [2]. The energy detected in this case is that of the spread spectrum signal entering the main lobe of the Shuttle's antenna pattern.

Referring to the block diagram of Figure 1, the spatial acquisition and detection unit* works at the second IF and it uses a portion of

*In Hughes (Ku-band system subcontractor) documents [3,4], this unit is referred to as the independent spatial acquisition detection (ISAD) unit.

Table 1. Salient Parameter Assumptions for Shuttle Ku-Band Receiver Channel

Parameter Description	Value*	Remarks
PN Code Rate	3.028 mcp	Reduced from 11.232 mcs
PN Code Length	1023 chips	Reduced from 2047 chips
Incoming carrier doppler and drift uncertainty	(±7.5 kHz)	Corrected at TDRS. Without correction: ±1.0 MHz
Residual received carrier uncertainty	±150 kHz	Receiver oscillator(s) drift contribution
Incoming code clock doppler uncertainty	(≤ 2 Hz)	Coherent with carrier. Corrected at TDRS. Without correction: ±400 Hz
Residual code clock oscillator uncertainty	±100 Hz	Reduced from ±300 Hz for 11.223 mcs code rate

*Values in brackets () have negligible effect on threshold calculations.

*Hughes documents refer to this circuit as Independent Spacial Acquisition Detector (ISAD).

**Az and El Δ-information time-multiplexed.

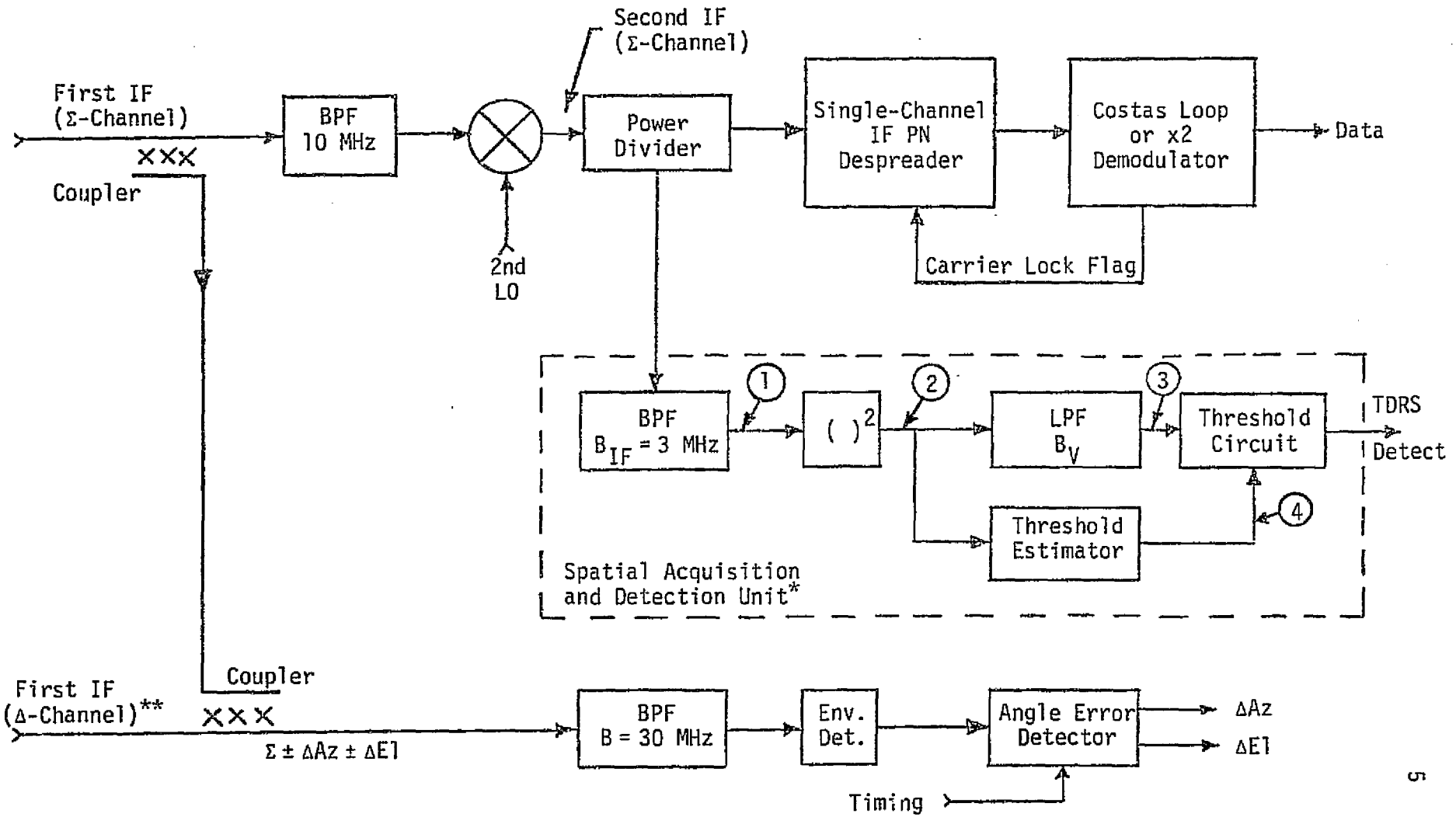

Figure 1. Signal Processing Portion of Shuttle Ku-Band Receiver - Simplified Block Diagram

the sum-channel (Σ) signal. The spread PN signal is passed through a 3 MHz bandpass filter and applied to a square-law detector. The output of the square-law detector is, in turn, applied to a low-pass filter and a threshold estimator. The function of the low-pass filter is to reduce the magnitude of the fluctuating component of the detected noise. The function of the threshold estimator is to provide a well-smoothed value of the DC component of the detected noise. This DC component is then scaled and applied to the threshold circuit to provide the reference for the "signal present" condition. The threshold estimator circuit is essentially a low-pass filter whose bandwidth is at least several orders of magnitude narrower than B_V. Consequently, the detection of the signal in the main beam of the antenna depends on the ability of the B_V filter to respond to the DC level change at the output of the square-law detector, such change being due to the antenna beam scanning across the TDRS signal. The actual value of B_V is therefore a compromise between the detection reliability and the antenna scan rate.

2.2.1.2 Spiral Scan Considerations

For a constant scan frequency* spiral search pattern, the relationship between the minimum antenna dwell time and the scan frequency is given by [2]:

$$t_{dm} = \frac{\beta}{(2\pi)\,\theta_m\, f_s} \qquad (1)$$

where: t_{dm} = minimum antenna dwell time over 3 dB beamwidth (seconds)

β = antenna 3 dB beamwidth (degrees)

f_s = scan frequency (Hz)

θ_m = maximum half-cone scan limit (degrees).

It must be noted that, with a constant scan frequency search, the t_{dm} occurs at the outer limit of the scan volume boundary defined by θ_m. The time required to spiral out to the maximum scan limit, i.e., area search time, is

*This type of scan requires minimum implementation complexity.

$$T_m = \frac{\theta_m}{(\Delta\theta)\, f_s} \tag{2}$$

where T_m = area search time

$\Delta\theta$ = angular advance of antenna beam per revolution (degrees/rev).

Making use of the relationship

$$f_s = \frac{\dot{\phi}}{360^\circ} \tag{3}$$

where $\dot{\phi}$ is the gimbal rate in deg/sec, one can rewrite (1) and (2) as follows:

$$t_{dm} = \frac{360\,\beta}{(2\pi)\,\theta_m\,\dot{\phi}} \tag{4a}$$

$$T_m = \frac{360\,\theta_m}{(\Delta\theta)\,\dot{\phi}} \tag{4b}$$

Using (4a) and (4b), one can determine t_{dm} and T_m as the functions of gimbal rate $\dot{\phi}$. Also, assuming that $B_V \approx 1/t_{dm}$, one can establish the interdependence between B_V and $\dot{\phi}$. Figure 2 shows T_m, t_{dm}, and B_V as functions of gimbal rate, $\dot{\phi}$, for the specific case which assumes:

$\theta_m = 10^\circ$ (20° cone)

$\beta = 1.6^\circ$

$\Delta\theta = 0.72^\circ$ (0.6 dB pointing loss during search).

From the data in Figure 2, it is evident that, with the constant frequency spiral scan, the maximum uncertainty area defined by the 20° cone ($\theta_m = 10^\circ$) can be searched in about 50 seconds if the nominal 102°/sec gimbal rate is assumed [3, Table 3.4-1]. With 90°/sec gimbal rate, the area search time is about 55 seconds. The corresponding values of B_V are 11 Hz and 10 HZ and, as will be shown in the next subsection, these relatively low bandwidths may not be required. It appears, therefore, that the area search time is limited primarily by the gimbal rates, rather than the requirements for narrow B_V. Such limitation, as shown by the data in Figure 2, is in the 50 to 55 seconds region, less than 1/3 of the specified 180-second limit.

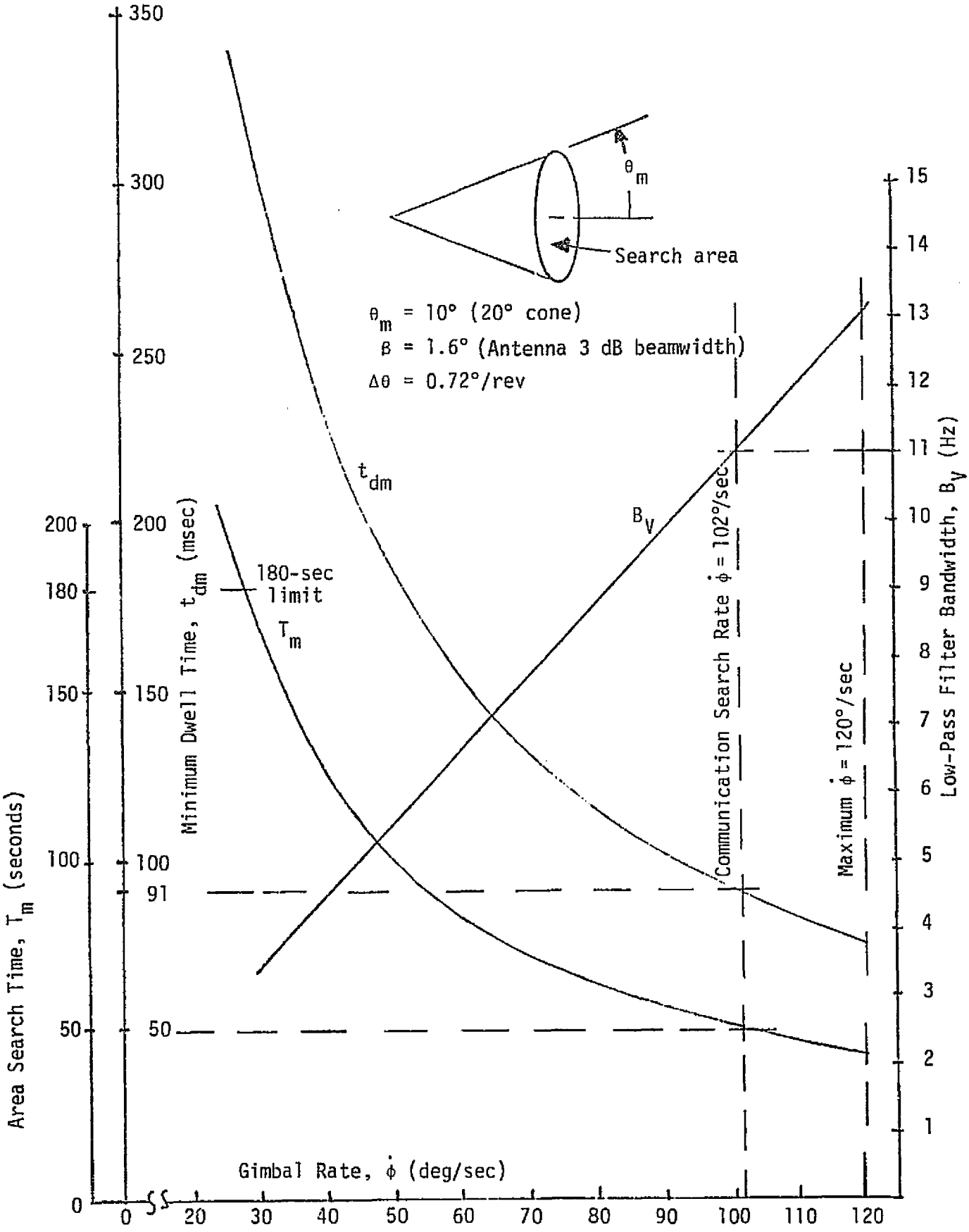

Figure 2. Area Search Time, Minimum Dwell Time, and Low-Pass Filter Bandwidth as Functions of Gimbal Rate (constant frequency spiral scan)

2.2.1.3 Signal Detection Considerations

The statistics of the signal detection during angular search for TDRS will now be considered. Specifically, TDRS detection at C/N_0 = 60.2 dB-Hz will be considered. Square-law detector theory will be used to simplify the pertinent analysis. Thus, assuming a square-law detector between IF output (Point ①, Figure 1) and the LPF input (Point ②), the expression for rms noise value at the LPF output is

$$\sigma = \sqrt{\frac{2\,B_V}{B_{IF}}}\,\sqrt{1+2(S/N)_{IF}} \qquad (5)$$

where σ = normalized rms value of the noise component at output of the LPF (Input ③ to threshold circuit)

B_{IF} = noise bandwidth of IF filter (Hz)

B_V = noise bandwidth of the low-pass filter (Hz)

$(S/N)_{IF}$ = signal-to-noise ratio in IF filter.

It must be noted that σ in (5) is normalized with respect to the average (DC) value of "noise only" output of the square-law detector. This DC value is

$$\bar{N} = N_{IF} = B_{IF}N_0 \qquad (6)$$

where $N_0 = kT_s$ = Boltzmann's constant × System noise temperature = system noise density in dBW/Hz.

Equation (5) can be used for calculating the location of the TDRS detection threshold, as well as for the estimates of the threshold tolerances commensurate with the statistical constraints imposed on the TDRS acquisition. Specifically, the location of the threshold(s) must be such that, with a given σ, a certain probability of detection, P_D, is obtained for the mainlobe signal and, at the same time, an acceptably low probability of false alarm, P_{fa}, is maintained for the worst case sidelobe signal. The condition of the worst case sidelobe signal occurs when the TDRS is within the first sidelobe of the Shuttle's antenna, yet the detection thresholds have been deliberately lowered to insure mainlobe acquisition under degraded conditions listed in Table 2.

Table 2. Factors Contributing to Sidelobe Suppression Degradation

Parameter	Maximum	Minimum	Degradation (dB)
TDRS EIRP	48.0 dBw	36.6 dBw	11.4
Path Loss	208.5 dB	205.7 dB	2.8
Pointing Loss (GPC designate)	3 dB	0 dB	3.0
		Total Degradation	17.2 dB

Therefore, if the measured sidelobe level of an antenna is 22 dB down (baseline value), the effective level during TDRS acquisition is only

$$\Delta_{eff} = 22 \text{ dB} - 17.2 \text{ dB} = 4.8 \text{ dB} . \quad (7)$$

The value of Δ_{eff} of 4.8 dB will be used in calculations which follow. First, we compute the $(S/N)_{IF}$ for the worst case mainlobe signal:

$$(S/N)_{ML} = C/N_0(\text{dB-Hz}) - \text{Spectrum loss (dB)} - 10 \log B_{IF} \text{ (dB)}$$

$$= 60.2 \text{ dB-Hz} - 1.2 \text{ dB} - 64.8 \text{ dB-Hz}$$

(1.2 dB: in 3.0 MHz; 64.8 dB-Hz: 3.0 MHz noise BW)

$$= -5.8 \text{ dB} \quad \text{or} \quad \underline{0.265} \text{ numeric.} \quad (8)$$

Next, we compute $(S/N)_{IF}$ for the highest sidelobe signal, i.e., worst case:

$$(S/N)_{SL} = (S/N)_{ML} - 4.8 \text{ dB} = -5.8 \text{ dB} - 4.8 \text{ dB}$$

$$= -10.6 \text{ dB} \quad \text{or} \quad \underline{0.087} \text{ numeric.} \quad (9)$$

The numeric values given by (8) and (9) represent the increase in the DC input to the threshold device due to the mainlobe and the sidelobe signals, respectively. Both of these values are superimposed on the unity magnitude of the DC term due to noise alone.

Disregarding the effects of possible DC term changes due to either the earth or the sun detection, the threshold level must be set between the values of 1.087 and 1.265. The lower bound on the threshold is determined by P_{fa} which, for this case, is taken as 10^{-7}. This implies that the lower bound of the threshold must be at 5.2 σ_{SL} above the 1.087

level. The upper bound of the threshold setting is determined by the required $P_D = 0.99$ and, therefore, it lies about 2.4 σ_{ML} below the 1.265 level.

The actual values of σ_{ML} and σ_{SL} are determined by substituting the corresponding values of $(S/N)_{ML}$ and $(S/N)_{SL}$ into equation (5). Thus, for $B_{IF} = 3.0$ MHz, one obtains

$$\sigma_{ML} = \sqrt{\frac{2\,B_V}{3 \times 10^6}}\ \sqrt{1 + (2)(0.265)} = 1.01 \times 10^{-3} \sqrt{B_V} \qquad (10)$$

$$\sigma_{SL} = \sqrt{\frac{2\,B_V}{3 \times 10^6}}\ \sqrt{1 + (2)(0.087)} = 0.85 \times 10^{-3} \sqrt{B_V} \qquad (11)$$

Table 3 shows the magnitudes of σ_{ML} and σ_{SL} for several most likely values of B_V. Using $B_V = 20$ Hz, we obtain the lower and the upper bounds on the threshold setting:

$$Th_{lower} = 1.087 + 5.2\,\sigma_{SL} = 1.087 + (5.2)(0.0038)$$

$$= 1.107 \qquad (12)$$

$$Th_{higher} = 1.265 - 2.4\,\sigma_{ML} = 1.265 - (2.4)(0.0045)$$

$$= 1.254\ . \qquad (13)$$

Table 3. Magnitudes of σ_{ML} and σ_{SL} vs. B_V

B_V (Hz)	σ_{ML} (mV)	σ_{SL} (mV)	
20	4.52	3.82	$C/N_0 = 60.2$ dB-Hz
15	3.91	3.31	$L_s = 1.2$ dB
10	3.19	2.70	$B_{IF} = 3.0$ dB

Numerical values given by (12) and (13) define the threshold tolerance region. Figure 3 depicts the location of this region with respect to other pertinent low-pass filter output levels. The magnitude of the threshold region may correspond either to an uncertainty of an analog-to-digital converter or to the drift resulting from changes in system parameters. In either case, the threshold region shown in

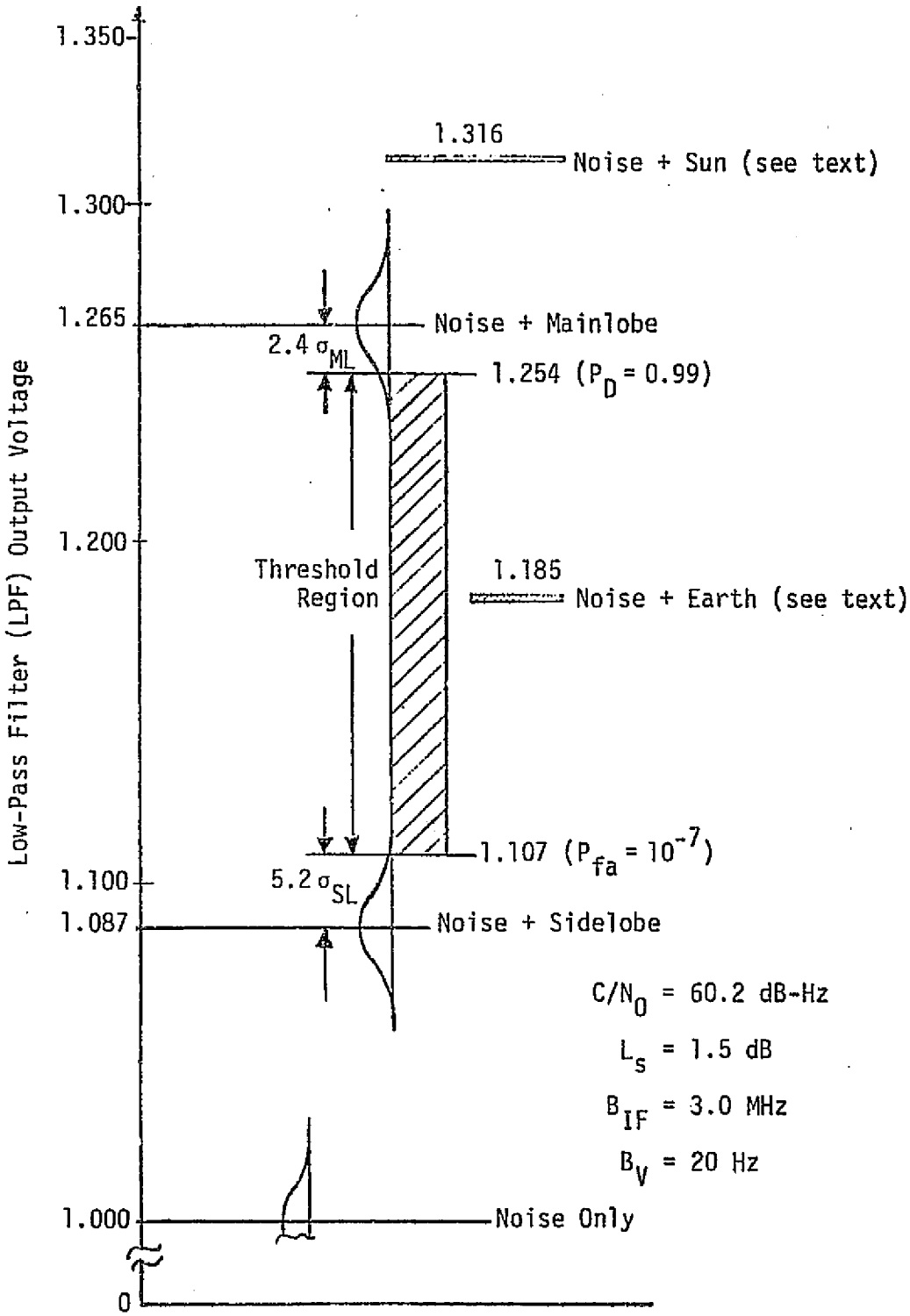

Figure 3. TDRS Spatial Acquisition Threshold and Tolerances

Figure 3 permits an implementation tolerance of about ±2 dB, a rather reasonable figure.

It remains to determine the relative magnitudes of the earth and the sun signals. For this, we compute the S/N ratios for these sources using their respective temperatures and the system temperature, T_{sys}. Consequently,

$$(S/N)_{earth} = \frac{T_E}{T_{sys}} = \frac{290°K}{1565°K} = \underline{0.185} \text{ or } \begin{matrix}-7.5 \text{ dB below} \\ \text{system noise}\end{matrix} \quad (14)$$

$$(S/N)_{sun} = \frac{T_M}{T_{sys}} = \frac{495°K}{1565°K} = \underline{0.316}^{*} \text{ or } \begin{matrix}-5.0 \text{ dB below} \\ \text{system noise}\end{matrix} \quad (15)$$

The locations of the earth-plus-noise and the sun-plus-noise signals are shown in Figure 3. The location of the earth signal is shown for reference only, because this signal will be rejected by the earth discriminator [5]. Of most importance is the fact that the sun signal is <u>above</u> the noise-plus-mainlobe signal for the case at hand, i.e., $C/N_0 = 60.2$ dB-Hz, and thus, <u>special means</u>, possibly optical, may have to be used for the rejection of the sun lock-up.

One concludes therefore that, with the exception of requiring a "sun discriminator," the performance of the spatial acquisition unit is not significantly degraded at C/N_0 of 60.2 dB-Hz. In other words, a reasonable implementation tolerance can be assumed, about ±2 dB, and the values of B_V which will result in lowering the scan rate below the baseline 102°/sec are not required. Consequently, the spatial acquisition time at C/N_0 of 60.2 dB-Hz is determined by the servo system and thus will not exceed the estimated 55-second period required to scan the 20° uncertainty region [5, p. 18].

After the spatial detector circuit provides a signal, thus indicating that the TDRS is within the mainlobe of the antenna, the antenna is returned to the angular position at which detection has occurred and the miniscan program is initiated [5]. During the miniscan, the antenna beam is moved in a spiral pattern around the initial "signal detect"

---

*Sun temperature of 495° is based on averaging over the equivalent antenna beamwidth (Hughes Aircraft Company estimate, Vu-graph titled "ISAD Detection in Search Mode - 3.028 M Chip PN").

position and thus it is reasonable to assume that the TDRS signal provided to the receiver is no worse than that at which the initial space detection has occurred. Consequently, one can also assume that the next step, i.e., the PN code search and acquisition, takes place with at least the same C/N_0 ($\geq$ 60.2 dB-Hz) as the spatial detection. Section 2.2.2 considers the PN search and acquisition performance.

2.2.2 PN Code Search and Acquisition

2.2.2.1 General Description

The purpose of the code search and acquisition stage of the signal acquisition procedure is to align the phases of the incoming and the locally generated PN codes. The alignment is achieved by shifting the phase of the locally generated code until the coincidence of the two codes is detected and the shifting is terminated. If the termination of the code phase shift is due to a true coincidence, the PN code tracking begins and the remainder of the acquisition sequence, i.e., carrier lock, bit and frame synchronization, is carried out.

Figure 4 shows the simplified block diagram for the PN code search implementation. The logic flow diagram for the PN code search, as well as for the acquisition and track phases is given in Figure 5. Referring to Figure 4, the code search is performed as follows:

The frequency of the code clock applied to the PN register is changed so as to cause the phases of the incoming and the locally generated codes to slip past each other. The change in code clock frequency is such that even for the worst case of code clock drift (assumed at 100 Hz, see Table 1), the relative code phase slippage does not exceed 1/2 chip in the post-detection bandwidth B_V. Note that B_V is the bandwidth of one of the low-pass filters (LPF) which are placed at the output of the square-law envelope detector.

Consequently, as shown in Figure 4, the output of the correlator is passed through the post-correlation IF filter of bandwidth B_{IF} is square-law detected and is applied to low-pass filters B_V and b_V, as well as to the threshold estimator. As the code phase difference approaches 1/4 chip width, the output of the B_V filter exceeds the threshold Th_1. Crossing of threshold Th_1 results in a 10 msec pulse at the output of the one-shot multi-vibrator (MV). This pulse inhibits the code search process for 10 msec.

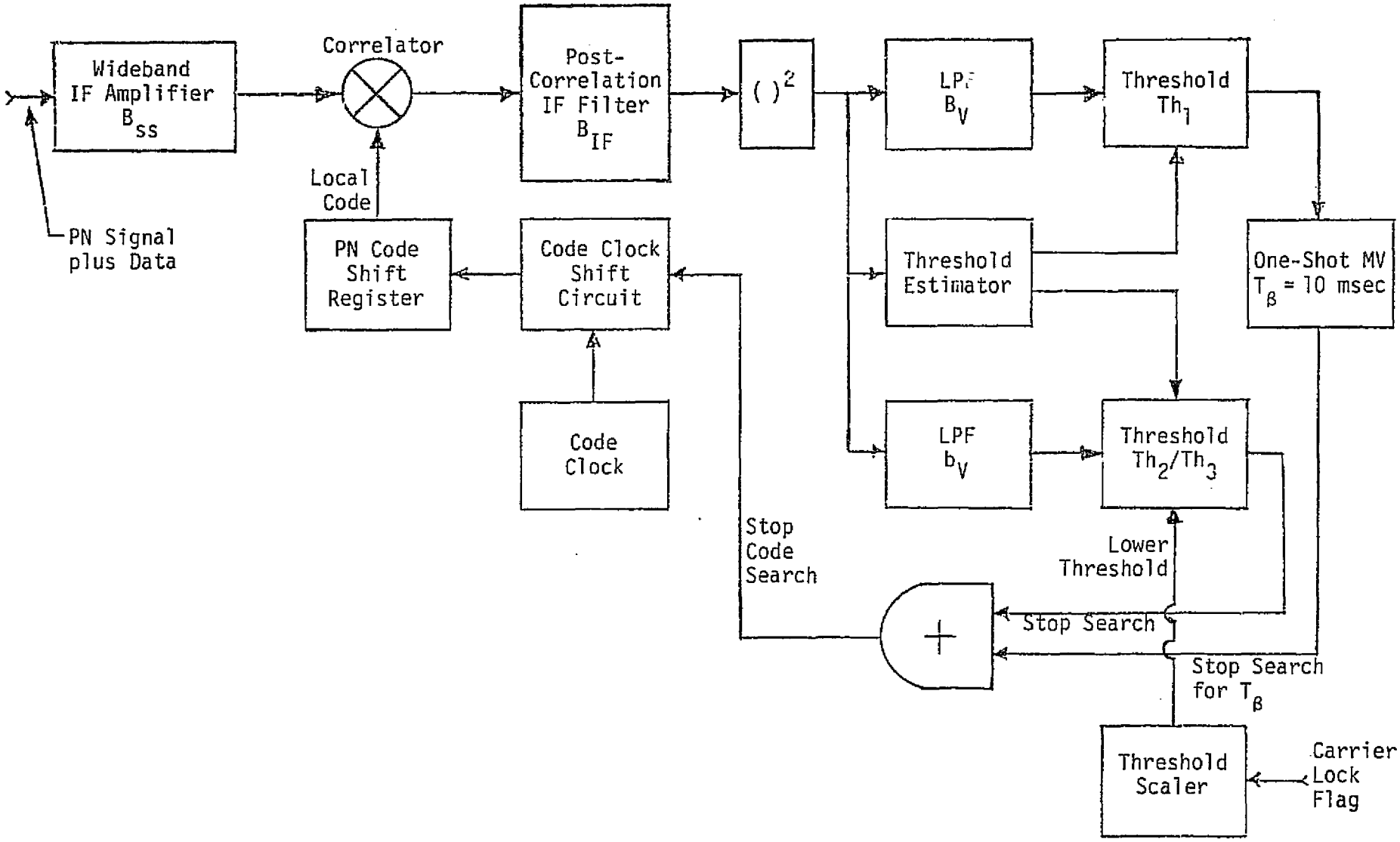

Figure 4. Simplified Block Diagram for PN Code Search Implementation (Single-Channel Version)

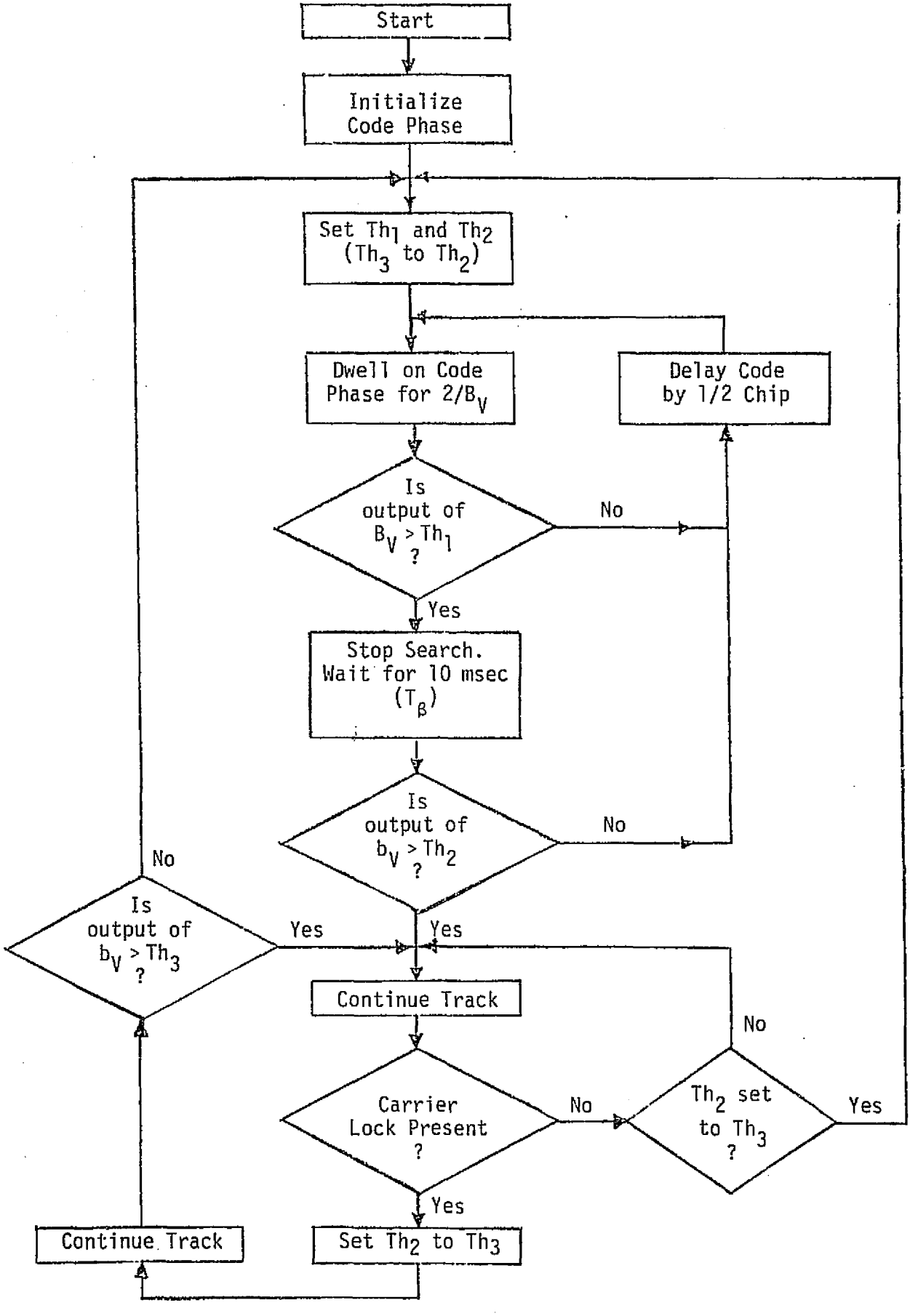

Figure 5. Logic Flow Diagram for PN Code Search, Acquisition and Track

If the crossing of Th_1 is due to partial correlation, which is the beginning phase of the full correlation, the code tracking loop (not shown in Figure 4) pulls into code sychronism.* The pull-in causes the output of the b_V to exceed the secondary threshold Th_2 and the search is terminated. The subsequent acquisition of the carrier causes the secondary threshold to be lowered to Th_3, a value which prevents the code search from re-occurring unless the C/N_0 drops below a predetermined tracking threshold value.

On the other hand, if the crossing of Th_1 is due to a noise pulse, i.e., due to a false alarm, the Th_2 is not exceeded after 10 msec and the code search is resumed upon the expiration of the 10 msec interval. Therefore, each false alarm triggering halts the search process for only 10 msec. The logic flow diagram of Figure 5 shows both the true and the false alarm paths.

2.2.2.2 Quantitative Considerations - PN Synchronization Detection

The process of PN synchronization detection will now be considered quantitatively. As the first step, we determine the post-correlation IF bandwidth, B_{IF}:**

$$B_{IF}\ (\text{post-correlation}) = 2\ (|\Delta f_0| + 2 \times \text{Data Rate}) \qquad (16)$$

where Δf_0 = residual carrier uncertainty due to local oscillator drifts in the receiver. Thus, for 216 kbps (Manchestered) and $|\Delta f_0|$ = 150 kHz, one obtains:

$$B_{IF} = 2(150 \times 10^3 + 2 \times 216 \times 10^3) = 1.164 \times 10^6 \text{ Hz}$$

$$= 1.164 \text{ MHz} \qquad (17)$$

or 60.7 dB-Hz.

The next step is to calculate the expected signal losses for the cases of: (1) an uncorrelated and (2) a correlated signal. For the uncorrelated signal, the loss is that due to the passage of the 3.03 mcs PN

---

*It is assumed that a 10 msec interval is sufficiently long for the code tracking loop to pull in.

**It is assumed that the bandwidth B_{ss} of the wideband IF amplifier is sufficiently wide (10 to 30 MHz) so as to introduce only a negligible loss of the spread spectrum signal.

code spectrum through the 1.164 MHz IF. Consulting the $\int_0^{B_{IF}/2} (\sin x/x)^2\, dx$ curve indicates that this loss is about 4.6 dB.

The loss for the correlated signal is computed based on the assumption that the crossing of threshold Th_1 takes place at the displacement from the peak of $\epsilon = \pm 0.25$ chips along the idealized, triangular voltage correlation funtions. In terms of power, such displacement results in a correlation loss of

$$L_s\,(\text{corr}) = (1-\epsilon)^2 = (0.75)^2 = 0.56 \qquad (18)$$

or 2.5 dB.

It must also be noted that the threshold crossing for the correlated case can take place in the vicinity of the peak of the correlation function, which is, by definition (see footnote, page 2), 1.5 dB below the threshold maximum.

The signal-to-noise ratios which determine the DC levels at the outputs of the low-pass filters for the uncorrelated and the correlated signals can be computed as follows:

$$(S/N)_{\text{Uncorrelated}} = C/N_0\ (\text{dB-Hz}) - L_s\ (\text{dB}) - 10 \log B_{IF}\ (\text{dB-Hz})$$
$$= 60.2\ \text{dB-Hz} - 4.6\ \text{dB} - 60.7\ \text{dB-Hz}$$
$$= -5.1\ \text{dB} \quad \text{or} \quad 0.309\ \text{numeric} \qquad (19)$$

$$(S/N)_{\text{Corr/ 0.25 chip}} = 60.2\ \text{dB-Hz} - 2.5\ \text{dB} - 60.7\ \text{dB-Hz}$$
$$= -3.0\ \text{dB} \quad \text{or} \quad 0.501\ \text{numeric} \qquad (20)$$

$$(S/N)_{\text{Corr/Maximum}} = 60.2\ \text{dB-Hz} - 1.5\ \text{dB} - 60.7\ \text{dB-Hz}$$
$$= -2.0\ \text{dB} \quad \text{or} \quad 0.631\ \text{numeric} \qquad (21)$$

The numeric values computed above are referred to the value of unity, which is the normalized ($\bar{N}$) baseline level corresponding to the DC voltage due to the thermal noise only. The difference in the DC levels corresponding to the uncorrelated and the correlated signals, in conjunction with the rms values of filtered noise at the respective LPF outputs, determine the statistical performance of the PN code search process.

The normalized rms values of noise at the outputs of the respective LPFs are, as for the spatial acquisition, derived from the square-law detector theory. For the various cases of signal input conditions, the normalized rms values are defined below. The primes indicate the σ-values prior to the normalization.

Uncorrelated Signal Plus Thermal Noise

$$\sigma_1 = \frac{\sigma_1'}{\bar{N}} = \sqrt{\frac{2B_{LPF}}{B_{IF}}}\,(1 + P_s/N) \tag{22}$$

where

$$P_s/N = (C/N_0)(1/B_{IF})\,L_s\,(\text{spread spectrum}) = (S/N)_{Uncorr} \tag{23}$$

Note that P_s/N is given by equation (19) and the numeric value for this term is 0.309 for the set of conditions assumed.

Correlated Signal Plus Thermal Noise

$$\sigma_2 = \frac{\sigma_2'}{\bar{N}} = \sqrt{\frac{2B_{LPF}}{B_{IF}}}\,\sqrt{1 + 2(S/N)_{IF}} \tag{24}$$

Thermal Noise Only

$$\sigma_0 = \frac{\sigma_0'}{\bar{N}} = \sqrt{\frac{2B_{LPF}}{B_{IF}}} \tag{25}$$

Note that (25) is simply a special case of (24) for $(S/N)_{IF} = 0$.

When equations (22), (24) and (25) are used for determining the acquition time, various values of B_V are substituted for B_{LPF} and the corresponding values of acquisition times are computed. Because the acquisition detection is based on discriminating between the conditions of either an uncorrelated or a correlated signal present, it is the σ_1 and σ_2 that play the major role in determining the detection statistics. For $B_{IF} = 1.16$ MHz and $(S/N)_{IF} = -3.0$ dB, the values of σ_1 and σ_2 are

$$\sigma_1 = \sqrt{\frac{2\,B_V}{1.16\times10^6}}\,(1 + 0.309) = 0.0017\sqrt{B_V} \tag{26}$$

$$\sigma_2 = \sqrt{\frac{2\,B_V}{1.16\times10^6}}\sqrt{1+(2)(0.501)} = 0.0018\sqrt{B_V} \qquad (27)$$

The value of B_V also determines the dwell time per sample cell [4]. For a noiseless case, maximum dwell time t_s is

$$t_s = \frac{2}{B_V - 4|\Delta f_c|} \qquad (28)$$

where B_V = primary threshold circuit (Th_1) low-pass filter bandwidth

Δf_c = total code clock uncertainty due to doppler and drift. (In this report, Δf_c = 100 Hz and is due mainly to VCO residual drifts.)

From (28), the total time to search out a PN code sequence is

$$T_{ss} = t_s \times n \times N \qquad (29)$$

where n = samples per chip

N = code length (chips).

In the case considered here, a search step of $\tau/2$ (1/2 chip) is assumed, resulting in n = 2. Thus, for the code length of 1023 chips, the nN product is 2046.

Because the value of B_V determines many critical parameters of the code search and acquisition process, the values of these parameters versus B_V are given in Table 4.

Table 4. Code Search Parameters Determined by B_V (See notes for conditions)

B_V (Hz)	σ_1 (Volts)	σ_2 (Volts)(1)	t_s (msec)(2)	T_{ss} (sec)(2,3)
3000	0.093	0.100	0.77	1.57
2500	0.085	0.090	0.83	1.70
2000	0.076	0.082	1.25	2.56
1500	0.066	0.070	1.82	3.72
1000	0.054	0.058	3.33	6.75

(1) Values of σ_2 are based on C/N_0 = 60.2 dB-Hz and L_s(corr) = 2.5 dB ($\epsilon = \tau/4$).

(2) Values of t_s and T_{ss} are for a noiseless case and Δf_c = 100 Hz.

(3) Values of T_{ss} are based on code search step of $\tau/2$ and N = 1023 chips.

Using the values of σ_1 and σ_2 given by Table 4, we can determine the code search time required for 0.99 probability of detection, $T_{ss}(0.99)$, as the function of B_V. For this, we select the nominal threshold setting so that, at the $\tau/4$-chip offset, we have a detection probability of 0.9. But, because for each pass, we have two samples ($+\tau/4$ and $-\tau/4$) with this probability, the cumulative probability per pass is 0.99. Furthermore, examination of other cases, such as sampling at $\varepsilon > \tau/4$ on one side of the correlation peak and $\varepsilon < \tau/4$ on the other side indicates that the cumulative probability for two samples remains very close to 0.99 if the threshold is set for 0.90 probability of detection for $\varepsilon = \tau/4$.

Note that, so far, the probability of false alarm has not been discussed. This is because the actual probability of declaring lock and stopping search "for good" is determined by crossing of threshold Th_2. This threshold, however, as will be shown later, is associated with an extremely small probability of crossing due to noise.

In comparison, the probability of stopping search for 10 msec due to false alarm at each code phase sample is relatively high for the set of conditions under consideration. It is this false alarm probability which determines the average dwell time per cell $\bar{t}_s$. Specifically,

$$\bar{t}_s = t_s + P_a\left(T_\beta + \frac{P'_{fa}\, T_\beta}{1 - P'_{fa}}\right) \tag{30}$$

where $\bar{t}_s$ = average dwell time per cell

t_s = dwell time per cell for a noiseless case

P_a = probability of crossing threshold Th_1 per each test cell

T_β = time to test the validity of Th_1 crossing (in our case, $T_\beta = 10$ msec)

P'_{fa} = probability of false alarm crossing of Th_2 threshold.

For small values of P'_{fa} (i.e., $P'_{fa} < 10^{-2}$), equation (30) can be simplified to

$$\bar{t}_s = t_s + P_a T_\beta \ . \tag{31}$$

Consider now the method for determining $\bar{t}_s$ and $T_{ss}(0.99)$ for various values of B_V.

To keep the $P_D = 0.90$, one sets the threshold at a level $K_2\sigma_2$ below the S(corr) + $\bar{N}$ level, as shown in Figure 6. The value of $K_2 = 1.27$ for $P_D = 0.90$. Therefore, the magnitude of K_1 is

$$K_1 = \frac{\Delta S - K_2\sigma_2}{\sigma_1} \tag{32}$$

or

$$K_1 = \frac{(S/N)_{Corr} - (S/N)_{Unc} - K_2\sigma_2}{\sigma_1} \tag{33}$$

Once the value of K_1 is known, the magnitude of P_a can be determined by consulting the appropriate error function curves [6].

As a numerical example, consider the case when $B_V = 2500$ Hz. From equations (19) and (20) and Table 4, one obtains the appropriate values and solves for K_1. Thus,

$$K_1(2500) = \frac{0.501 - 0.309 - (1.27)(0.090)}{0.085}$$

$$= \frac{0.192 - 0.114}{0.085} = \frac{0.078}{0.085} = 0.914 \; . \tag{34}$$

This value of K_1 correpsonds to $P_a = 0.17$ or 17% of false Th_1 crossing at each sample. The corresponding $\bar{t}_s$ is

$$\bar{t}_s(2500) = t_s + P_a T_\beta$$

$$= 0.83 \times 10^{-3} + (0.17)(10^{-2})$$

$$= 0.83 \times 10^{-3} + 1.70 \times 10^{-3})$$

$$= 2.53 \times 10^{-3} \quad \text{or} \quad 2.53 \text{ msec} \; . \tag{35}$$

Note that the relatively high value of P_a ($P_a > 0.01$) contributes significantly to the lengthening of $\bar{t}_s$. Finally, the total time $T_{ss}(0.99)$ is computed:

$$T_{ss}(0.99) = \bar{t}_s(2500) \times n \times N$$

$$= (2.53)(10^{-3})(2)(1023) = \underline{5.18 \text{ sec}}. \tag{36}$$

By repeating this procedure for other values of B_V, the corresponding values of $T_{ss}(0.99)$ were obtained. Figure 7 shows the plot of $T_{ss}(0.99)$ versus B_V. From this plot, it is evident that a broad minimum

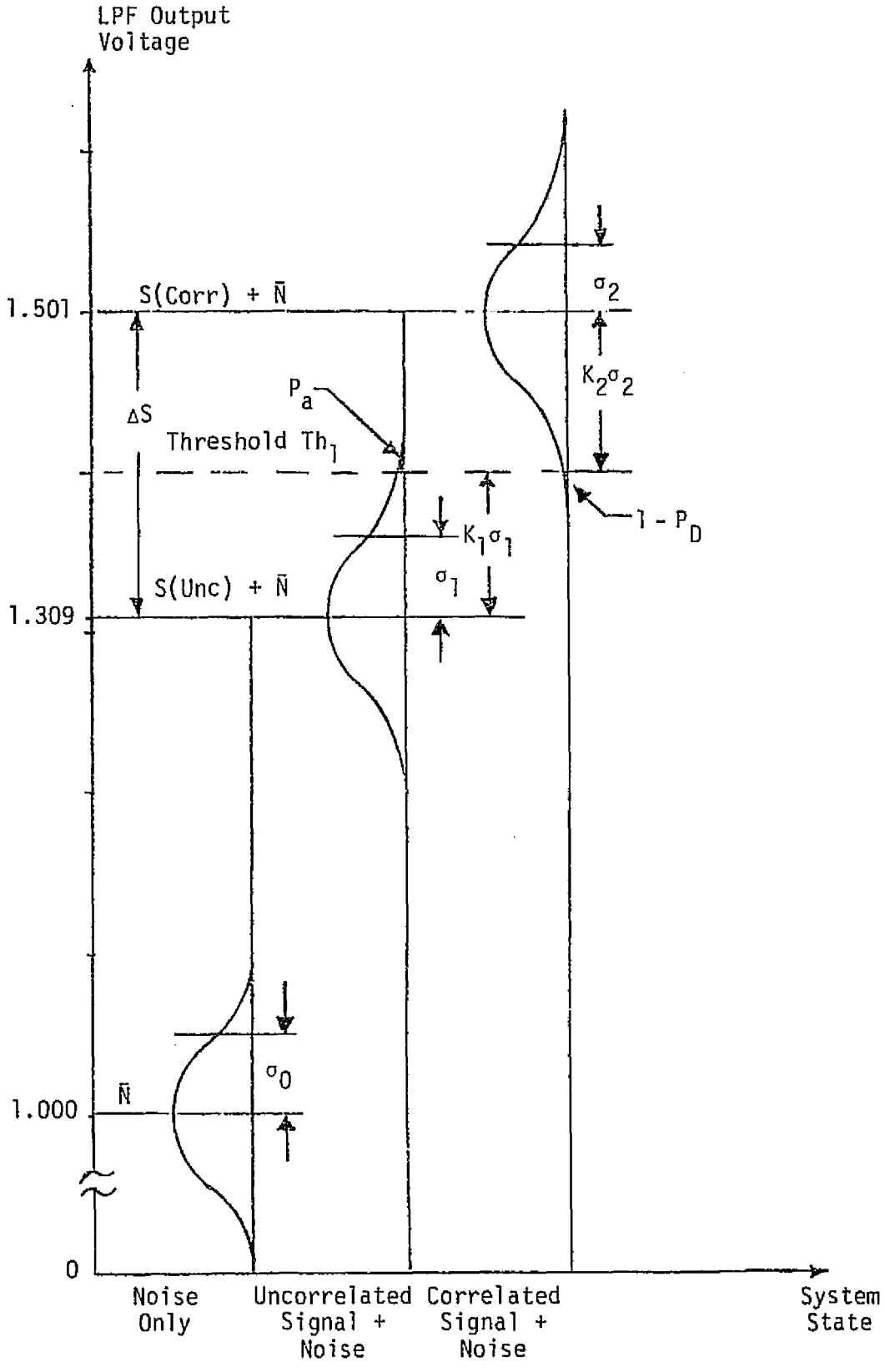

Figure 6. Primary Threshold (Th_1) Setting for C/N_0 = 60.2 dB-Hz

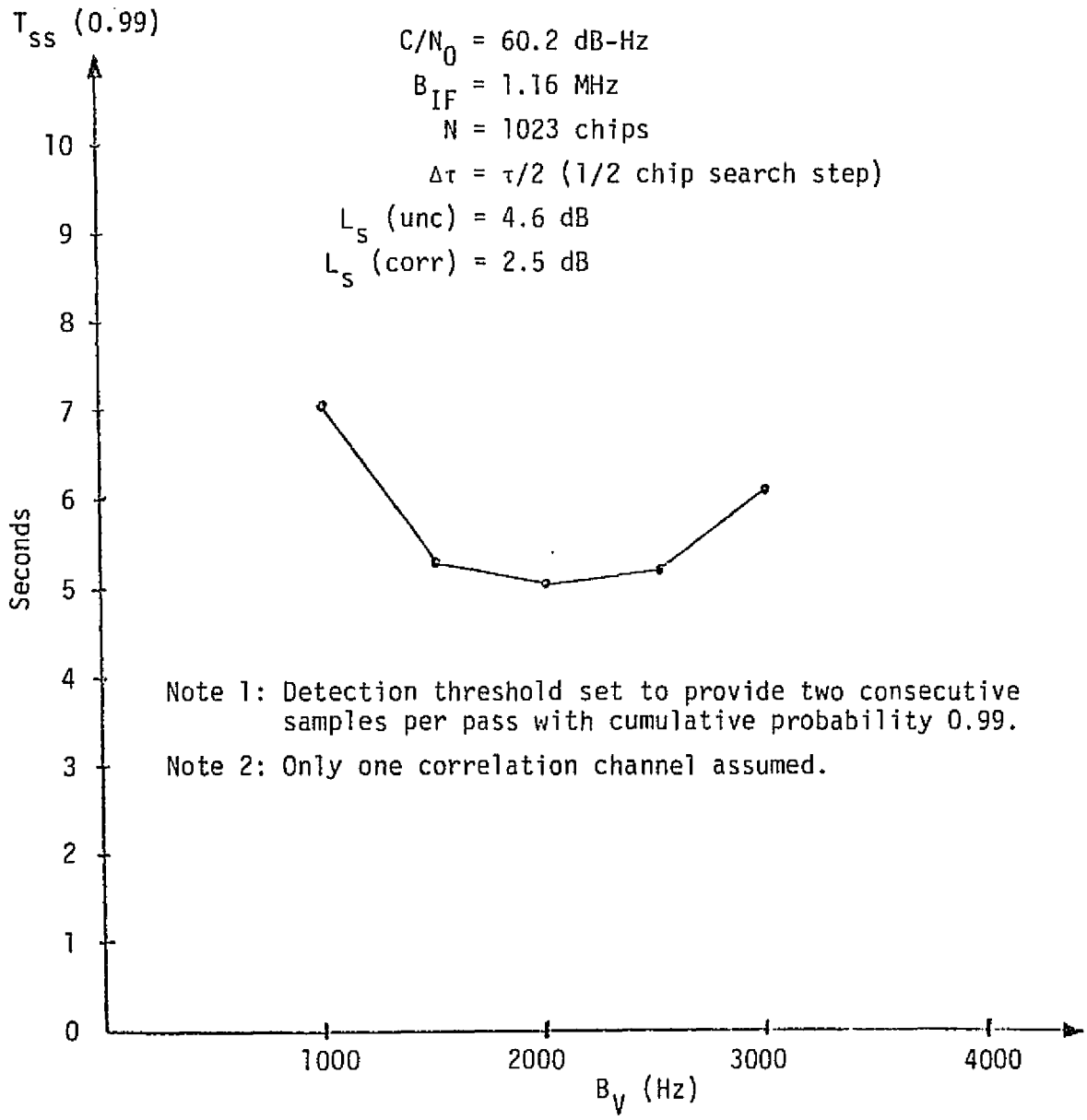

Figure 7. PN Code Search Time Versus Post-Detection LPF Bandwidth B_V

for $T_{ss}(0.99)$ values lies in the region of B_V from 1500 Hz to 2500 Hz. It must be emphasized, however, that the plot shown pertains only to the set of conditions indicated and $C/N_0 = 60.2$ dB. Other sets of conditions would result in different relationships between B_V and T_{ss}. It must also be pointed out that the plot in Figure 7 is based on a threshold setting commensurate with two samples contributing to the cumulative probability of PN sync detection per pass of 0.99. Furthermore, the acquisition times indicated are below the 10 seconds value given by the equipment specification [1]. The PN code acquisition time of 8 seconds would therefore be a reasonable value to assume as a revised goal. Requiring PN code acquisition times less than 8 seconds is not warranted, however, in view of the fact that practically no threshold tolerance (or margin) is available at C/N_0 of 60.2 dB-Hz. Furthermore, because of acquisition time optimization at C/N_0 of 60.2 dB-Hz, there may not be a marked decrease in acquisition time as the C/N_0 increases. This is due to an assumption that threshold Th_1 is set for constant false alarm rate with respect to the level of the uncorrelated signal plus noise. Therefore, unless other threshold setting criteria are used, the acquisition time will not decrease appreciably with increased C/N_0.

2.2.2.3 Acquisition Decision and Hold-On Performance

So far only the initial sync detection statistics, i.e., crossing of threshold Th_1 and holding the search for 10 msec, have been discussed. We will now consider the statistics associated with crossing the secondary threshold Th_2. As stated previously, threshold Th_2 is crossed only if the crossing of Th_1 is due to true correlation and not due to noise pulse.

Assuming that the bandwidth of the low-pass filter b_v is 100 Hz (commensurate with 10 msec averaging time), the corresponding σ-values are found from equations (26) and (27) by replacing B_V with b_v. Thus,

$$\text{Uncorrelated:} \quad \sigma_1' = 0.0017\sqrt{b_1} = 0.0017\sqrt{100} = 0.017 \text{ volts} \qquad (37)$$

$$\text{Correlated:} \quad \sigma_2' = 0.0018\sqrt{b_1} = 0.0018\sqrt{100} = 0.018 \text{ volts.} \qquad (38)$$

The number of sigmas available in the DC change ΔS of 0.192 volts is then, at least,

$$n_\sigma = \frac{\Delta S}{\sigma_2'} = \frac{0.192}{0.018} \cong 10.7 . \quad (39)$$

Consequently, meeting the detection probability far in excess of 0.99 probabilities of the Th_1 circuit is not difficult and the driving factor in setting the Th_2 threshold should be the false alarm probability.

Because the original (A-version) of the specification [1] for the Ku-band communication/radar equipment states only that the false alarm probability of code acquisition be 10^{-6}, we propose that this P_{fa} value be applied to the maximum allowable code acquisition time of 10 sec. If this is the case, we can solve for the setting of Th_2 based on $b_V = 100$ Hz. The relationship between P'_{fa}, i.e., probability of crossing Th_2 and the total false alarm probability P_a for the 10-second period is

$$P_{fa} = n_d \times P'_{fa} = 10^{-6} \quad (40)$$

where P_{fa} = false alarm probability (of lock decision) in 10-sec interval

P'_{fa} = false alarm probability of crossing Th_2

n_d = number of dwells in 10 seconds.

Solving (36) for P'_{fa}:

$$P'_{fa} = \frac{10^{-6}}{n_d} = \frac{10^{-6}}{(2)(100)(10)} = 0.5 \times 10^{-9} . \quad (41)$$

This corresponds to a threshold setting of 6.1 σ'_1, or 0.104 volts above the S(unc) + Noise value of 1.309 volts. If the threshold Th_2 is set exactly at this value, i.e., 1.413 volts, the distance from the correlated value (at 2.5 dB down) is

$$K'_2 = \frac{1.501 - 1.413}{\sigma_2'} = \frac{0.088}{0.018} = 4.9 . \quad (42)$$

This corresponds to a detection probability of well over 0.999999.

The next problem to consider is the tracking threshold for the PN code loop. Based on a PN tracking noise loop bandwidth (two-sided) of 500 Hz, the loop SNR at approximately 60 dB-Hz is

$$\begin{aligned} \text{PN Loop SNR} &= 60 \text{ dB-Hz} - 10 \log 2B_L \\ &= 60 - 10 \log (500) \\ &= 60 - 27 = 33 \text{ dB} . \end{aligned} \quad (43)$$

Thus, it is evident that the SNR in the PN code tracking loop is not a thresholding factor—even at C/N_0 as low as 50 dB-Hz, this SNR is still 23 dB! A decrease in C/N_0, however, does affect the hold-in capability of the secondary threshold circuit. Therefore, the setting of Th_2 must be lowered after acquisition to prevent re-activation of the PN code search mode.

A reasonable threshold to define would be about 57 dB-Hz. The criterion for lower setting of Th_2 would then be to provide a probability of 0.99 of staying in lock during a 100 minute communication interval. In this case, "staying in lock" implies not resuming the code search due to a spurious false alarm. Based on this criterion, the lower setting of Th_2, i.e., Th_3, can be computed. Thus, at $C/N_0 = 57$ dB-Hz:

$$(S/N)_{IF\ Corr} = 57\ \text{dB-Hz} - L_s(\text{corr}) - 10 \log B_{IF}$$
$$= 57 - 1.5 - 60.7 = -5.2 \qquad (44)$$
$$\text{or}\quad 0.302 \text{ numeric} .$$

Note that we are using 1.5 dB correlation loss for this calculation because it is valid to assume that the PN tracking loop has positioned the punctual correlator at its optimum position. The standard deviation in $b_V = 100$ Hz at 57 dB-Hz is

$$\sigma_2'' = \sqrt{\frac{2b_V}{B_{IF}}}\sqrt{1 + 2(S/N)_{IF}}$$
$$= \sqrt{\frac{(2)(100)}{1.16\times10^6}}\sqrt{1 + (2)(0.302)}$$
$$= 0.0166 \text{ volts} . \qquad (45)$$

For 0.99 probability of staying in lock for 100 minutes, the probability of unlocking is 0.01. In other words,

$$P_{UL} = n_s \times P'_{UL} = 0.01 \qquad (46)$$

where P_{UL} = probability of unlocking (resuming search)

P'_{UL} = probability of crossing Th_2' in the downward direction

n_s = number of independent samples in $b_V = 100$ Hz over 100-minute interval.

Solving (46) for P'_{UL}:

$$P'_{UL} = \frac{0.01}{(2)(100)(60)(100)} = 8.33 \times 10^{-9} \approx 10^{-8} \qquad (47)$$

The probability of 10^{-8} corresponds to 5.6 σ''_2. Therefore, the numerical value of the Th'_2 setting is

$$Th_3 = S(corr) + \bar{N} - 5.6\,\sigma''_2$$

$$= 1.302 - (5.6)(0.0166) = 1.302 - 0.093$$

$$= 1.209 \text{ volts} \qquad (48)$$

Figure 8 shows the settings of Th_2 and Th_3 for the case of initial acquisition and subsequent tracking, respectively. As can be seen from Figure 8, the setting of Th_3 is below the level of the uncorrelated signal-plus-noise for the case of $C/N_0 = 60.2$ dB-Hz. It is for this reason that the switch-over to Th_3 is performed after the carrier acquisition. In this manner, the code search can be resumed if the code sync is lost, and the problem of the decision circuit being latched by an uncorrelated PN signal in the "no search" state is eliminated.

2.2.3 Carrier Acquisition

Following the completion of the PN code search, the carrier acquisition takes place. For carrier acquisition, the Costas loop demodulator's VCO frequency is swept over the residual carrier uncertainty range which, for the case under consideration, is ±150 kHz. Thus, the total range over which the VCO is swept is about 300 kHz.

Not considering the effect of the low-pass filters within the I and Q arms of the Costas loop, the signal-to-noise ratio in the loop, SNR_L, is related to system input C/N_0 in the following manner:

$$SNR_L = \frac{1}{4 B_L (N_0/C) L_s} \cdot \frac{1}{\left[1 + (N_0/C) L_s W K_L\right]} \qquad (49)$$

where B_L = loop noise bandwidth, one-sided

W = low-pass (arm) filter noise bandwidth

L_s = signal loss between system input and Costas demodulator

C/N_0 = carrier-to-noise ratio at system input

K_L = factor determined by filter type.

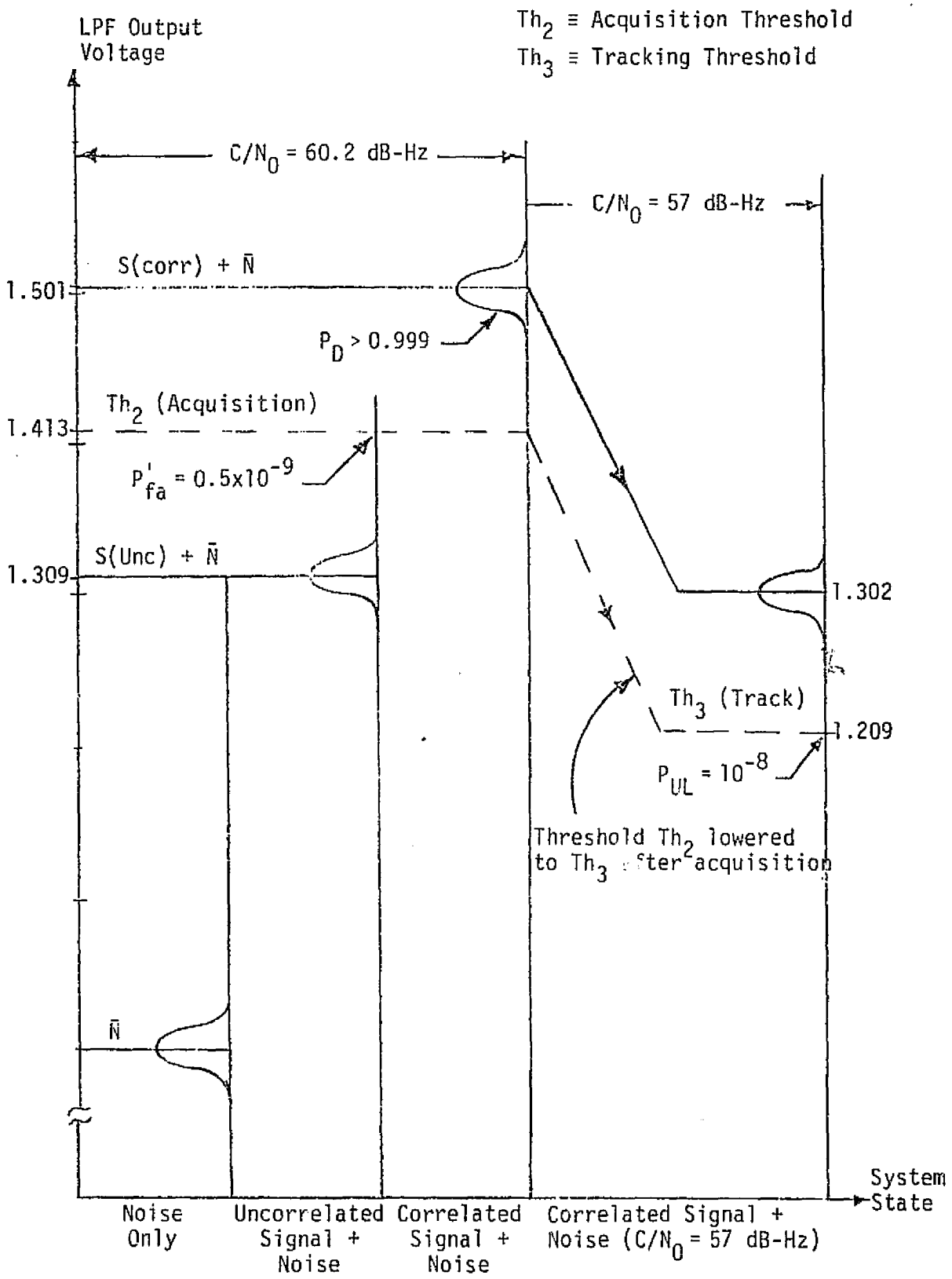

Figure 8. Acquisition (Th_2) and Tracking (Th_3) Threshold Settings

For an ideal low-pass filter, $K_L = 1$ in equation (49), but for an n-pole Butterworth filter, $K_L = (2n-1)/2n$.

Assuming that the low-pass filters single-pole RC circuits with 3 dB cutoff at 436 kHz, or twice the data rate, the noise bandwidth of these filters, W, is

$$W = \pi/2 \times f_c(3\ \text{dB}) = \pi/2 \times 436\ \text{kHz} = 678.8\ \text{kHz} . \quad (50)$$

Figure 9 shows the plot of SNR_L versus the C/N_0 at the input to the PN despreader. Curve 1 is the direct plot of equation (49) for which the following values were assumed:

B_L = 2500 Hz

W = 678.8 kHz

K_L = 1/2

L_s = 1.5 dB (correlation loss).

Because equation (49) takes into account only a squaring loss, curve 2 was added to show the degradation which results from the finite bandwidth of the arm filters. The corrections required for generating Curve 2 from Curve 1 were obtained from Figure 3 in [7].

The results of SNR_L values shown in Figure 9 indicate that reliable acquisition can be obtained at C/N_0 of about 60 dB-Hz. Specifically, at $C/N_0 = 60.2$ dB-Hz, loop SNR is 15.9 dB, i.e., a ratio of 38.9 according to Curve 2. The maximum sweep rate commensurate with this loop SNR can now be obtained from a modified (and simplified) version of equation (4-33) in [8]. Thus, for $\zeta = 0.707$,

$$\dot{\Delta f}_{max} \cong 0.566 \left(1 - \frac{1}{\sqrt{SNR_L}}\right) B_L^2 \ \text{Hz/sec}$$

$$\cong 0.566 \left(1 - \frac{1}{\sqrt{38.9}}\right) (2500)^2$$

$$\cong 2.97 \times 10^6 \ \text{Hz/sec} . \quad (51)$$

When the loop acquires at the sweep rate indicated above, the tracking stress error will be

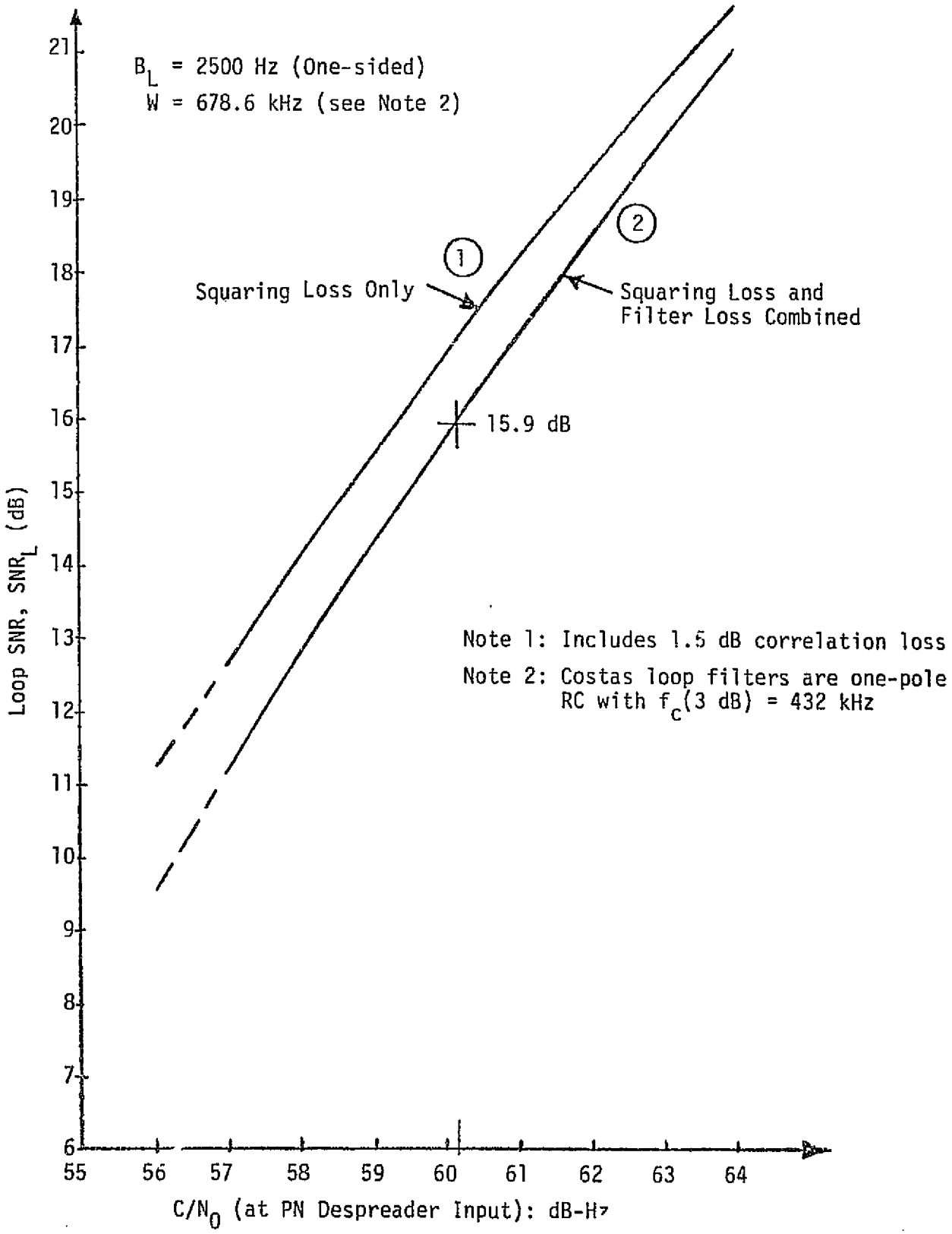

Figure 9. Carrier Acquisition (Costas) Loop SNR vs. C/N_0 Ratio at PN Despreader Input

$$\theta_a = 1.77 \frac{\dot{\Delta f}_{max}}{B_L^2} \text{ radians}$$

$$= \frac{(1.77)(2.97)\,10^6}{(2500)^2} = 0.84 \text{ radians} . \qquad (52)$$

To reduce the tracking error stress during acquisition and to improve probability of acquisition, the sweep rate should be decreased by a factor of at least 2, or preferably, by 4. Consequently, for $\Delta f_c = 300$ kHz,

$$T_{acq}(\text{carrier}) \cong \frac{4\ \Delta f_c}{\dot{\Delta f}_{max}} = \frac{(4)(300)(10^3)}{2.97 \times 10^6}$$

$$= 0.404 \text{ seconds.} \qquad (53)$$

With the sweep rate reduced by a factor of 4, the tracking error prior to stopping of the sweep is reduced to less than 0.25 radians for a B_L = 2500 Hz loop. Furthermore, because of relatively high SNR_L at $C/N_0 \approx 60$ dB-Hz, trade-off can be carried out if necessary between B_L, θ_a, and carrier acquisition time. It may also be noted that, because of relatively high SNR_L at C/N_0 of 60.2 dB-Hz, the acquisition time is not likely to be shortened at increased values of C/N_0 although the cumulative probability of lock per pass will increase.

2.2.4 Bit and Frame Synchronization

The performance of the bit and frame synchronization subunits is difficult to predict analytically and, therefore, empirically derived data must be relied upon. Of specific interest is the bit synchronizer performance described in [9]. According to that reference, mean acquisition times of less than 0.7 seconds are obtained at E_b/N_0 values as low as 0 dB. Referring to the data rate of 216 kbps, the corresponding C/N_0 is

$$C/N_0 \text{ dB-Hz} = 10 \log (216 \times 10^3) - 0 \text{ dB}$$

$$= 53.3 \text{ dB-Hz} . \qquad (54)$$

This means that bit sync acquisition time of 1 sec at $C/N_0 = 60.2$ dB-Hz can be easily achieved with at least a 6 dB margin.

No exact data on frame sychronization time is available, except for a statement in [9], most likely based on empirical data, that average frame synchronization time is less than 10 msec. Because it is also stated in [9] that total time for bit and frame acquisition is approximately 0.5 seconds at 0 dB of E_b/N_0, we conclude that 1.0 sec combined bit and frame sync acquisition at $C/N_0 = 60.2$ dB-Hz is quite realistic and does not impose unnecessary complexity requirements on the Ku-band equipment design.

2.3 TRACKING THRESHOLD PERFORMANCE

In the preceding section, the acquisition performance of the various subunits was considered at C/N_0 of about 60 dB-Hz. It was shown that reasonable acquisition performance can be obtained at the nominal C/N_0 value of 60.2 dB-Hz. The tracking threshold performance will now be considered.

2.3.1 Angle Tracking Threshold

Angle tracking threshold can be defined as that value of C/N_0 at which the angle tracking loops (1) either break lock or (2) the angle noise in these loops becomes sufficiently high so as to degrade significantly the BER performance. Thus, by examining the behavior of the rms angle tracking error as a function of C/N_0, the threshold performance of the angle tracking loops can be defined. Although there are two tracking loops in the system under consideration, one for the Az axis and one for the El axis, examination of the angle tracking error in either one of these loops is indicative of the angle tracking threshold performance.

An expression for the square of the angle tracking error can be obtained by modifying the equation on page 3-37 of [3] into a more directly useable form:

$$\sigma_a^2 = \frac{4\beta^2 B_s A}{K_m^2 \left(\frac{C}{N_0 D}\right)} \times \frac{1 + \frac{B_{IF}}{2\left(\frac{C}{N_0 L_t}\right)}}{1 - \frac{2B_s}{\left(\frac{C}{N_0 D}\right)}} \qquad (55)$$

where σ_a = rms value of angle tracking error

β = antenna 3 dB beamwidth (1.6°)

B_s = angle servo loop noise bandwidth (1.0 Hz)

K_m = antenna tracking slope coefficient (ranges from 0.5 to 1.0. Use 0.5)

A = coupling factor for the monopulse channel (assumed at 2 dB, or 1.585 numeric)

D = effective increase in thermal noise N_0 due to coupling of noise from Δ channel (assume D = 2.1 dB or 1.622 numeric)

B_{IF} = IF bandwidth of the angle tracking channel (B_{IF} = 30 MHz)

C/N_0 = carrier-to-noise ratio (dB-Hz) at receiver input.

Substituting the values indicated into equation (55), one obtains the relationship between σ_a and C/N_0. Figure 10 shows this relationship. From Figure 10, it is evident that, if the criterion for threshold is $\sigma_a \leq 0.2°$, the tracking threshold, based on the thermal noise alone is at about 54 dB.

On the other hand, if we consider the requirement for the antenna pointing loss not to exceed 0.3 dB, with probability of 0.99 over the average interval of one minute, the "threshold" criteria is different. Specifically, the pointing angle error which results in 0.3 dB loss is given by

$$\theta = \sqrt{\frac{M\,\beta^2}{12}} \qquad (56)$$

where M = pointing loss in dB (0.3 dB)

β = antenna 3 dB beamwidth (1.6°)

θ = pointing error resulting in loss of M dB.

Substituting the appropriate values in (52) and solving for θ, one obtains

$$\theta\ (\Delta G = 0.3\ \text{dB}) = \sqrt{\frac{0.3(1.6)^2}{12}} = 0.253°. \qquad (57)$$

Now, with the 1 Hz servo loop noise bandwidth, the number of independent samples within a 1-minute interval is 120. Thus, the probability of <u>not</u> exceeding 0.253° is

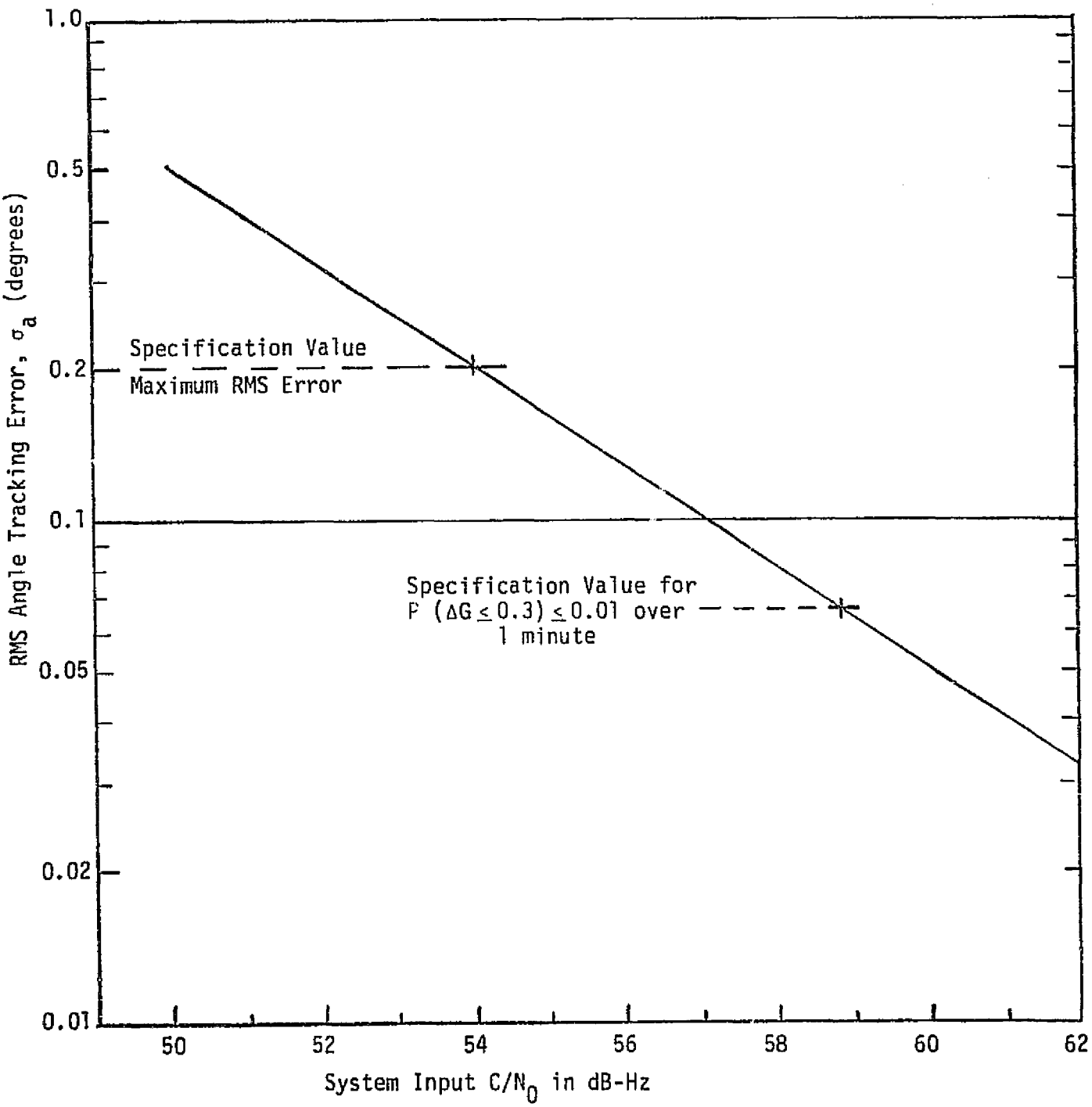

Figure 10. RMS Angle Tracking Error Versus C/N$_0$

$$P\ (\theta \leq 0.253°) \ = \ (1 - P_s)^{120} \ = \ 0.99 \qquad (58)$$

where P_s is the probability of the angle error exceeding 0.253° during any one of the 120 independent subintervals of the 1-minute averaging period. Solving (58) for P_s, one obtains

$$P_s \ = \ 1.0 - (0.99)^{1/120} \ \cong \ 8.4 \times 10^{-5} \qquad (59)$$

which corresponds to 3.75 σ_a. Therefore, solving for σ_a, one obtains

$$\sigma_a \ = \ \frac{0.253°}{3.75} \ = \ 0.067° \ . \qquad (60)$$

According to Figure 10, this value of σ_a corresponds to $C/N_0 = 58.9$ dB-Hz. This is a relatively high threshold compared to the 54 dB-Hz commensurate with $\sigma_a = 0.2°$. On the other hand, because of the low slope of the BER curve in the 10^{-2} region and below, the 0.3 dB gain loss due to pointing error does not appear to be a significant threat. Considering that the $\sigma_a \leq 0.2°$ is the threshold-determining factor, the pointing loss corresponding to this σ_a is

$$M\ (dB) \ = \ \frac{12\,\sigma_a^2}{\beta^2} \ = \ \frac{(12)(0.2)^2}{(1.6)^2} \ = \ 0.19 \text{ dB} \ . \qquad (61)$$

This loss should result in only a negligible degradation in threshold performance of all of the subunits. Consequently, the 54 dB-Hz value may be considered as the limiting value for the angle tracking threshold.

2.3.2 PN Unlock Threshold

The PN tracking threshold has been discussed in detail in section 2.2.2.3. As stated there, the secondary threshold Th_3 is lowered to insure that PN search mechanism is not initiated within 100 minutes at C/N_0 = 57 dB-Hz. The corresponding probability of staying in lock is set at 0.99. These considerations suggest that 57 dB-Hz be adopted as the threshold value for the PN tracking, although this limitation is arbitrarily imposed in view of the fact the code tracking loop may still be functioning below the 57 dB-Hz value.

2.3.3 Carrier Tracking Threshold

The logical criterion for establishing the carrier tracking threshold is to determine the C/N_0 value at which the mean time for the carrier loop to unlock is 100 minutes. In terms of loop parameters, this time is given by

$$\bar{T} = \frac{\pi}{4B_L} e^{1.5\rho} \tag{62}$$

where $\bar{T}$ = mean time to unlock

B_L = carrier loop noise bandwidth (one-sided)

ρ = loop signal-to-noise ratio (SNR_L) .

Substituting the appropriate values into (62) and solving for ρ, one obtains

$$\frac{(60)(100)(4)(2500)}{\pi} = e^{1.5\rho} \tag{63}$$

$$1.91 \times 10^7 = e^{1.5\rho}$$

$$16.8 = 1.5\rho$$

or

$$\rho = 11.2 \text{ or } 10.5 \text{ dB} .$$

Extrapolation of Curve 2 in Figure 9 indicates that, for B_L = 2500 Hz, the SNR_L of 10.5 dB corresponds to C/N_0 of about 56.5 dB-Hz. Consequently, C/N_0 of 57 dB-Hz may be considered as a conservative threshold value for the carrier tracking loop.

2.3.4 Bit Synchronizer Threshold

The bit synchronizer threshold, according to Table 5-5 in [9] is at about E_b/N_0 of -5 dB. For 216 kbps data rate, this corresponds to

$$C/N_0 \text{ dB-Hz} = 53.3 \text{ dB-Hz} - 5 \text{ dB}$$

$$= 48.3 \text{ dB-Hz} . \tag{64}$$

Thus, it appears that the bit synchronizer threshold is not the limitation on any of the other system subunits.

3.0 CONCLUSIONS AND RECOMMENDATIONS

The summary of the acquisition and tracking threshold performance estimates for the Shuttle Ku-band receiver is given in Table 5. From these estimates, it is evident that the requirement to acquire at C/N_0 = 60.2 dB does not violate any of the parameters included in the procurement specification [1]. Moreover, because the estimates in Table 5 are derived from a rather basic, simple system configuration, it is recommended that these estimates be used as guidelines for the Ku-band forward link performance. In this manner, any improvements in system configuration should result in a better performance.

Table 5. Summary of Acquisition and Tracking Threshold Performance for the Shuttle Ku-Band Communication Receiver Subunits (Forward Link)

Subunit	Acquisition		Tracking	
	Estimated Acquisition Time at C/N_0 = 60.2 dB-Hz	Aquisition Performance Limitation	Tracking Threshold C/N_0	Tracking Threshold Limitation or Driving Factor
Angle Search and Track	55 sec	Maximum gimbal rate of 120°/sec	54 dB-Hz	RMS angle track error of 0.2°
PN Code Search and Acquisition f_c = 3.03 Mcps N = 1023 bits	5-8 sec	1) SNR 2) Code clock uncertainty of 100 Hz due to receiver VCO	57 dB-Hz	Time to remain within lock for 100 minutes and P_{lock} = 0.99
Carrier Search and Lock	$\leq$ 0.5 sec	1) Probability of acquisition 0.9 or better 2) B_L of 2500 Hz	57 dB-Hz	Mean time to unlock of 100 minutes
Bit sync	1 sec	SNR	48.3 dB-Hz	SNR
Frame Sync	10 msec	SNR	Limited by bit sync threshold	SNR

REFERENCES

1. "Procurement Specification MC409-0025, Ku-Band Integrated Radar and Communications Equipment," Volume II, Space Division, Rockwell International, March 15, 1976.

2. S. Udalov, "Signal Detection and Angular Search Procedure for Shuttle Ku-Band Communication System," Axiomatix Report No. R7410-2 (under NASA Contract NAS 9-13467), October 2, 1974.

3. "Proposal for Ku-Band Integrated Radar and Communication Equipment for the Space Shuttle Orbiter Vehicle," Volume II, Hughes Aircraft Company, Ref. No. D7768/SCG60176P, May 1976.

4. "Space Shuttle Ku-Band Integrated Rendezvous Radar/Communications System Study," Hughes Aircraft Company Report No. D4148 SCG60041R, for NASA-JSC under Contract NAS 9-14595, March 1976.

5. "Ku-Band Integrated Radar and Communication Equipment for the Space Shuttle Orbiter Vehicle," Conceptual Design Review Booklet, Hughes Aircraft Company Ref. No. D7768/SCG66722V, January 18-20, 1977.

6. J. V. DiFranco and W. L. Rubin. Radar Detection. New Jersey: Prentice-Hall, Inc., 1968, pp. 368-369.

7. M. K. Simon and W. C. Lindsey, "Optimum Performance of Costas Type Receivers," Axiomatix Report No. R7502-1, February 18, 1975.

8. F. Gardner. Phaselock Techniques. New York: John Wiley & Sons, Inc., 1966, p. 49.

9. "Signal Design Study for Shuttle/TDRSS Ku-Band Uplink," Final Report, TRW Report No. 29210, CDRL No. 2, for NASA-JSC under Contract No. NAS 9-14842, August 1976.

APPENDIX B

STEADY STATE PERFORMANCE OF DELAY LOCK LOOPS

STEADY STATE PERFORMANCE OF DELAY LOCK LOOPS

by

Waddah Alem

In this appendix, an expression is derived for the normalized mean square tracking error in a delay lock loop (DLL). To generalize all previous analysis of the DLL, the loop is assumed to have an arbitrary correlator spacing with an envelope detector implementation for noncoherent PN tracking. The results apply when the period of the PN sequence being tracked is large. The bandlimiting effects of the bandpass arm filters are considered in Appendix C. The receiver front end filter is assumed wide enough to pass the PN code without any effect on its correlation function.

The delay lock loop under consideration is shown in Figure 1. The received signal is assumed to consist of a signal component and a bandlimited white Gaussian noise component $n_i(t)$ with the two-sided spectral density of $N_0/2$. The signal component is

$$\sqrt{2P_s}\, s(t-T) \cos(\omega_0 t + \phi)$$

where $s(t)$ is a PN code with a long period and ∓ 1 amplitude, P_s is the average signal power, ω_0 is the carrier frequency including any doppler, T is the signal transmission delay, and ϕ is a random phase uniformly distributed between 0 and 2π.

The received signal is multiplied at the phase detector with a delayed and an advanced replica of the signal component. The amount of correlator spacing is assumed to be $\mp\Delta/N$, where Δ is the chip time and N is any number larger than or equal to 2.

The outputs of the phase detectors assume the form

$$y_{12} = \sqrt{2P_s}\, s(t-T)\, s\left(t-\hat{T}\pm\frac{\Delta}{N}\right) \cos(\omega_0 t + \phi) + \text{Noise} \qquad (1)$$

where $\hat{T}$ is the estimated propagation delay. The delay error is denoted by $\varepsilon = T - \hat{T}$. In the analysis, the error is assumed to be in the region $|\varepsilon| < \Delta/N$.

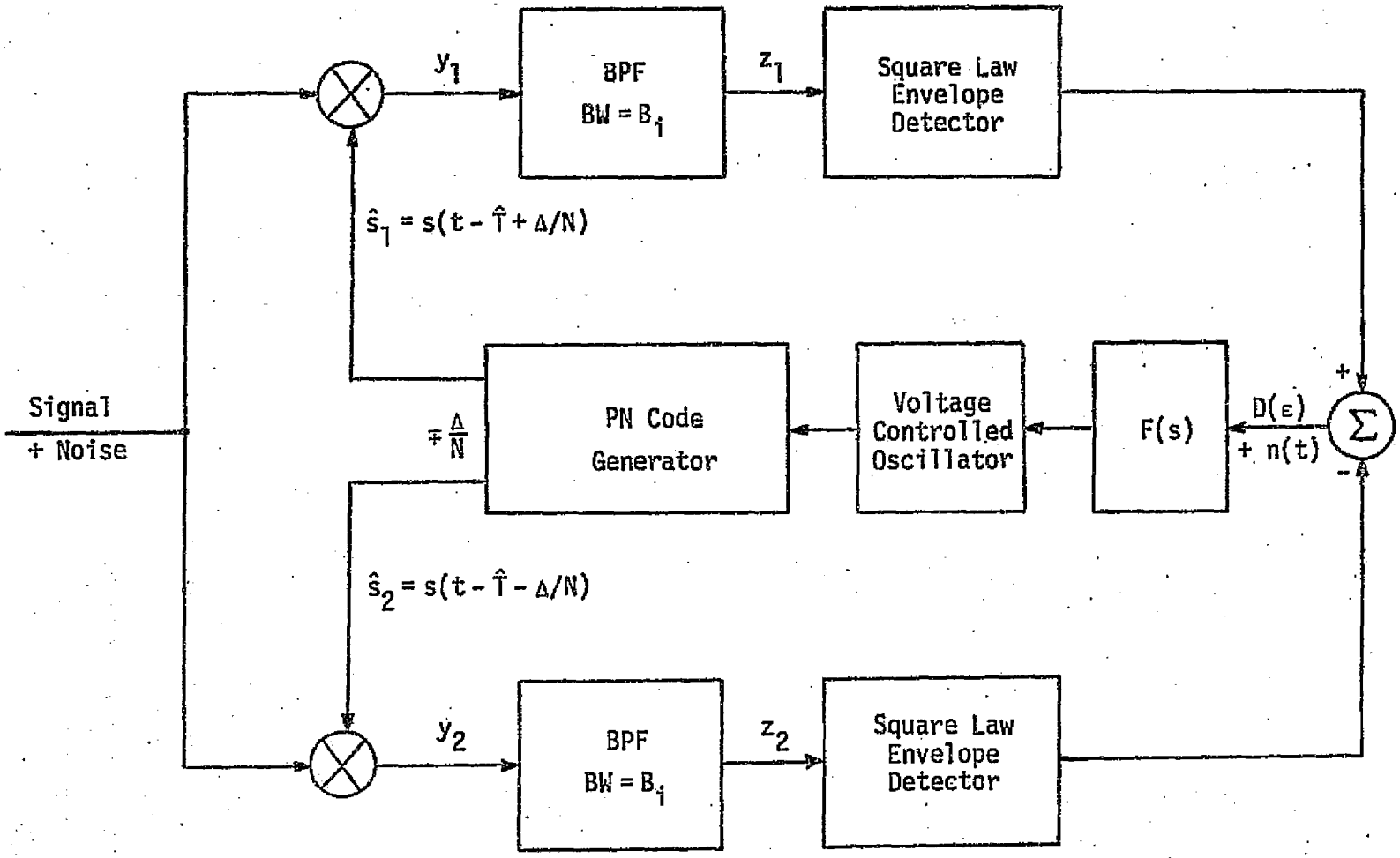

Figure 1. Block Diagram of the Delay Lock Loop

It is assumed that the bandwidth of the arm filters is symmetrically located around $f_0 = \omega_0/2\pi$ and that the bandwidth of these filters is wide enough to pass any data with negligible distortion. In addition, the PN code self-noise effect on the loop performance can be neglected in most cases of interest when the single-sided loop bandwidth is small compared to the chip rate of the PN code. Hence, the outputs of the bandpass filters can be written as

$$z_{12} = \sqrt{2P_s}\,(1 - \frac{1}{N} \mp \frac{\varepsilon}{\Delta}) \cos(\omega_0 t + \phi) + \text{Noise} \tag{2}$$

or, alternately,

$$z_i = S_{zi} + n_{zi}\,, \qquad i = 1,2 \tag{3}$$

where

$$S_{z_{12}} = \sqrt{2P_s}\,(1 - \frac{1}{N} \mp \frac{\varepsilon}{\Delta}) \cos(\omega_0 t + \phi)\,.$$

The square law detectors are used because the loop is supposed to track the PN code noncoherently, which is the case of interest when tracking is required without carrier synchronization. The outputs of the square law detectors assume the form

$$z_{12}^2 = S_{z12}^2 + 2S_{z12} \cdot n_{z12} + n_{z12}^2\,. \tag{4}$$

The signal part of (4) is S_{z12}^2, while $n_e(t) = (2S_{z12} \cdot n_{z12} + n_{z12}^2)$ constitutes the noise component. Hence,

$$S_{z12}^2 = (1 - \frac{1}{N} \mp \frac{\varepsilon}{\Delta})^2 P_s + \text{harmonics filtered by loop filter } (F(p/p_0))\,. \tag{5}$$

The signal part of the output of the difference circuit is $D(\varepsilon) = S_{z1}^2 - S_{z2}^2$. In the region where $|\varepsilon| \leq \Delta/N$, $D(\varepsilon)$ is a linear function of ε, given by

$$D(\varepsilon) = P_s \frac{4(N-1)}{N} \frac{\varepsilon}{\Delta} = k P_s (\frac{\varepsilon}{\Delta}) \tag{6}$$

where $K \triangleq \frac{4(N-1)}{N}$.

The normalized delay estimate is then given by

$$\frac{\hat{T}}{\Delta} = g_f F(s/\omega_n)\, g_c [D(\epsilon) + n_e(t)]/s \tag{7}$$

where g_f = gain of the loop filter

g_c = gain of the VCO

$F(s)$ = transfer function of the loop filter

ω_n = loop natural frequency.

Defining the open loop gain as

$$G = k P_s\, g_f\, g_c / p_0 ,$$

equation (7) becomes

$$\frac{\hat{T}}{\Delta} = G \frac{F(s/\omega_n)}{(s/\omega_n)} \left[\frac{\epsilon}{\Delta} + n_e(t)/(k P_s)\right]$$

or

$$\frac{\hat{T}}{\Delta} = H(s/\omega_n) \left[\frac{\epsilon}{\Delta} + n_e(t)/(k P_s)\right] \tag{8}$$

where the linearized closed loop transfer function $H(s)$ is defined as

$$H(s) = \frac{G F(s)}{s + G F(s)} . \tag{9}$$

For a second-order loop,

$$H(s/\omega_n) = \frac{1 + 2\zeta s/\omega_n}{(s/\omega_n)^2 + (2\zeta/\omega_n)s + 1} . \tag{10}$$

For a critically damped loop, the damping factor (ζ) is equal to $\sqrt{2}/2$; hence,

$$H(s/\omega_n) = \frac{1 + \sqrt{2}\, s/\omega_n}{1 + \sqrt{2}\,(s/\omega_n) + (s/\omega_n)^2} .$$

Using (10) and (8), the normalized mean square tracking error is given as

$$\sigma_T^2 = \frac{1}{(k P_s)^2} \int_{-\infty}^{\infty} S_{ne}(f)\, |H(f/f_n)|^2 \, df , \tag{11}$$

where $S_{ne}(\omega)$ is the noise power spectral density of $n_e(t)$. Defining the loop equivalent noise bandwidth B_L as

$$B_L = \int_0^\infty |H(f/f_n)|^2 \, df \, . \tag{12}$$

For the linearized loop filter in (10), the equivalent noise bandwidth becomes

$$B_L = \frac{\omega_n}{8\zeta}(1 + 4\zeta^2)$$

which, for a critically damped loop ($\zeta = \sqrt{2}/2$), is equal to

$$B_L = \frac{3}{4\sqrt{2}}\omega_n = 0.5303\ \omega_n \, . \tag{13}$$

In order to be able to evaluate the mean square tracking error σ_T^2, the power spectral density $S_{ne}(f)$ has to be found. Since the received noise $n_i(t)$ is assumed to be a bandlimited white Gaussian noise, it can be represented as

$$n_i(t) = \sqrt{2}\,[N_c(t)\cos\omega_0 t - N_s(t)\sin\omega_0 t] \, . \tag{14}$$

The processes $N_c(t)$ and $N_s(t)$ are statistically independent with a two-sided spectral density $(N_0/2)$ w/Hz and a one-sided bandwidth $B_H \ll \omega_0/2\pi$ [1].

The autocorrelation function of the output of the difference circuit is given by

$$\begin{aligned} R(\tau) &= E\langle\{[s_{z1}(t) + n_{z1}(t)]^2 - [s_{z2}(t) + n_{z2}(t)]^2\} \\ &\quad \cdot \{[s_{z1}(t+\tau) + n_{z1}(t+\tau)]^2 - [s_{z2}(t+\tau) - n_{z2}(t+\tau)]^2\}\rangle \\ R(\tau) &= (s_{z1}^2(t) - s_{z2}^2(t))^2 + 4(s_{z1}^2(t) + s_{z2}^2(t))\, R_{nz_1}(\tau) \\ &\quad - 8\, s_{z1}(t)\, s_{z2}(t)\, R_{nz_1 nz_2}(\tau) + 4R_{nz_1}^2(\tau) - 4R_{nz_1 \cdot nz_2}^2(\tau) \, . \end{aligned} \tag{15}$$

The first term in (15) is $D(\varepsilon)$ and the rest of the terms represent the autocorrelation of the noise. $R_{nz_1}(\tau)$ and $R_{nz_2}(\tau)$ are the autocorrelation functions of $n_{z1}(t)$ and $n_{z2}(t)$, respectively $[R_{nz_1}(\tau) = R_{nz_2}(\tau)]$, and $R_{nz_1 \cdot nz_2}(\tau)$ represents the cross-correlation between $n_1(t)$ and $n_2(t)$.

After some algebraic manipulations, the power spectral density $s_{ne}(f)$ is found to be

$$S_{ne}(f) = \begin{cases} \left(s_{z1}^2(t) + s_{z2}^2(t) - 2r\, s_{z1}(t)\, s_{z2}(t)\right)\frac{N_0}{2} + 4(1-r^2)\,(2B_i - |f|)\left(\frac{N_0}{2}\right)^2 ; \\ \qquad\qquad |f| < B_i \\ 0 \ ; \text{ otherwise} \end{cases} \tag{16}$$

where the bandpass filters have been assumed to be ideal with a rectangular bandwidth B_i. The constant r is the correlation between the advanced and the delayed signals in the correlation circuit,

$$r = \lim_{T\to\infty} \frac{1}{T}\int_0^T s(t-\hat{\tau}+\tfrac{\Delta}{N})\; s(t-\hat{\tau}-\tfrac{\Delta}{N})\; dt \ .$$

For long PN codes

$$r = 1 - \frac{2}{N} \ .$$

Using this result and the fact that, for small tracking errors ($\varepsilon << \Delta/N$), equation (5) results in

$$s_{z1}^2(t) = s_{z2}^2(t) = s_{z1}(t)\, s_{z2}(t) = P_s/2\,(1-\tfrac{1}{N})^2 \ .$$

The noise power spectral density becomes

$$S_{ne}(f) = \begin{cases} \frac{8(N-1)}{N^3}\left[P_s N_0(N-1) + N_0^2 B_i N\right] ; & |f| < B_i \\ 0 ; & \text{otherwise.} \end{cases} \tag{17}$$

It is assumed, as it is always the case, that the loop equivalent noise bandwidth is usually small when compared to the BPF bandwidth (B_i); hence, power spectral density of $S_{ne}(f)$ can be considered flat over the loop bandwidth. Therefore, (11) becomes

$$\sigma_T^2 = \frac{1}{(k P_s)^2} S_{ne}(0)\, 2B_L \ .$$

Substituting in the value of $S_{ne}(f)$ from (17), the normalized mean square delay error becomes

$$\sigma_T^2 = \frac{1}{N}\left[\rho_i^{-1} + (\rho_i)^{-2}\,\frac{N}{N-1}\right]\frac{B_L}{B_i} \tag{18}$$

where $\rho_i \triangleq P_s/(N_0 B_i)$ is the signal-to-noise ratio at the output of the arm filters.

Substituting N = 2 in (18),

$$\sigma_T^2 = \frac{1}{2}[\rho_i^{-1} + 2\rho_i^{-2}]\frac{B_L}{B_i}$$

which is the special case result of one-Δ loop obtained by Gill [2].

It is important at this stage to present the tau-jitter loop results for the sake of comparison. The tau-jitter loop shown in Figure 2 was analyzed by Hartman [3]. The normalized mean square delay error was shown to be

$$\sigma_T^2 = \left[0.905(\rho_i)^{-1} + [0.453 - T_d B_i/10]\left(\frac{N}{N-1}\right)^2(\rho_i)^{-2}\right]\frac{B_L}{B_i}, \qquad (19)$$

where the dithering frequency $f_d = 1/(2T_d)$ is usually taken in the range $B_i/8$ to $B_i/4$.

Figures 3 and 4 show the comparison between the DLL and the tau-jitter loop (for N = 4) for two values of arm filter bandwidth as a function of the input signal-to-noise ratio P_s/N_0. The loop bandwidth (B_L) defined in (12) is taken as a parameter. The range of values shown in the figures are chosen to include the design values of the Shuttle Ku-band radar/communication system.

As expected, the percent tracking jitter, σ_T%, decreases with the increase of input signal-to-noise ratio P_s/N_0. Furthermore, the performance of the tau-jitter loop is approximately 3 dB worse than that of the DLL because of the time-sharing between the early and late channels. This was found to be case by Hartman [3] for the case when N = 2.

Figure 5 compares the performance of the two loops for $B_i/2 = 432$ kHz, which is the suggested bandwidth for the arm filters in the video implementation of the Ku-band tracking loop. The 3 dB difference in performance between the DLL and the tau-jitter loop can be reduced by decreasing the dithering frequency of the latter, as long as it is not so small that it is attenuated by the loop filter. The variation of the tau-jitter performance with the product $T_d B_i$ is shown in Figure 6.

Finally, Figure 7 illustrates the effect of varying N on the percent tracking jitter in DLL. It is apparent that the performance improves with the decrease of N or, in other words, with the decrease of the correlator spacing Δ/N.

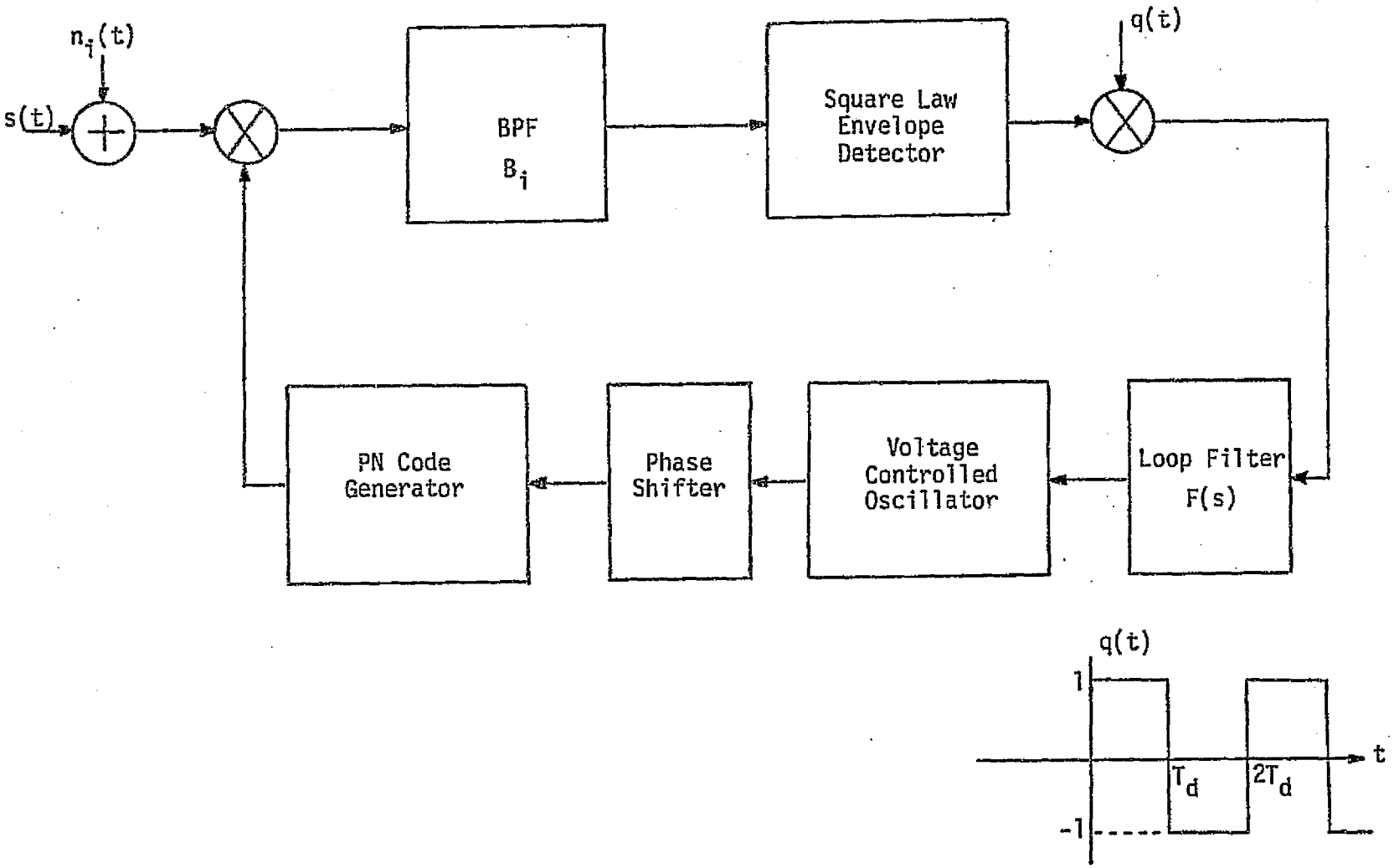

Figure 2. Block Diagram of Tau-Jitter Loop

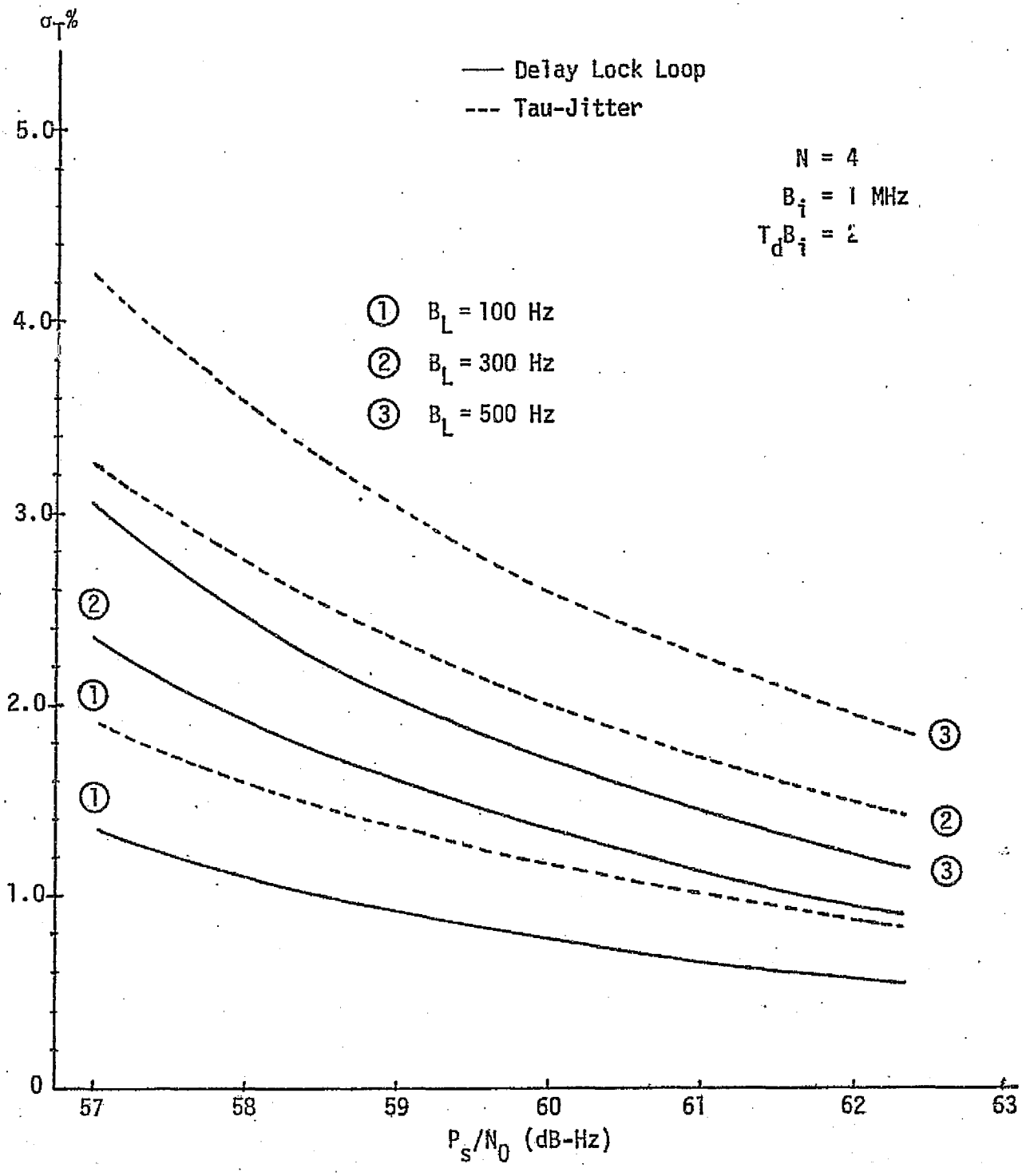

Figure 3. Percent Jitter Versus Signal-to-Noise Ratio (B_i = 1 MHz)

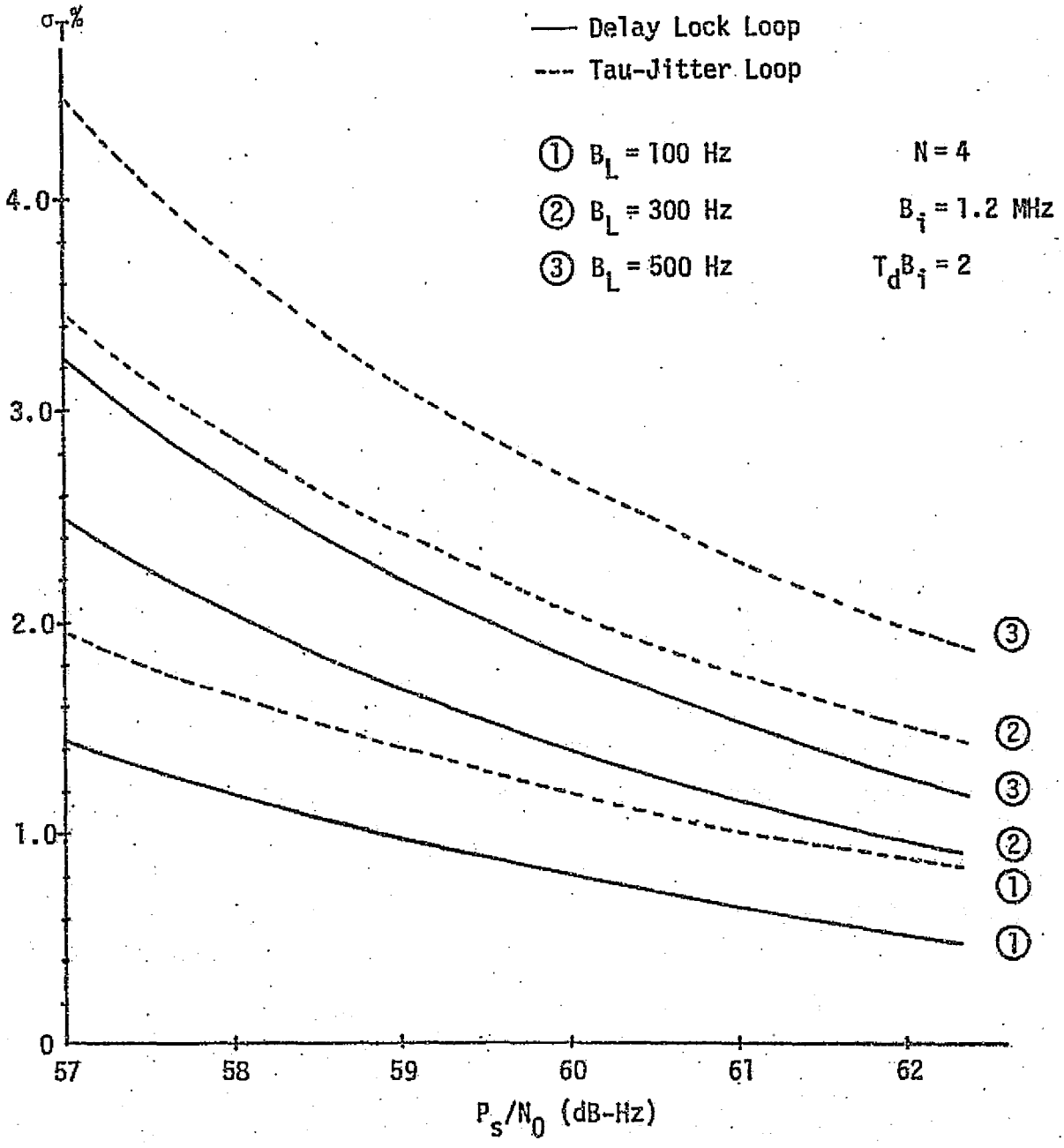

Figure 4. Percent Jitter Versus Signal-to-Noise Ratio (B_i = 1.2 MHz)

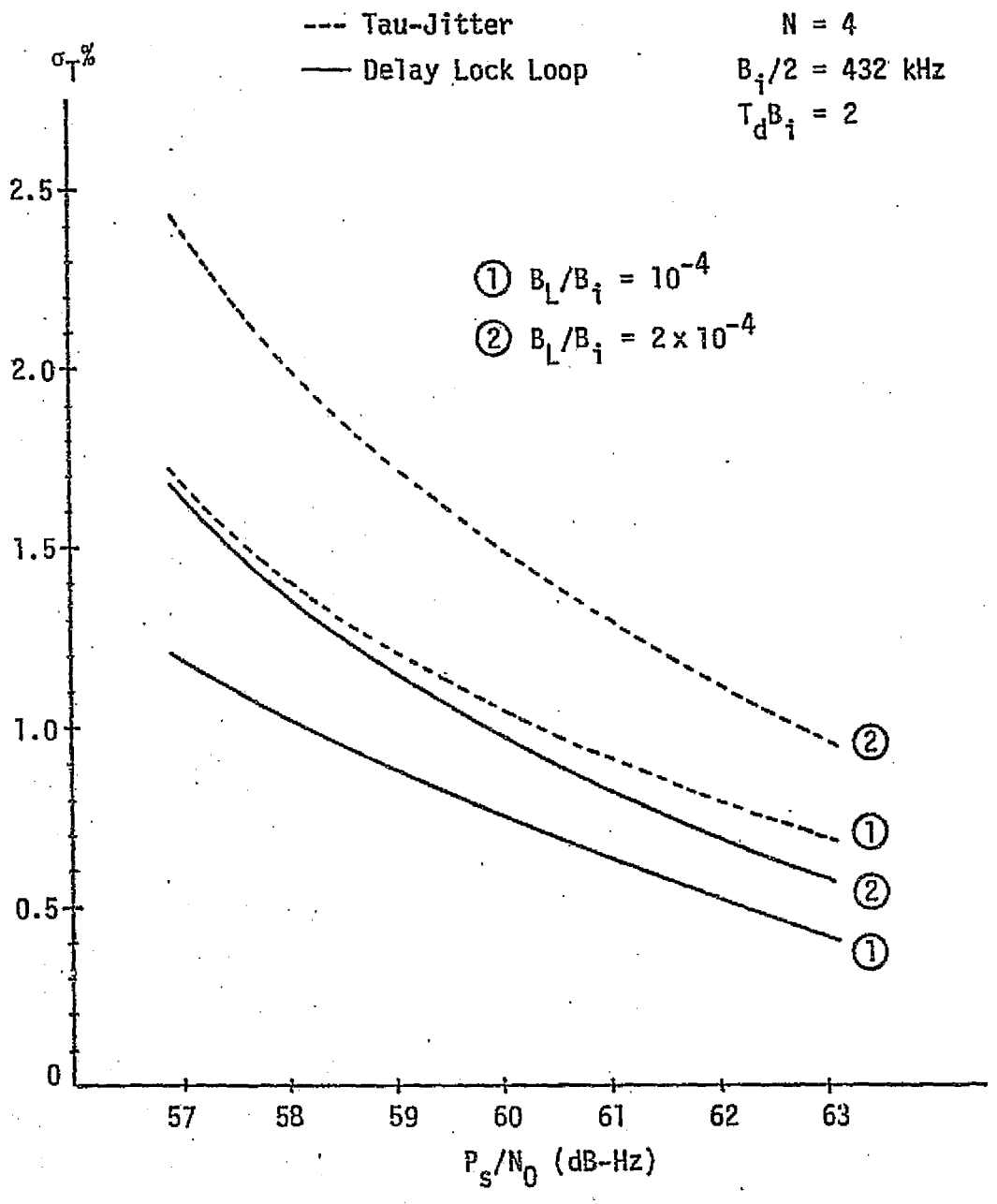

Figure 5. Comparison Between Delay Lock Loop and Tau-Jitter Loop

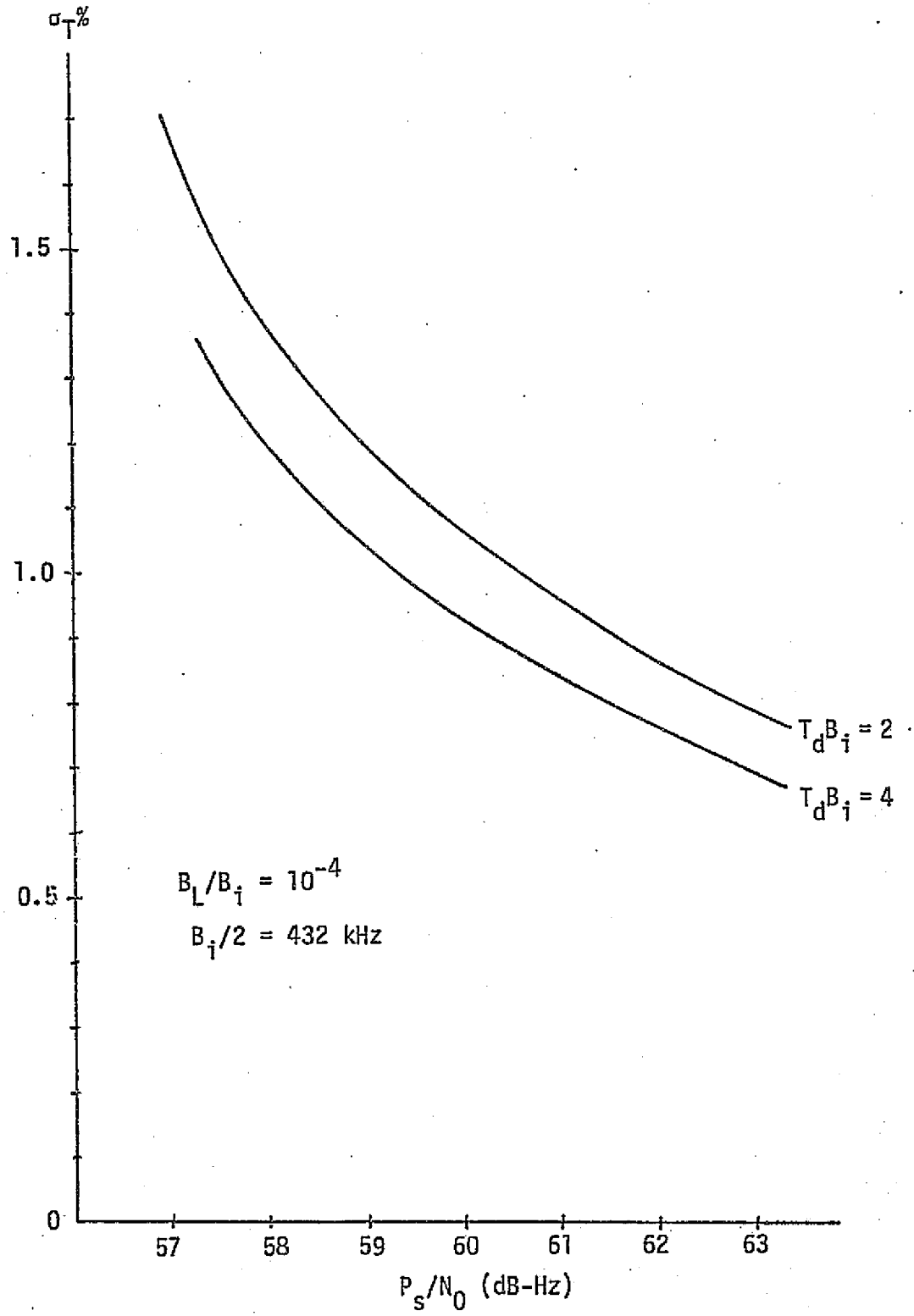

Figure 6. Tau-Jitter Loop Performance Variations With B_iT_d

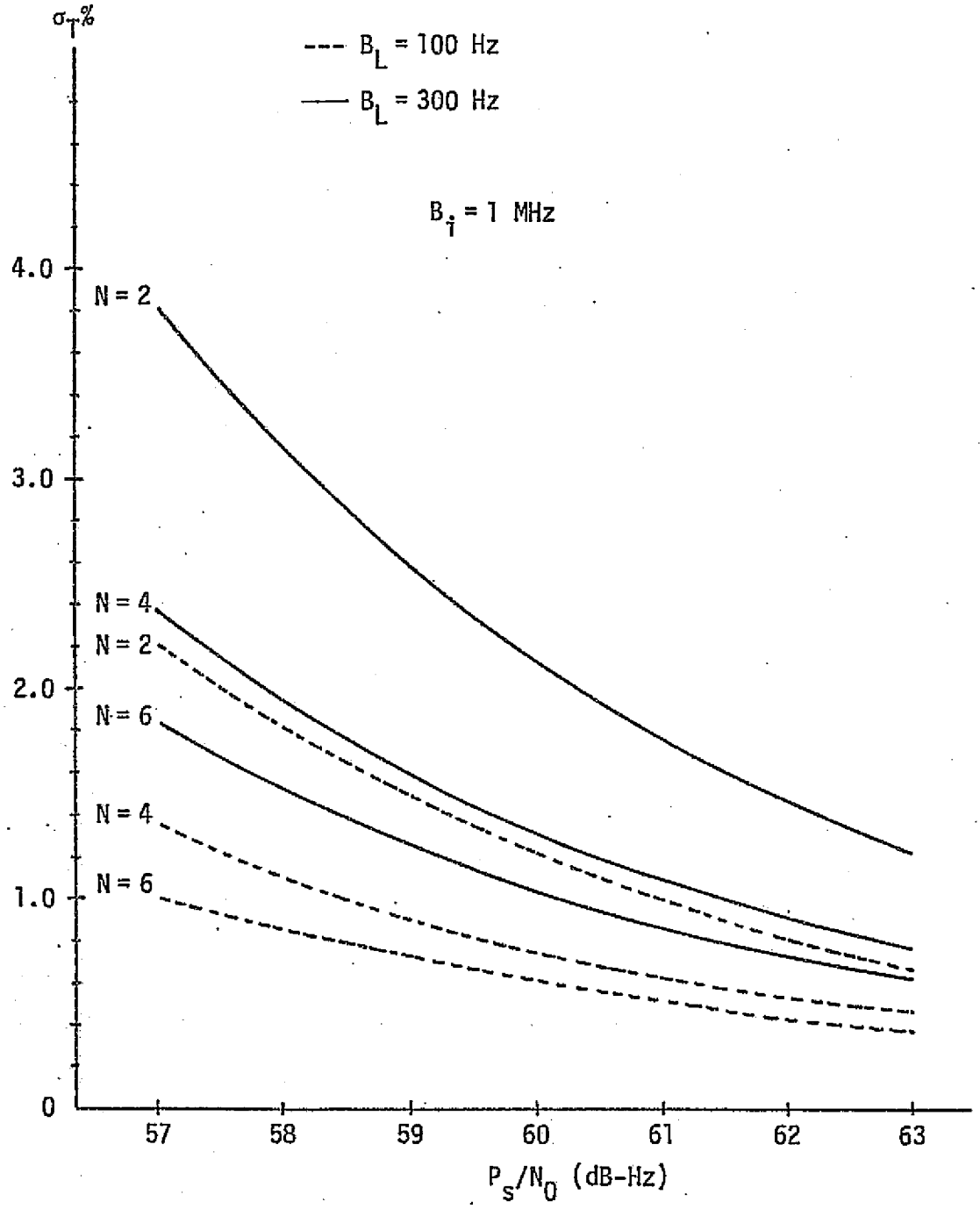

Figure 7. Variation in Performance of Delay Lock Loop with N

REFERENCES:

1. W. C. Lindsey and M. K. Simon. Telecommunication Systems Engineering. Englewood Cliffs, N.J.: Prentice-Hall, Inc., 1973.

2. W. J. Gill. "A Comparison of Binary Delay-Lock Implementations," IEEE Transactions on Aerospace and Electronic Systems, Vol. AES-2, July 1966, pp. 415-424.

3. H. P. Hartman. "Analysis of a Dithering Loop for PN Code Tracking," IEEE Transactions on Aerospace and Electronic Systems, Vol. AES-10, No. 1, January 1974, pp. 2-9.

APPENDIX C

THE EFFECT OF THE ARM FILTER ON DELAY LOCK LOOP PERFORMANCE

THE EFFECT OF THE ARM FILTER ON DELAY LOCK LOOP PERFORMANCE

by

Waddah Alem

The effect of the arm filter on the performance of the delay lock loop (DLL) has been investigated [1] for one-Δ ($N = 2$) implementation. The purpose of this appendix is to generalize those results to any amount of correlator spacing (Δ/N, $N \geq 2$). Contrary to what is done in practice, the bandwidth of the arm filter will not be chosen on the order of the data rate; instead, a comparison (in performance) between different arm filter bandwidths is presented. Only the case of a linear loop is treated here; however, extending the results to the nonlinear case is a straightforward procedure. The envelope implementation (noncoherent DLL) which is discussed here is shown in Figure 1. The advanced and retarded signals are $2\Delta/N$ apart. A loop such as this is sometimes said to have Δ/N of correlator spacing. The received signal is a sum of a transmitted signal $s_t(t)$ and additive noise $n_i(t)$ which is assumed to be a bandlimited white Gaussian noise. The signal can be denoted as

$$s_t(t) = \sqrt{2P_s}\, s(t-T)\, m(t-T) \cos(\omega_0 t + \phi) \tag{1}$$

and $n_i(t)$ has the representation

$$n_i(t) = \sqrt{2}\,[N_c(t) \cos(\omega_0 t + \phi) - N_s(t) \sin(\omega_0 t + \phi)] \tag{2}$$

where P_s is the average signal power, T is the transmission delay, $m(t)$ is the modulated data, $s(t)$ is a PN sequence with a long period, ω_0 is the carrier frequency with possible doppler included, and ϕ is a random phase uniformly distributed between 0 and 2π. As for the noise, $N_c(t)$ and $N_s(t)$ are statistically independent lowpass white Gaussian noise processes with two-sided spectral density, $N_0/2$ w/Hz. The bandwidth of the noise is assumed to be much less than the carrier frequency $\omega_0/2\pi$.

The phase detector outputs in the two arms are given by

$$y_{\mp}(t) = \sqrt{2P_s}\, m(t-T)\, s(t-T)\, s\left(t-\hat{T}\mp\frac{\Delta}{N}\right) \cos[\omega_0 t + \phi] + s\left(t-\hat{T}\mp\frac{\Delta}{N}\right) n_i(t)\,, \tag{3}$$

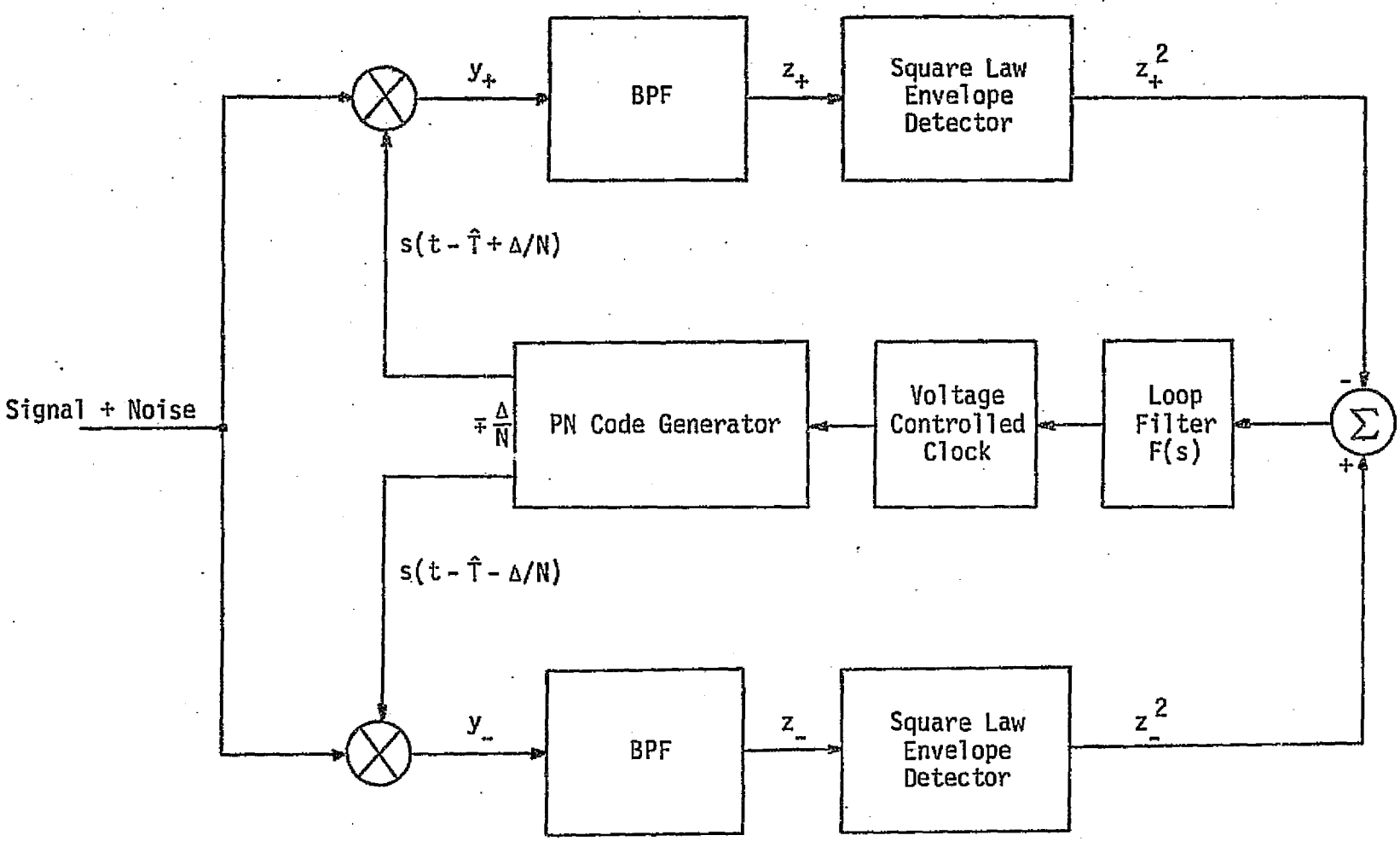

Figure 1. Block Diagram of the Delay Lock Loop

where $\hat{\tau}$ is the receiver's estimate of the transmission delay T. For all practical purposes, it can be shown that, for a loop with small single-sided loop bandwidth, when compared to the PN code chip rate, (3) can be written as

$$y_{\mp}(t) = \sqrt{2P_s}\, m(t-\tau)\, \overline{s(t-\tau)\, s(t-\hat{\tau} \mp \tfrac{\Delta}{N})}\, \cos[\omega_0 t + \phi] + s(t-\hat{\tau} \mp \tfrac{\Delta}{N})\, n_i(t)\,, \quad (4)$$

where the product of the two PN codes has been replaced by their statistical expectation (autocorrelation function), neglecting the effect of self-noise.

$$s(t-\tau)\, s(t-\hat{\tau}+\tfrac{\Delta}{N}) \triangleq R_+(\tfrac{\varepsilon}{\Delta}) = \begin{cases} 0\,; & \tfrac{\varepsilon}{\Delta} < \tfrac{-1}{N} - 1 \\ 1 + \tfrac{1}{N} + \tfrac{\varepsilon}{\Delta}\,; & -1 - \tfrac{1}{N} < \tfrac{\varepsilon}{\Delta} < \tfrac{-1}{N} \\ 1 - \tfrac{1}{N} - \tfrac{\varepsilon}{\Delta}\,; & -\tfrac{1}{N} < \tfrac{\varepsilon}{\Delta} < 1 - \tfrac{1}{N} \\ 0\,; & \tfrac{\varepsilon}{\Delta} > 1 - \tfrac{1}{N} \end{cases} \quad (5)$$

and

$$R_-(\tfrac{\varepsilon}{\Delta}) = R_+(\tfrac{\varepsilon}{\Delta} - 1)\,.$$

Both R_+ and R_- are periodic with a period equal to that of the PN code. Figure 2 illustrates the two autocorrelation functions.

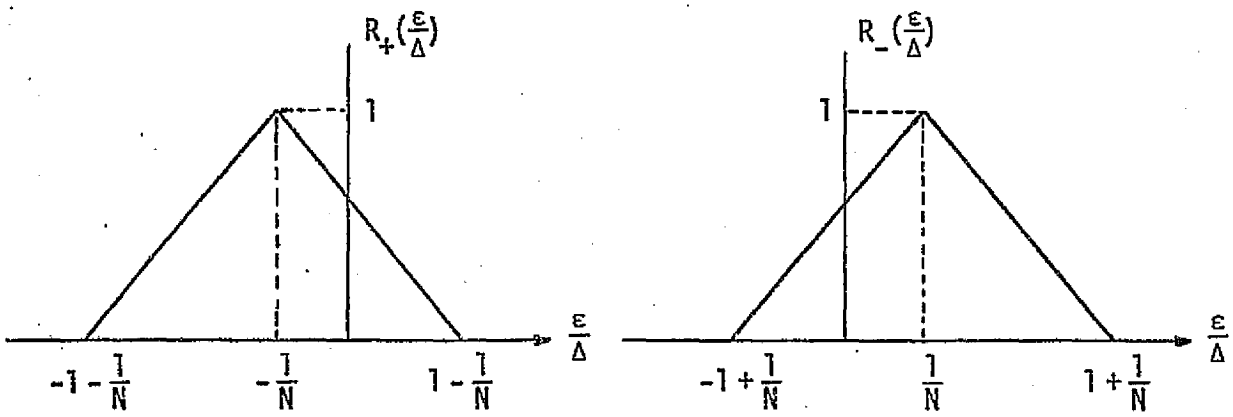

Figure 2. Autocorrelation Functions of the PN Code

Let $H_L(s)$ denote the lowpass equivalent transfer functions of the arm bandpass filters; then the output of these filters can be written as

$$z_{\mp}(t) = \sqrt{2P_s}\,\hat{m}(t-T)\,R_{\mp}(\tfrac{\varepsilon}{\Delta})\cos[\omega_0 t+\phi] + \sqrt{2}\,\hat{N}_{c\mp}(t)\cos[\omega_0 t+\phi] - \sqrt{2}\,\hat{N}_{s\mp}(t)\sin[\omega_0 t+\phi] \tag{6}$$

where, in operator notation,

$$\hat{m}(t) = H_\ell(s)\,m(t)$$

$$\hat{N}_{c\mp}(t) = H_\ell(s)\,[s(t-\hat{T}\mp\tfrac{\Delta}{N})\,N_c(t)]$$

$$\hat{N}_{s\mp}(t) = H_\ell(s)\,[s(t-\hat{T}\mp\tfrac{\Delta}{N})\,N_s(t)]\,.$$

After subtracting the outputs of the square law envelope detectors, the input to the loop filter becomes

$$e(t) = z_-^2(t) - z_+^2(t) = P_s\,\hat{m}^2(t-T)\,D(\tfrac{\varepsilon}{\Delta}) + n_e(t,\tfrac{\varepsilon}{\Delta})\,, \tag{7}$$

where $D(\varepsilon/\Delta)$ is the discriminator characteristic and $n_e(t,\varepsilon/\Delta)$ is the equivalent additive noise. The discriminator characteristic is given as

$$D(\tfrac{\varepsilon}{\Delta}) = R_-^2(\tfrac{\varepsilon}{\Delta}) - R_+^2(\tfrac{\varepsilon}{\Delta}) = \begin{cases} 0\,; & \tfrac{\varepsilon}{\Delta} < -1-\tfrac{1}{N} \\ -(1+\tfrac{1}{N}+\tfrac{\varepsilon}{\Delta})^2\,; & (-1-\tfrac{1}{N}) < \tfrac{\varepsilon}{\Delta} < (-1+\tfrac{1}{N}) \\ -\tfrac{4}{N}(1+\tfrac{\varepsilon}{\Delta})\,; & -1+\tfrac{1}{N} < \tfrac{\varepsilon}{\Delta} < -\tfrac{1}{N} \\ 4\,\tfrac{\varepsilon}{\Delta}(1-\tfrac{1}{N})\,; & |\tfrac{\varepsilon}{\Delta}| < \tfrac{1}{N} \\ 4(1-\tfrac{\varepsilon}{\Delta})\,; & \tfrac{1}{N} < \tfrac{\varepsilon}{\Delta} < 1-\tfrac{1}{N} \\ (1+\tfrac{1}{N}-\tfrac{\varepsilon}{\Delta})^2\,; & 1-\tfrac{1}{N} < \tfrac{\varepsilon}{\Delta} < 1+\tfrac{1}{N} \\ 0\,; & \tfrac{\varepsilon}{\Delta} > 1+\tfrac{1}{N} \end{cases} \tag{8}$$

Equation (8) is illustrated in Figure 3.

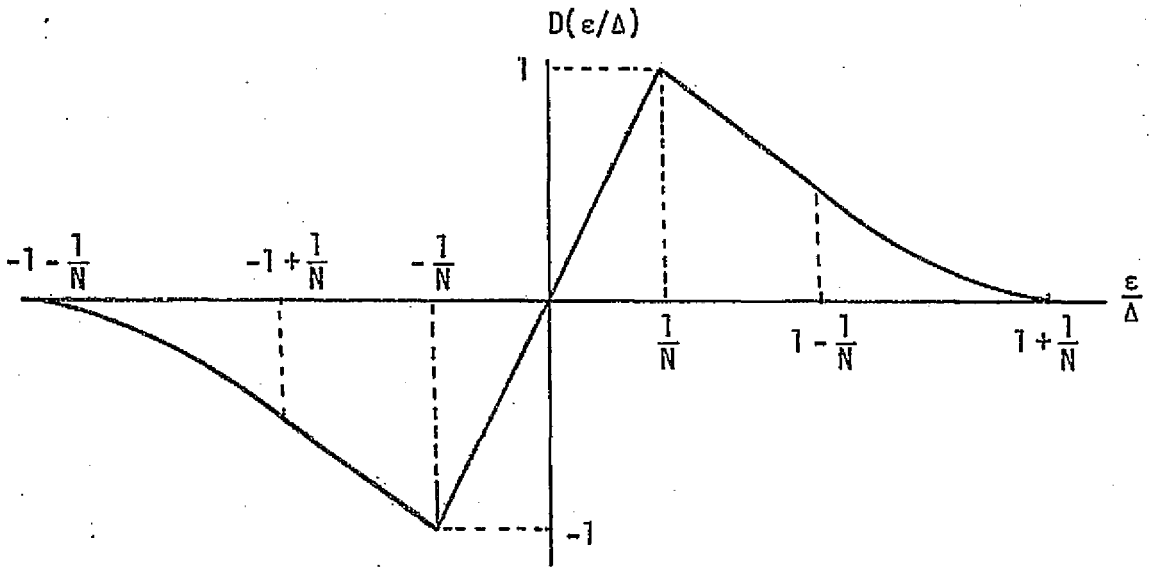

Figure 3. Discriminator Characteristic

The equivalent noise $n_e(t,\varepsilon/\Delta)$ is defined as

$$n_e(t,\tfrac{\varepsilon}{\Delta}) = \hat{N}^2_{c-}(t) - \hat{N}^2_{c+}(t) + \hat{N}^2_{s-}(t) - \hat{N}^2_{s+}(t)$$

$$+ 2\sqrt{P_s}\,\hat{m}(t-T)\left\{R_-(\tfrac{\varepsilon}{\Delta})\,\hat{N}_{c-}(t) - R_+(\tfrac{\varepsilon}{\Delta})\,\hat{N}_{c+}(t)\right\}. \qquad (9)$$

The resulting estimate of the normalized transmission delay is expressed as:

$$\frac{\hat{T}}{\Delta} = \frac{g_c\,g_f\,F(s)}{s}\,e(t)$$

which, after a little manipulation, results in

$$\frac{\varepsilon}{\Delta} = \frac{T}{\Delta} - \frac{g_c\,g_f\,F(s)}{s}\left[P_s\,\hat{m}^2(t-T)\,D(\tfrac{\varepsilon}{\Delta}) + n_e(t,\tfrac{\varepsilon}{\Delta})\right] \qquad (10)$$

Decomposing $\hat{m}^2(t-T)\,D(\frac{\varepsilon}{\Delta})$ into a mean and modulation self-noise results in

$$\hat{m}^2(t-T)\,D(\tfrac{\varepsilon}{\Delta}) = \overline{\hat{m}^2(t-T)}\;D(\tfrac{\varepsilon}{\Delta}) + [\hat{m}^2(t-T) - \overline{\hat{m}^2(t-T)}]\,D(\tfrac{\varepsilon}{\Delta}) \qquad (11)$$

where

$$\overline{\hat{m}^2(t-T)} \triangleq M_m = \int_{-\infty}^{\infty} S_m(f)\,|H_\ell(j2\pi f)|^2\,df\,. \qquad (12)$$

$S_m(f)$ is the power spectral density of the data modulation. It is a known fact [2] that, when the loop bandwidth B_L is much less than the data symbol

rate $R_s = 1/T_s$, the modulation self-noise can be neglected. This results in

$$\frac{\dot{\varepsilon}}{\Delta} = \frac{\dot{T}}{\Delta} - G F(s) M_m \left[D_n\left(\frac{\varepsilon}{\Delta}\right) + \frac{n_e(t,\frac{\varepsilon}{\Delta})}{k P_s M_m} \right] \tag{13}$$

where G is defined as the open loop gain.

$$G = k P_s g_c g_f$$

$$k = \frac{4(N-1)}{N}$$

and $D_n(\varepsilon/\Delta)$ is the normalized discriminator characteristic with a unit slope at the origin.

To find the mean square jitter in the loop, it is essential to determine the autocorrelation function of the equivalent noise $n_e(t,\varepsilon/\Delta)$, which is defined as

$$R_e(\tau,\frac{\varepsilon}{\Delta}) \triangleq \overline{n_e(t,\frac{\varepsilon}{\Delta})\, n_e(t+\tau,\frac{\varepsilon}{\Delta})} \,. \tag{14}$$

After some algebraic manipulation, it is found that

$$R_e(\tau,\frac{\varepsilon}{\Delta}) = 8 R_{\hat{N}}^2(\tau) + 4 P_s R_{\hat{m}}(\tau) R_{\hat{N}}(\tau) f(\frac{\varepsilon}{\Delta}) \,, \tag{15}$$

where

$$f(\frac{\varepsilon}{\Delta}) \triangleq R_+^2(\frac{\varepsilon}{\Delta}) + R_-^2(\frac{\varepsilon}{\Delta}) = \begin{cases} 0 \,; & \frac{\varepsilon}{\Delta} < -1 - \frac{1}{N} \\ (1 + \frac{1}{N} + \frac{\varepsilon}{\Delta})^2 \,; & -1 - \frac{1}{N} < \frac{\varepsilon}{\Delta} < -1 + \frac{1}{N} \\ 2[\frac{1}{N^2} + (1 + \frac{\varepsilon}{\Delta})^2] \,; & -1 + \frac{1}{N} < \frac{\varepsilon}{\Delta} < -\frac{1}{N} \\ 2[(1 - \frac{1}{N})^2 + (\frac{\varepsilon}{\Delta})^2] \,; & |\frac{\varepsilon}{\Delta}| < \frac{1}{N} \\ 2[\frac{1}{N^2} + (1 - \frac{\varepsilon}{\Delta})^2] \,; & \frac{1}{N} < \frac{\varepsilon}{\Delta} < 1 - \frac{1}{N} \\ (1 + \frac{1}{N} - \frac{\varepsilon}{\Delta})^2 \,; & 1 - \frac{1}{N} < \frac{\varepsilon}{\Delta} < 1 + \frac{1}{N} \\ 0 \,; & \frac{\varepsilon}{\Delta} > 1 + \frac{1}{N} \end{cases} \tag{16}$$

$$R_{\hat{N}}(\tau) = \frac{N_0}{2}\int_{-\infty}^{\infty} |H_\ell(j2\pi f)|^2 \, e^{j2\pi f\tau} \, df$$

$$R_{\hat{m}}(\tau) = \frac{N_0}{2}\int_{-\infty}^{\infty} |H_\ell(j2\pi f)|^4 S_m(f) \, e^{j2\pi f\tau} \, df \, .$$

Since the DLL equivalent bandwidth is usually much narrower than that of $n_e(t,\varepsilon/\Delta)$, the spectral density of the noise can be assumed flat over the loop bandwidth with one-sided spectral density of

$$N_e(\tfrac{\varepsilon}{\Delta}) = 2\int_{-\infty}^{\infty} R_e(\tau,\tfrac{\varepsilon}{\Delta}) \, d\tau \, . \tag{17}$$

Using the above information, it can be shown that

$$N_e(\tfrac{\varepsilon}{\Delta}) = 4N_0^2 \int_{-\infty}^{\infty} |H_\ell(j2\pi f)|^4 \, df + 4P_s N_0 f(\tfrac{\varepsilon}{\Delta}) M_m \, ,$$

which can be written as

$$N_e(\tfrac{\varepsilon}{\Delta}) = 2P_s N_0 M_m^2 \left[\frac{2K_D f(\tfrac{\varepsilon}{\Delta}) + 2\frac{K_L}{\rho_i M_m}}{M_m}\right] \tag{18}$$

where

$$K_L \triangleq \frac{\int_{-\infty}^{\infty} |H_\ell(j2\pi f)|^4 \, df}{\int_{-\infty}^{\infty} |H_\ell(j2\pi f)|^2 \, df}$$

$$K_D \triangleq \frac{\int_{-\infty}^{\infty} S_m(f) \, |H_\ell(j2\pi f)|^4 \, df}{\int_{-\infty}^{\infty} S_m(f) \, |H_\ell(j2\pi f)|^2 \, df}$$

$$\rho_i = \frac{P_s}{N_0 B_i} \tag{19}$$

where B_i denotes the <u>two-sided</u> bandwidth of the equivalent lowpass filter $H_\ell(s)$; that is,

$$B_i = \int_{-\infty}^{\infty} |H_\ell(j2\pi f)|^2 \, df \, . \tag{20}$$

For large signal-to-noise ratios or when the error ϵ/Δ is restricted to the linear region of the discriminator characteristic ($|\epsilon/\Delta| < 1/N$), $D_n(\epsilon/\Delta)$ is replaced by ϵ/Δ. If it is further assumed that $\hat{\tau} = 0$, the normalized mean square tracking jitter can be expressed as

$$\sigma_T^2 = \left(\frac{\bar{\epsilon}^2}{\Delta^2}\right) = \frac{\overline{N_e}\left(\frac{\epsilon}{\Delta}\right) B_L}{(G M_m)^2} . \tag{21}$$

Substituting the values of $\overline{N_e}(\epsilon/\Delta)$ and G, it can be concluded that

$$\sigma_T^2 = \frac{1}{2\rho}\left[\frac{K_D + \frac{8 K_L}{\rho_i M_m^2 k^2}}{M_m}\right] = \frac{1}{2\rho\, \zeta_L} , \tag{22}$$

where $\rho = P_s/(N_0 B_L)$ and ζ_L is called the squaring loss of the DLL. In terms of data signal-to-noise ratio $R_d = P_s T_s/N_0 = P_s/(N_0 R_s)$, one can write

$$\zeta_L = \frac{M_m}{K_D + K_L \frac{B_i/R_s}{2 R_d M_m}\left(\frac{N}{N-1}\right)^2} . \tag{23}$$

Comparing (23) and the results obtained by Simon [1], it can be concluded that the squaring loss of a DLL with a correlator spacing of Δ/N is equal to the squaring loss of a DLL with a correlator spacing of $\Delta/2$ and a data rate of $4\left(\frac{N-1}{N}\right)^2 R_s$. Equivalently, it is only required to plot curves of ζ_L for the case of DLL with correlator spacing of $\Delta/2$. All other cases can be derived from the same curves by appropriately modifying the data rate R_s.

Figure 4 shows the percent jitter $\sigma_T\%$ for a delay lock loop with correlator spacing of $\Delta/4$. In plotting this curve, the data is assumed to be Manchester encoded and the arm filters are assumed to be 2-pole Butterworth filters. It can be concluded that, for all practical purposes, the performance is identical, for the two values of B_i under consideration, at $P_s/N_0 > 60$ dB-Hz and is different by only 0.3 dB at $P_s/N_0 = 57$ dB-Hz.

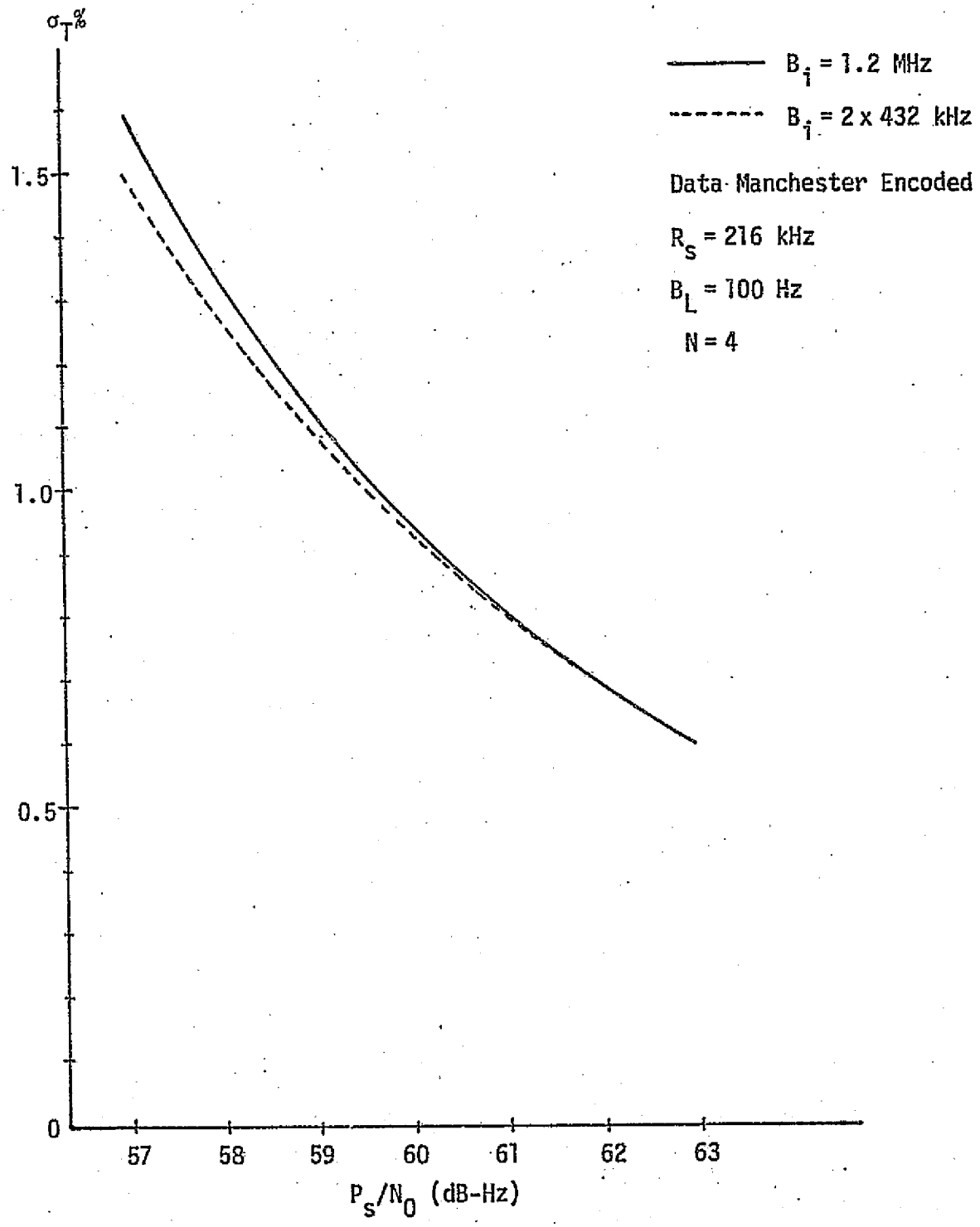

Figure 4. Percent Jitter With Manchester Encoded Data and Two-Pole Butterworth Arm Filters

REFERENCES:

1. M. K. Simon. "Noncoherent Pseudonoise Code Tracking Performance of Spread Spectrum Receivers," IEEE Transactions on Communications, Vol. COM-25, No. 3, March 1977, pp. 327-348.

2. W. C. Lindsey and M. K. Simon. Telecommunication Systems Engineering. Englewood Cliffs, N.J.: Prentice-Hall, Inc., 1973.

TRANSIENT RESPONSE OF DELAY LOCK LOOPS

by

Waddah Alem

The transient response of a delay lock loop (DLL) with an arbitrary correlator spacing is studied. The model of the DLL used is the same as that in Appendixes B and C. It is shown again in Figure 1 for convenience. The transient performance is studied in the absence of noise.

The system equation which was derived in Appendix B can be written in the absence of noise as

$$s(y-x) = GF(s)\,D_n(x) \tag{1}$$

where the various parameters have been normalized such that $x \triangleq \epsilon/\Delta$, $y \triangleq T/\Delta$, $s = d/d\tau$, $\tau \triangleq \omega_n t$, and $D_n(x)$ is the normalized discriminator characteristic which has a slope of unity at the stable point ($x = 0$). $D_n(x)$ was found in Appendix C to have the form

$$D_n(x) = \begin{cases} 0\ ; & x < -1-\frac{1}{N} \\ \frac{-N}{4(N-1)}\left(1+\frac{1}{N}+x\right)^2\ ; & -1-\frac{1}{N} < x < -1+\frac{1}{N} \\ \frac{-1}{N-1}\left(1+x\right)\ ; & -1+\frac{1}{N} < x < -\frac{1}{N} \\ x\ ; & |x| < \frac{1}{N} \\ \frac{1}{N-1}\left(1-x\right)\ ; & \frac{1}{N} < x < 1-\frac{1}{N} \\ \frac{N}{4(N-1)}\left(1+\frac{1}{N}-x\right)^2\ ; & 1-\frac{1}{N} < x < 1+\frac{1}{N} \\ 0\ ; & x > 1+\frac{1}{N} \end{cases} \tag{2}$$

$F(s)$ is the transfer function of the loop filter.

For a critically damped loop,

$$GF(s) = \frac{1+\sqrt{2}\,s}{\frac{1}{G}+s}$$

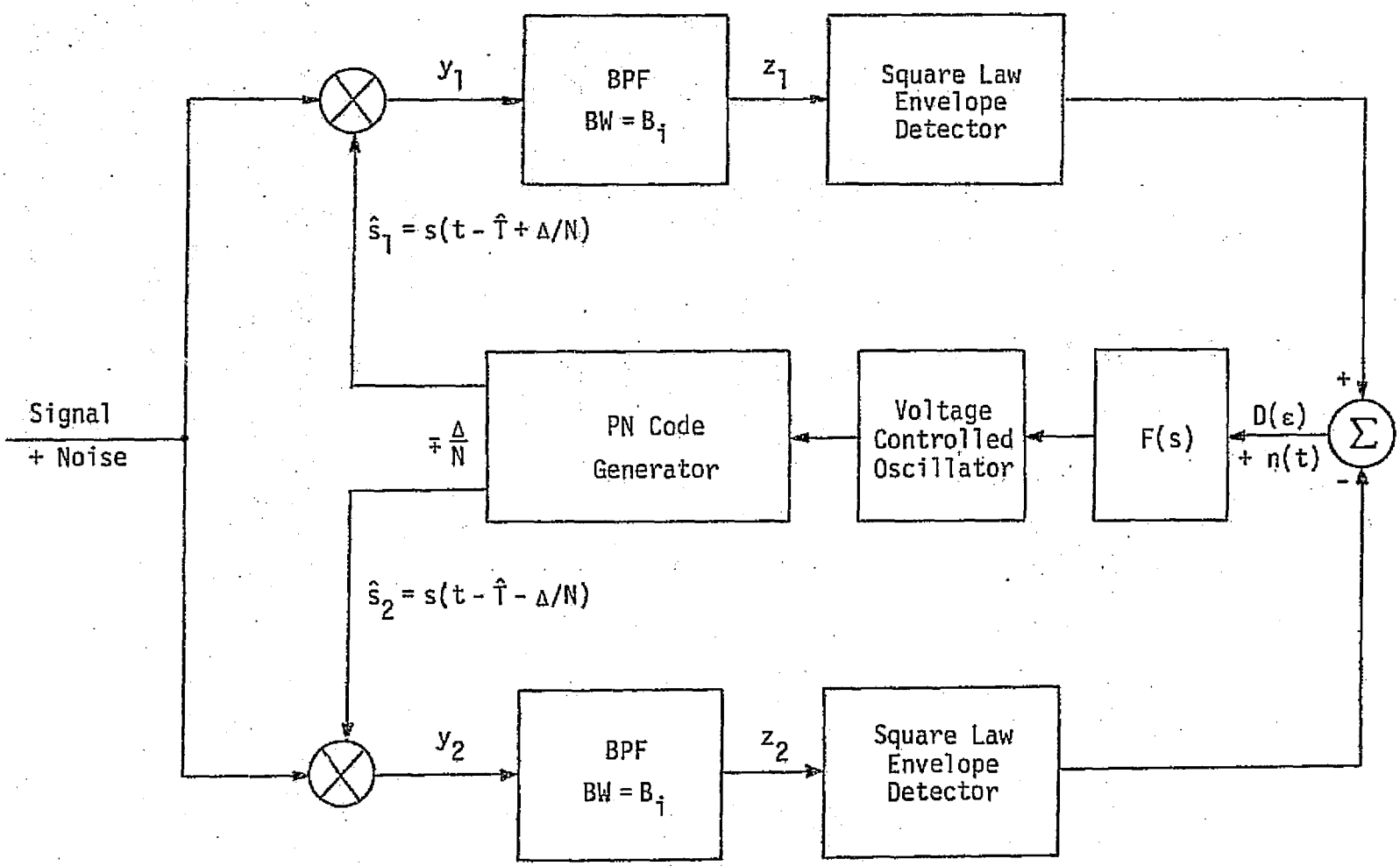

Figure 1. Block Diagram of the Delay Lock Loop

which, upon substituting into (1), yields

$$\dot{y}/G + \ddot{y} \overset{\cdot}{=} \dot{x}/G + \ddot{x} + D_n(x) + \sqrt{2}\, D_n'(x)\dot{x} . \tag{3}$$

The dot denotes the derivative with respect to normalized time (τ) and the prime denotes the derivative with respect to the normalized error (x). The solution of the second-order partial differential equation in (3) is facilitated by defining $\gamma \triangleq \ddot{x}/\dot{x} = d\dot{x}/dx$, which results in

$$\gamma[x,\dot{x},y,\dot{y}] = -\frac{D_n(x) + [\sqrt{2}\, D_n'(x) + 1/G]\dot{x} - \dot{y}/G - \ddot{y}}{\dot{x}} .$$

For a constant search velocity, $\ddot{y} = 0$, the above equation becomes

$$\gamma[x,\dot{x},y,\dot{y}] = \frac{D_n(x) + [\sqrt{2}\, D_n'(x) + 1/G]\dot{x} - \dot{y}/G}{\dot{x}} .$$

Two questions have to be answered when discussing transient performance of a delay lock loop:

1. What is the maximum velocity of the transmitter (relative to the receiver) so that the received signal can still be acquired?
2. How long do the transients last?

The first question is answered by computing the trajectories in the $(x,\dot{x})$ plane for given initial conditions and then finding the maximum $\dot{y}$ for which the DLL would still be able to lock. The second question can be dealt with by using the definition of γ as a starting point and computing the acquisition transients as a function of time and then finding the acquisition time.

Using Newton's method of numerically solving differential equations and fact that $\gamma = d\dot{x}/dx$, it is easily found that the difference equations to be solved are

$$\dot{x}_{n+1} - \dot{x}_n = \gamma_n \delta_n$$

$$\tau_{n+1} - \tau_n = \frac{\delta_n}{\dot{x}_n}$$

where $\delta_n \triangleq x_{n+1} - x_n$ is the interval size in the nth extrapolation step. It is usually taken as

$$|\delta_n| = \frac{\delta}{1 + |\gamma_n|}$$

where δ is a number to be chosen according to the required accuracy. It can be taken in the range of 0.01 to 0.1.

The acquisition trajectories for N = 2 and N = 4 are shown in Figures 2 and 3, respectively. It is apparent from Figure 2 that the results are different from those obtained in [1] and [2], which were shown to be in error by [3]. The results, however, are in complete agreement with those obtained in [3]. It was found that the maximum normalized search rate for N = 2 is $\dot{y} = 1.0$. For N = 4, the maximum normalized search rate is $\dot{y} = 0.5$. The open loop gain showed little effect on the trajectories for G > 10.

Figure 4 shows the transient response of the DLL for N = 2 and N = 4. The search rate is chosen to be $\dot{y} = 0.9$ for the first case and $\dot{y} = 0.45$ for the second case, respectively. The graphs show that the acquisition time (time required for the transient to subside within $|x| = 0.1$) for N = 2 is shorter than that for N = 4. The actual acquisition time can be computed from the definition of the normalized time for critically damped loops, where

$$t = \frac{0.5303\ \tau}{B_L} .$$

Table 1 summarizes the results for different values of loop bandwidth.

Table 1. Acquisition Time (sec)

B_L (Hz)	100	200	300	400	
N = 2	0.0244	0.0122	0.0081	0.0061	$\dot{y} = 0.9$
N = 4	0.0292	0.0146	0.0097	0.0073	$\dot{y} = 0.45$

NOTE: B_L is a one-sided bandwidth.

Finally, the actual maximum search velocity in chips/sec (which can be interpreted as the maximum allowable drift in the code) can be found from the definition of the normalized search velocity $\dot{y}$. As a function of the single-sided loop noise bandwidth B_L, the search velocity (v_s) is

$$v_s = 1.8857\, \dot{y}\, B_L \quad \text{chips/sec} .$$

For B_L = 100 Hz, the maximum search velocity is 188.57 chips/sec for N = 2 and 94.29 chips/sec for N = 4.

REFERENCES:

1. W. J. Gill, "A Comparison of Binary Delay-Lock Implementations," IEEE Transactions on Aerospace and Electronic Systems, Vol. AES-2, July 1966, pp. 415-424.

2. J. J. Spilker, Jr. "Delay-Lock Tracking of Binary Signals," IEEE Transactions on Space Electronics and Telemetry, Vol. SET-9, No. 1, March 1963, pp. 1-8.

3. P. T. Nielsen. "On the Acquisition Behavior of Binary Delay-Lock Loops," IEEE Transactions on Aerospace and Electronic Systems, Vol. AES-11, May 1975, pp. 415-418.

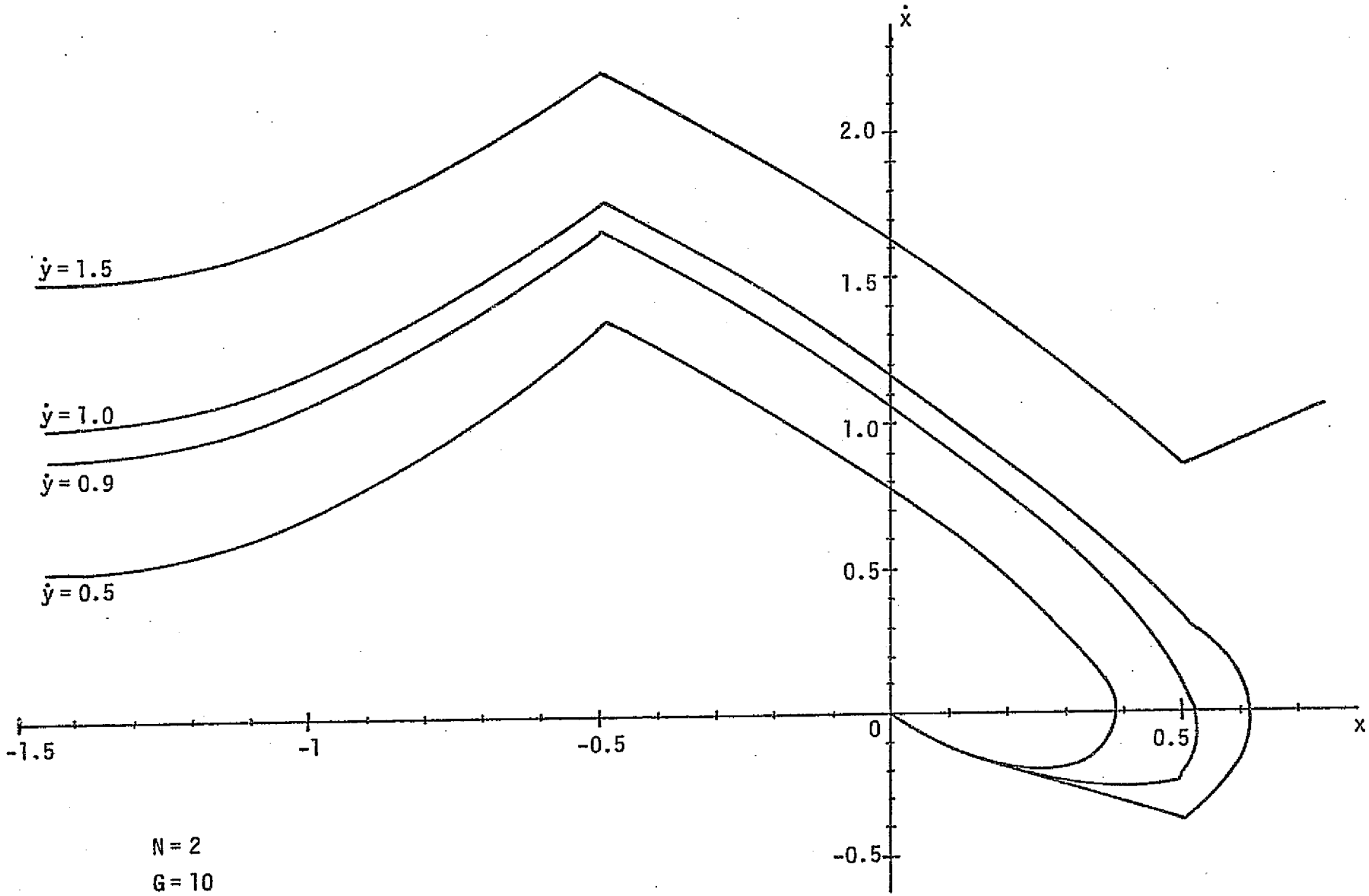

Figure 2. Lock-On Trajectories for N = 2

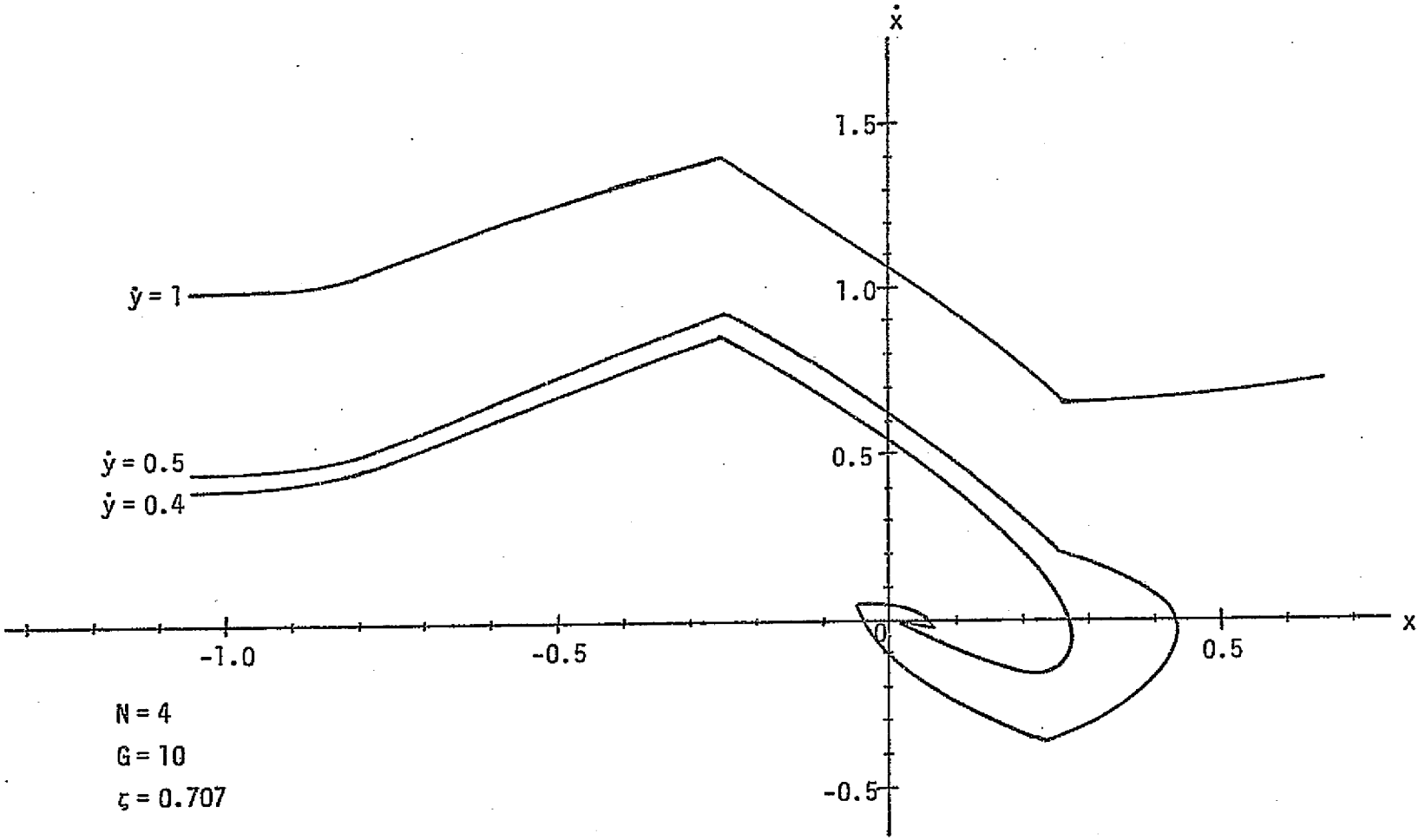

Figure 3. Lock-On Trajectories for N = 4

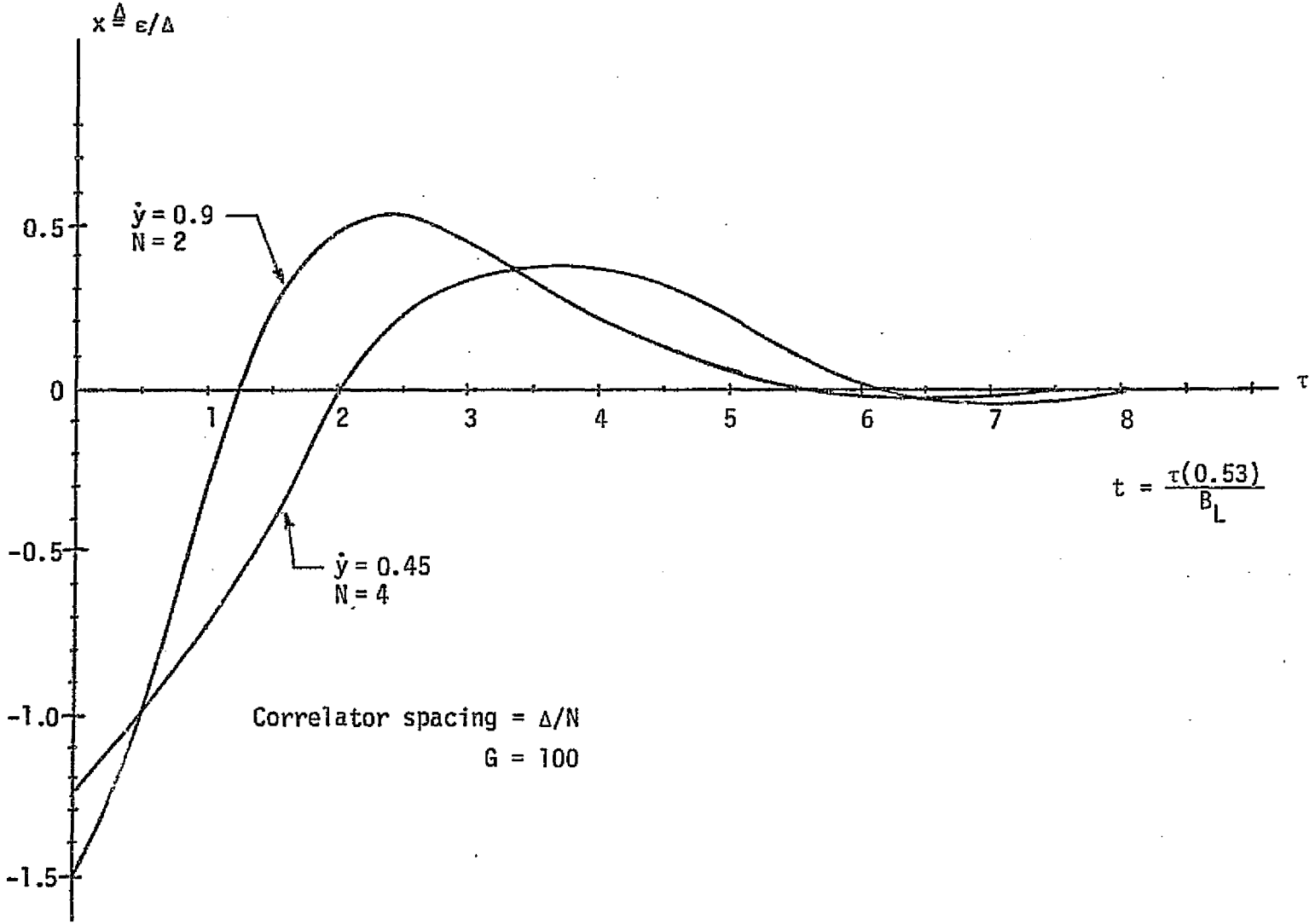

Figure 4. Transient Response of Delay Lock Loop

OUTPUT SIGNAL AND NOISE STATISTICS OF A BENT-PIPE PAYLOAD DATA PREPROCESSOR FOR SHUTTLE ORBITER

by

Marvin K. Simon

INTRODUCTION

The bent-pipe mode for payloads allows transmission of data that is not in the standard NASA format. Thus, multiple formats and multiple modulator/demodulators can be used by the payloads. The design goal for the bent-pipe mode is to minimize the signal processing in the Orbiter for data that does not meet the standard NASA format. Therefore, no Orbiter control of command or telemetry for the bent-pipe data is proposed. Rather, the Orbiter will act as a relay which will either merely make a frequency translation at IF or perform RF demodulation and remodulation on a new carrier.

A technique for accommodating narrowband bent-pipe payload data is presented in Figure 1. In this concept, the payload data can be in any modulation format and can be analog or digital, but its highest frequency must be less than 2 MHz. To guarantee this maximum frequency limitation, the input payload data is first low-pass filtered. The filtered payload data plus payload-Orbiter link noise is then hardlimited, making the resultant waveform appear as a pseudo-2 Mbps digital data stream which, for high signal-to-noise ratio, resembles the normal 2 Mbps NRZ data input for Modes 1 and 2 Ku-band communication. Thus, this concept allows for the normal Mode 2 operational data (192 kbps) and the 4.5 MHz analog or the 4 Mbps digital data or the 4.5 MHz TV to be transmitted along with the bent-pipe payload data. Alternately, in Mode 1, the bent pipe payload data can be transmitted along with the 192 kbps operational data and the 10-50 Mbps convolutionally coded digital data.

Previous designs of the FM Mode 2 and PM Mode 1 Ku-band return links have not considered the effects of a bent-pipe signal on the other two data channels nor the interfering effects of these channels on the preprocessed bent-pipe waveform. Before addressing these issues, however, one must first examine the nonlinear processing of the payload data plus noise which takes place in the bent-pipe preprocessor itself. In general,

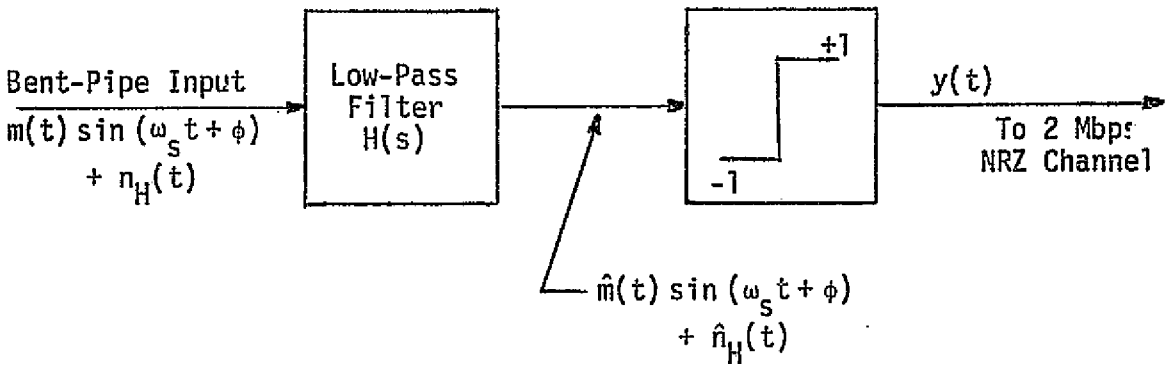

Figure 1. A Bent-Pipe Payload Data Preprocessor

one would like to be able to statistically characterize the signal and noise components in the preprocessor output when its input is as unspecified as possible. As we shall see from the development which follows, this general task leads to mathematically intractable solutions. Fortunately, however, sufficient information is known about many of the payloads so that they can be characterized by specific data formats. Among the possible candidates are analog and various digital formats, including composite digital signals. One specific example which corresponds to NASA and DoD payloads is a 16 kbps Manchester coded telemetry data stream biphase modulated on a 1.024 MHz subcarrier. This signal has been tested over a Mode 2 return link and the results of these tests reported in [1].

In this appendix, we shall focus our attention on characterizing the output signal and noise statistics of the bent-pipe preprocessor when the input signal is of the above form, namely, a low rate digital modulation on a subcarrier. Since the bent-pipe preprocessor output becomes modulated onto an 8.5 MHz unbalanced QPSK subcarrier, together with the 192 kbps Manchester coded operational data, one should then be able to modify previous analyses [2,3] of unbalanced QPSK demodulator performance to account for the presence of the noisy preprocessed bent-pipe signal as opposed to the noise-free 2 Mbps NRZ data stream which is normally transmitted on that channel. These modifications, along with the predictions of performance which follow from them, are the subject of further investigation.

CHARACTERIZATION OF THE OUTPUT CORRELATION FUNCTION OF A ZERO MEMORY NONLINEARITY

The general problem of characterizing the output correlation function of a zero memory nonlinearity whose input is signal plus bandlimited noise can be handled by a variety of analytical techniques. For simple nonlinear devices such as a full-wave square-law detector and a half-wave linear detector, the so-called "direct method" [4,5], wherein the output correlation function is directly evaluated as a statistical average over the joint probability density function of the output random variables, is useful. When one tries to apply this method to more complicated types of nonlinearities, considerable analytical difficulties often arise. In these situations, a less direct method which involves the use of the

Fourier transform of the transfer characteristic of the nonlinear device is particularly helpful [4,5]. This so-called "transform method" will be used in the development which follows. One other method which is also quite often used in problems of this type and deserves mention is based on Price's theorem [6]. While this method is certainly applicable, it was judged to be less convenient for the particular case of interest here.

We begin our analysis by defining $y = g(x)$ as the transfer characteristic of the zero memory nonlinearity in question. Then assuming that $g(x)$ is such that its two-sided Fourier transform exists, we have

$$f(j\xi) = \int_{-\infty}^{\infty} g(x)\, e^{-j\xi x}\, dx \tag{1}$$

The Fourier transform $f(j\xi)$ is often referred to as the transfer function of the nonlinear device. If $F_{y_1,y_2}(j\xi_1,j\xi_2;\tau)$ denotes the joint characteristic function of the output random variables $y_1 \triangleq y(t_1)$ and $y_2 \triangleq y(t_2)$ with $\tau = t_2 - t_1$, then the autocorrelation function of the output of the nonlinear device is given by [4,5]:

$$R_y(t_1,t_2) = \frac{1}{(2\pi)^2} \int_C \int_C f(j\xi_1)\, f(j\xi_2)\, F_{y_1,y_2}(j\xi_1,j\xi_2;\tau)\, d\xi_1\, d\xi_2 \tag{2}$$

where C is an appropriately chosen contour in the complex ξ-plane. More will be said about the selection of C when we consider a specific nonlinearity.

Assuming that the input $x(t)$ to the nonlinearity is the sum of signal $s_x(t)$ plus bandlimited noise $n_x(t)$, and furthermore that $s_x(t)$ and $n_x(t)$ are sample functions of statistically independent processes, then $F_{y_1,y_2}(j\xi_1,j\xi_2;\tau)$ factors and (2) becomes

$$R_y(t_1,t_2) = \frac{1}{(2\pi)^2} \int_C \int_C f(j\xi_1)\, f(j\xi_2)\, F_{s_1,s_2}(j\xi_1,j\xi_2;\tau)\, F_{n_1,n_2}(j\xi_1,j\xi_2;\tau)\, d\xi_1\, d\xi_2 \tag{3}$$

where $F_{s_1,s_2}(j\xi_1,j\xi_2;\tau)$ is the joint characteristic function of $s_1 \triangleq s_x(t_1)$ and $s_2 \triangleq s_x(t_2)$, and $F_{n_1,n_2}(j\xi_1,j\xi_2;\tau)$ is the joint characteristic function of $n_1 \triangleq n_x(t_1)$ and $n_2 \triangleq n_x(t_2)$.

When the input noise $n_x(t)$ is a sample function of a stationary Gaussian process with zero mean, variance σ^2, and correlation function $R_n(\tau)$, then $F_{n_1,n_2}(j\xi_1,j\xi_2;\tau)$ is given by

$$F_{n_1,n_2}(j\xi_1,j\xi_2;\tau) = \exp\left\{-\frac{1}{2}(\sigma^2\xi_1^2 + \sigma^2\xi_2^2 + 2R_n(\tau)\,\xi_1\,\xi_2)\right\} \tag{4}$$

Expanding the exponential in (4) in a Maclaurin power series and substituting this result into (3) gives

$$R_y(t_1,t_2) = \frac{1}{(2\pi)^2}\sum_{k=0}^{\infty}(-1)^k\frac{R_n^k(\tau)}{k!}\int_C f(j\xi_1)\,\xi_1^k\exp\left(-\frac{\sigma^2\xi_1^2}{2}\right)d\xi_1$$

$$\times\int_C f(j\xi_2)\,\xi_2^k\exp\left(-\frac{\sigma^2\xi_2^2}{2}\right)d\xi_2\,F_{s_1,s_2}(j\xi_1,j\xi_2;\tau)\,. \tag{5}$$

To proceed any further with the evaluation of (5), we must specify the form of the input signal, and hence its joint characteristic function.

Consider the case where the input is of the form

$$s_x(t) = \sqrt{2S}\,m(t)\cos(\omega_s t+\phi)\,, \tag{6}$$

where $m(t)$ is a low rate digital modulation, ω_s is the radian frequency of the sinusoidal oscillation, ϕ is a random phase assumed to be uniformly distributed on the interval $(0,2\pi)$ and independent of $m(t)$, and S denotes the average power of the signal. Letting $m_i \triangleq m(t_i)$, then the joint characteristic function of $s_x(t)$ is given by

$$F_{s_1,s_2}(j\xi_1,j\xi_2;\tau) = E\left\{\exp(j\xi_1\sqrt{2S}\,m_1\cos\theta_1 + j\xi_2\sqrt{2S}\,m_2\cos\theta_2)\right\}\,, \tag{7}$$

where $\theta_i \triangleq \omega_s t_i+\phi$; $i=1,2$. Using the well-known expansion,

$$\exp(j\alpha\cos\beta) = \sum_{m=0}^{\infty} j^m\varepsilon_m J_m(\alpha)\cos m\beta\,, \tag{8}$$

where ε_m is the Neumann factor, i.e., $\varepsilon_0=1$, $\varepsilon_m=2$ $(m\geq 1)$, and $J_m(\alpha)$ is the Bessel function of the first kind of order m and argument α, and further observing that

$$E_\phi\left\{\cos m\theta_1\cos m\theta_2\right\} = \begin{cases}0; & n\neq m\\ (1/\varepsilon_m)\cos m\omega_s\tau\,; & n=m\end{cases} \tag{9}$$

Equation (7) simplifies to

$$F_{s_1,s_2}(j\xi_1,j\xi_2;\tau) = \sum_{\ell=0}^{\infty} j^{2\ell}\,\varepsilon_i\,E\left\{J_\ell(\xi_1\sqrt{2S}\,m_1)\,J_\ell(\xi_2\sqrt{2S}\,m_2)\right\}\cos\ell\omega_s\tau \tag{10}$$

Substituting (10) into (5) and defining,

$$h_{\ell k}(t_i) = \frac{1}{2\pi}\int_C j^{\ell+k} f(j\xi_i)\,\xi_i^k \exp\left(-\frac{\sigma_i^2\xi_i^2}{2}\right) J_\ell(\xi_i\sqrt{2S}\,m_i)\,d\xi_i\,;\quad i=1,2 \tag{11}$$

the autocorrelation function of the output of the nonlinearity becomes

$$R_y(t_1,t_2) = \sum_{\ell=0}^{\infty}\varepsilon_\ell \sum_{k=0}^{\infty}\frac{R_n^k(\tau)}{k!}E\left\{h_{\ell k}(t_1)\,h_{\ell k}(t_2)\right\}\cos\ell\omega_s\tau\,. \tag{12}$$

Typically, m(t) is specified in the form of a random pulse train, namely,

$$m(t) = \sum_{n=-\infty}^{\infty} a_n\,p(t-nT)\,, \tag{13}$$

where $a_n = \pm 1$ are random data bits, p(t) is the signaling pulse, and $R \triangleq 1/T$ denotes the signaling rate. Since the process defined in (13) is cyclostationary, we define

$$R_{\ell k}(\tau) \triangleq \langle E\left\{h_{\ell k}(t_1)\,h_{\ell k}(t_2)\right\}\rangle \tag{14}$$

where < > denotes time average. Finally, taking the time average of (12) and letting $R_y(\tau) \triangleq \langle R_y(t_1,t_2)\rangle$, we get the desired result, namely,

$$R_y(\tau) = \sum_{\ell=0}^{\infty}\varepsilon_\ell \sum_{k=0}^{\infty}\frac{R_n^k(\tau)}{k!}R_{\ell k}(\tau)\cos\ell\omega_s\tau \tag{15}$$

The correlation function of (15) can be split up into several parts, as follows

$$R_y(\tau) = R_{SxS}(\tau) + R_{NxN}(\tau) + R_{SxN}(\tau) \tag{16}$$

where

$$R_{SxS}(\tau) = \sum_{\ell=0}^{\infty}\varepsilon_\ell\,R_{\ell 0}(\tau)\cos\ell\omega_s\tau \tag{17a}$$

$$R_{N\times N}(\tau) = \sum_{k=1}^{\infty} \frac{R_n^k(\tau)}{k!} R_{0k}(\tau) \tag{17b}$$

$$R_{S\times N}(\tau) = 2 \sum_{\ell=1}^{\infty} \sum_{k=1}^{\infty} \frac{R_n^k(\tau)}{k!} R_{\ell k}(\tau) \cos \ell\omega_s \tau \tag{17c}$$

The first term in (16) corresponds to the interaction of the signal with itself and represents the periodic signal components present in the output of the nonlinearity. The second term is due to the interaction of the input noise with itself, while the third term corresponds to the interaction of the input signal with the input noise. These latter two terms together comprise the contribution of the total random variations of the output.

SIGNAL AND NOISE COMPONENTS IN THE CORRELATION FUNCTION OF THE BENT-PIPE PREPROCESSOR OUTPUT

In this section, we apply the general result just given to the bent-pipe preprocessor of Figure 1. Specifically, the zero memory nonlinearity is a hard limiter with transfer characteristic:

$$g(x) = g_+(x) + g_-(x) \tag{18}$$

where

$$g_+(x) = \begin{cases} 1 & x \geq 0 \\ 0 & x < 0 \end{cases}$$

$$g_-(x) = \begin{cases} 0 & x \geq 0 \\ -1 & x < 0 \end{cases} \tag{19}$$

The corresponding transfer function $f(j\xi)$ is then

$$f(j\xi) = f_+(j\xi) + f_-(j\xi) \tag{20}$$

where

$$f_+(j\xi) \triangleq \mathcal{F}\{g_+(x)\}$$

$$= \int_0^{\infty} e^{-j\xi x}\, dx = \frac{1}{j\xi} \qquad (\text{Im } \xi < 0)$$

$$f_-(j\xi) = \mathcal{F}\{g_-(x)\}$$

$$= -\int_{-\infty}^{0} e^{-j\xi x}\, dx = \frac{1}{j\xi} \qquad (\text{Im } \xi > 0) \tag{21}$$

with $\mathcal{F}$ denoting Fourier transform and Im denoting the imaginary part of what immediately follows this notation. Having now specified the regions of convergence of $f(j\xi)$ in the complex ξ-plane, we can be more specific as to the selection of the contour C required to evaluate (11). For $f_+(j\xi)$, the appropriate contour (denoted by C_+) extends along the real axis from $-\infty$ to ∞ and is indented <u>downward</u> around the possible singularity at $\xi = 0$ (see Figure 2). Similarly, for $f_-(j\xi)$, the appropriate contour, namely C_-, extends along the real axis from $-\infty$ to ∞, and indents <u>upward</u> around the same potential singularity point (Figure 2). Thus, substituting (20) and (21) into (11), we get:*

$$h_{\ell k}(t_i) = \frac{1}{2\pi}\int_{C_+} j^{\ell+k-1}\,\xi_i^{k-1}\exp\left(-\frac{\sigma_i^2\xi_i^2}{2}\right)J_\ell\left(\xi_i\sqrt{2S}\,\hat{m}_i\right)d\xi_i + \frac{1}{2\pi}\int_{C_-} j^{\ell+k-1}\,\xi_i^{k-1}\exp\left(-\frac{\sigma_i^2\xi_i^2}{2}\right)J_\ell\left(\xi_i\sqrt{2S}\,\hat{m}_i\right)d\xi_i;\quad i=1,2 \tag{22}$$

From [5], p. 1079, Eq. (A.154), we find that (except for $\ell = k = 0$)

$$\int_{\substack{C_+\\ \text{or } C_-}} \xi^{k-1}J_\ell(a\xi)\,e^{-q^2\xi^2}\,d\xi = \frac{\pi j^{1-\ell-k}\left(\frac{a}{2q}\right)^\ell {}_1F_1\left(\frac{\ell+k}{2};\,\ell+1;\,-\frac{a^2}{4q^2}\right)}{q^k\,\Gamma(\ell+1)\,\Gamma\left(1-\frac{\ell+k}{2}\right)} \tag{23}$$

and

$$\int_{C_+} \xi^{-1}J_0(a\xi)\,e^{-q^2\xi^2}\,d\xi = \frac{1}{2}$$

$$\int_{C_-} \xi^{-1}J_0(a\xi)\,e^{-q^2\xi^2}\,d\xi = -\frac{1}{2} \tag{24}$$

where ${}_1F_1(\alpha;\beta;-x)$ is the confluent hypergeometric function. Thus, applying (23) and (24) to (22) gives

---

*The "hat" on m_i is intended to denote the fact that the input to the nonlinearity is a filtered version of the actual input modulation, i.e., $\hat{m}(t) = H(p)\,m(t)$ where $H(s)$ is the transfer function of the preprocessor low-pass filter.

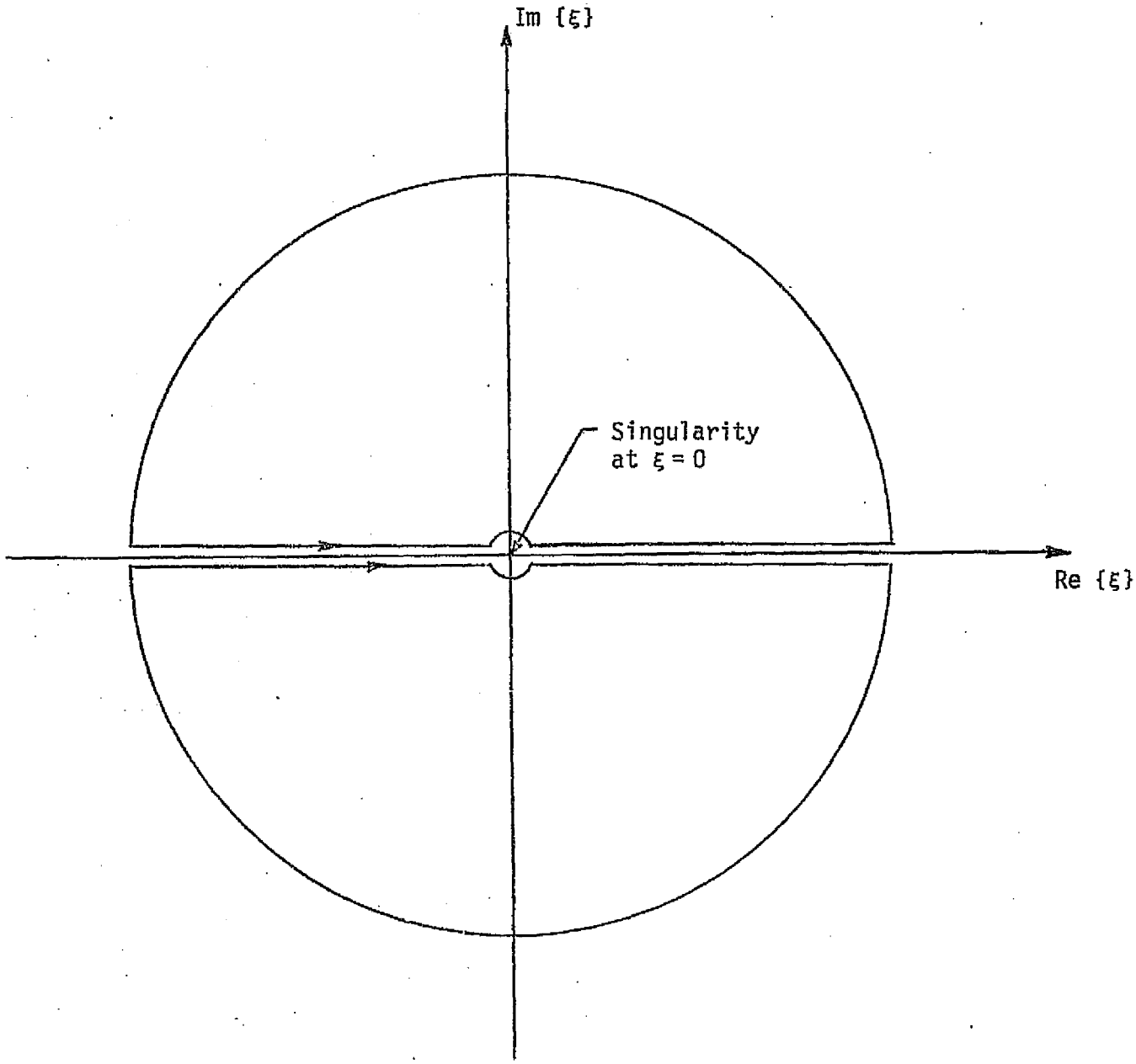

Figure 2. Integration Contours C_+ and C_-

$$h_{00}(t_i) = 0$$

$$h_{\ell k}(t_i) = \frac{\left(\frac{\sqrt{S}\,\hat{m}_i}{\sigma}\right)^{\ell} {}_1F_1\left(\frac{\ell+k}{2};\ \ell+1;\ -\frac{S\hat{m}_i^2}{\sigma^2}\right)}{\left(\frac{\sigma}{\sqrt{2}}\right)^{k} \Gamma(\ell+1)\ \Gamma\left(1-\frac{\ell+k}{2}\right)} \tag{25}$$

and from (14),

$$R_{00}(\tau) = 0$$

$$R_{\ell k}(\tau) = \left(\frac{\sqrt{S}}{\sigma}\right)^{2\ell} \frac{\left\langle \hat{m}^{\ell}(t)\,\hat{m}^{\ell}(t+\tau)\ {}_1F_1\left(\frac{\ell+k}{2};\ell+1;-\frac{S\hat{m}(t)}{\sigma^2}\right)\ {}_1F_1\left(\frac{\ell+k}{2};\ell+1;-\frac{S\hat{m}^2(t+\tau)}{\sigma^2}\right)\right\rangle}{\left(\frac{\sigma}{\sqrt{2}}\right)^{2k} \Gamma^2(\ell+1)\ \Gamma^2\left(1-\frac{\ell+k}{2}\right)} \tag{26}$$

where, for simplicity of notation, we have used the overbar to denote statistical expectation.

Unless one makes some additional simplifying assumptions, the statistical and time averages required in (26) cannot be evaluated. Since the payload-Orbiter link will, in general, be a strong link, we shall try to evaluate (26) for the large signal-to-noise ratio case, i.e., $S/\sigma^2 \gg 1$. In this regard, an asymptotic expansion for the confluent hypergeometric function is appropriate. From [5], p. 1073, Eq. (A.1.16), we have that

$${}_1F_1(\alpha;\beta;-x) \cong \frac{\Gamma(\beta)\ x^{-\alpha}}{\Gamma(\beta-\alpha)} \sum_{i=0}^{\infty} \frac{(\alpha)_i\ (\alpha-\beta+1)_i}{i!\ x^i} \tag{27}$$

where

$$(\alpha)_i \triangleq \alpha(\alpha+1)(\alpha+2)\cdots(\alpha+i-1); \quad (\alpha)_0 \triangleq 1. \tag{28}$$

Consider first the evaluation of $R_{SxS}(\tau)$ of (17a) using (27) to simplify $R_{\ell 0}(\tau)$. Letting $k=0$ in (26), we get

$$R_{\ell 0}(\tau) = \left\langle \frac{\hat{m}^{\ell}(t)\,\hat{m}^{\ell}(t+\tau)}{\Gamma^2\left(1+\frac{\ell}{2}\right)\Gamma^2\left(1-\frac{\ell}{2}\right)\left(\hat{m}^2(t)\right)^{\ell/2}\left(\hat{m}^2(t+\tau)\right)^{\ell/2}} \times \left[\sum_{i=0}^{\infty} \frac{\left(\frac{\ell}{2}\right)_i \left(-\frac{\ell}{2}\right)_i}{i!\left(\rho_H \hat{m}^2(t)\right)^i}\right]\left[\sum_{i=0}^{\infty} \frac{\left(\frac{\ell}{2}\right)_i \left(-\frac{\ell}{2}\right)_i}{i!\left(\rho_H \hat{m}^2(t+\tau)\right)^i}\right] \right\rangle \tag{29}$$

where

$$\rho_H \triangleq \frac{S}{\sigma^2} = \frac{S}{N_{0H} B_H} \tag{30}$$

is the signal-to-noise ratio in the noise bandwidth B_H of the preprocessor input filter $H(s)$, and N_{0H} is the noise spectral density on the payload-Orbiter link. From [7], p. 937, we have that

$$\Gamma(1-x)\,\Gamma(x) = \frac{\pi}{\sin \pi x} \tag{31}$$

But

$$\Gamma(1+x) = x\,\Gamma(x) \tag{32}$$

Thus,

$$\Gamma(1-x)\,\Gamma(1+x) = \frac{\pi x}{\sin \pi x} \tag{33}$$

and

$$\frac{1}{\Gamma^2\left(1+\frac{\ell}{2}\right)\Gamma^2\left(1-\frac{\ell}{2}\right)} = \frac{\sin^2 \frac{\pi \ell}{2}}{\left(\frac{\pi \ell}{2}\right)^2} = \begin{cases} 0; & \ell \text{ even} \\ \dfrac{1}{\left(\frac{\pi \ell}{2}\right)^2}; & \ell \text{ odd} \end{cases} \tag{34}$$

Suppose now we make the additional assumption that the power spectral density of the payload modulation $m(t)$ is narrowband with respect to the bandwidth B_H of $H(s)$. This is obviously a reasonable assumption when $m(t)$ has a data rate of 16 kbps and $H(s)$ has a bandwidth of 2 MHz. Thus, for this case, we have that $\hat{m}(t) \cong m(t)$, $\hat{m}^2(t) \cong m^2(t) = 1$, $\hat{m}^{\ell}(t) = m^{\ell}(t) = m(t)$ for ℓ odd. Furthermore,

$$\overline{\langle \hat{m}^{\ell}(t)\,\hat{m}^{\ell}(t+\tau)\rangle} \cong \overline{\langle m(t)\,m(t+\tau)\rangle} \triangleq R_m(\tau) \tag{35}$$

where $R_m(\tau)$ is the correlation function of the input payload modulation. For example, if m(t) is NRZ data, then

$$R_m(\tau) = \begin{cases} 1 - \frac{|\tau|}{T} ; & 0 \le |\tau| \le T \\ 0 ; & \text{otherwise} \end{cases} \tag{36}$$

Finally, using (34) and (35) in (29), we get

$$R_{\ell 0}(\tau) = \begin{cases} 0 ; & \ell \text{ even} \\ \frac{4}{\pi^2 \ell^2} \left[\sum_{i=0}^{\infty} \frac{(\frac{\ell}{2})_i (-\frac{\ell}{2})_i}{i!\, \rho_H^i} \right]^2 R_m(\tau) ; & \ell \text{ odd} \end{cases} \tag{37}$$

and from (17), with $\ell = 2\ell' + 1$,

$$R_{SxS}(\tau) = R_m(\tau) \frac{8}{\pi^2} \sum_{\ell'=0}^{\infty} \frac{1}{(2\ell'+1)^2} \left[1 + \sum_{i=1}^{\infty} \frac{(\ell' + \frac{1}{2})_i (-\ell' - \frac{1}{2})_i}{i!\, \rho_H^i} \right]^2 \cos (2\ell'+1)\, \omega_s \tau \tag{38}$$

This is a remarkably simple relation when compared with the formidable appearance of (26) from which we started this development. Furthermore, it soothes our intuition with regard to what we know is true in the limit as ρ_H approaches infinity, namely the output of the hard limiter becomes

$$\begin{aligned} y(t) &= \text{sgn} [\hat{m}(t) \cos (\omega_s t + \phi)] \\ &= \hat{m}(t) \text{ sgn} [\cos (\omega_s t + \phi)] \\ &\cong m(t) \text{ sgn} [\cos (\omega_s t + \phi)] \end{aligned} \tag{39}$$

and its correlation function is

$$R_y(\tau) = R_m(\tau) \frac{8}{\pi^2} \sum_{\ell'=0}^{\infty} \frac{1}{(2\ell'+1)^2} \cos (2\ell'+1)\, \omega_s \tau \tag{40}$$

Consider next the evaluation of $R_{NxN}(\tau)$ of (17b) using (27) to simplify $R_{0k}(\tau)$. Letting $\ell = 0$ in (26), we get

$$R_{0k}(\tau) = \frac{2^k}{\sigma^{2k}} \left\langle \frac{\left[\sum_{i=0}^{\infty} \frac{\left[\left(\frac{k}{2}\right)_i\right]^2}{i!\,(\rho_H \hat{m}^2(t))^i}\right]\left[\sum_{i=0}^{\infty} \frac{\left[\left(\frac{k}{2}\right)_i\right]^2}{i!\,(\rho_H \hat{m}^2(t+\tau))^i}\right]}{\left(\frac{S}{\sigma^2}\right)^k \Gamma^4\left(1-\frac{k}{2}\right)\left[\hat{m}^2(t)\right]^{k/2}\left[\hat{m}^2(t+\tau)\right]^{k/2}} \right\rangle \qquad (41)$$

Recalling (31), we have that

$$\frac{1}{\Gamma^4\left(1-\frac{k}{2}\right)} = \Gamma^4\left(\frac{k}{2}\right)\left(\frac{\sin\frac{k\pi}{2}}{\pi}\right)^4 = \begin{cases} 0\,; & k \text{ even} \\ \dfrac{\Gamma^4\left(\frac{k}{2}\right)}{\pi^2}\,; & k \text{ odd} \end{cases} \qquad (42)$$

Again assuming that the modulation is narrowband with respect to the bandwidth B_H of the preprocessor input filter, (41) simplifies to

$$R_{0k}(\tau) = \begin{cases} 0\,; & k \text{ even} \\ \dfrac{2^k\,\Gamma^4\left(\frac{k}{2}\right)}{\pi^4\,\sigma^{2k}\,\rho_H^{\,k}}\left[\sum_{i=0}^{\infty} \dfrac{\left[\left(\frac{k}{2}\right)_i\right]^2}{i!\,\rho_H^{\,i}}\right]^2\,; & k \text{ odd} \end{cases} \qquad (43)$$

and from (17) with $k = 2k'+1$,

$$R_{NxN}(\tau) = \frac{1}{\pi^4}\sum_{k'=0}^{\infty} \frac{2^{2k'+1}\,\Gamma^4\left(k'+\frac{1}{2}\right)}{(2k'+1)!\,\rho_H^{\,2k'+1}}\left[1+\sum_{i=1}^{\infty}\frac{\left[\left(k'+\frac{1}{2}\right)_i\right]^2}{i!\,\rho_H^{\,i}}\right]^2 \rho_{\hat{n}}^{\,2k'+1}(\tau) \qquad (44)$$

where

$$\rho_{\hat{n}}(\tau) \triangleq \frac{R_{\hat{n}}(\tau)}{\sigma^2} = \frac{N_{OH}}{2\sigma^2}\int_{-\infty}^{\infty} |H(j\omega)|^2\, e^{j2\pi f\tau}\,\frac{d\omega}{2\pi} \qquad (45)$$

Now from [5], p. 1077, Eq. (A.1.41a),

$$\Gamma\left(k'+\frac{1}{2}\right) = \frac{(2k')!\,\sqrt{\pi}}{2^{2k'}\,k'!} = \frac{(2k'-1)!!\,\sqrt{\pi}}{2^{k'}} \qquad (46)$$

where $(2k'-1)!! \triangleq 1\times 3\times 5\cdots\times(2k'-1)$, and $(-1)!! \triangleq 1$. Thus,

$$\frac{2^{2k'+1}\,\Gamma^4\left(k'+\frac{1}{2}\right)}{(2k'+1)!} = \frac{[(2k'-1)!!]^4\,\pi^2}{2^{2k'-1}\,(2k'+1)!} \qquad (47)$$

Using (47), equation (44) simplifies to

$$R_{NxN}(\tau) = \frac{1}{\pi^2} \sum_{k'=0}^{\infty} \frac{[(2k'-1)!!]^4}{2^{2k'-1}(2k+1)!\,\rho_H^{2k'+1}} \left[1 + \sum_{\ell=1}^{\infty} \frac{\left[(k'+\frac{1}{2})_i\right]^2}{i!\,\rho_H^{i}} \right]^2 \rho_{\hat{n}}^{k}(\tau) \qquad (48)$$

Finally, the evaluation of $R_{SxN}(\tau)$ of (17c) using (27) to simplify $R_{\ell k}(\tau)$ is all that remains. In particular, applying the same simplifying assumptions as used in arriving at expressions for $R_{SxS}(\tau)$ and $R_{NxN}(\tau)$, we get

$$R_{\ell k}(\tau) = \frac{2^k \left[\sum_{i=0}^{\infty} \frac{(\frac{k+\ell}{2})_i (\frac{k-\ell}{2})_i}{i!\,\rho_H^{i}} \right]^2}{\sigma^{2k}\, \Gamma^2(1-\frac{k+\ell}{2})\, \Gamma^2(1-\frac{k-\ell}{2})} R(\tau) \qquad (49)$$

where

$$R(\tau) = \begin{cases} R_m(\tau) ; & \ell \text{ odd} \\ 1 ; & \ell \text{ even} \end{cases}$$

Recalling (31), we have that

$$\Gamma(1-\tfrac{k+\ell}{2})\, \Gamma(1-\tfrac{k-\ell}{2}) = \left[\frac{\pi}{\Gamma(\frac{k+\ell}{2}) \sin\left[\frac{(k+\ell)\pi}{2}\right]} \right] \left[\frac{\pi}{\Gamma(\frac{k-\ell}{2}) \sin\left[\frac{(k-\ell)\pi}{2}\right]} \right] \qquad (51)$$

or

$$\frac{1}{\Gamma^2(1-\frac{k+\ell}{2})\, \Gamma^2(1-\frac{k-\ell}{2})} = \frac{\Gamma^2(\frac{k+\ell}{2})\, \Gamma^2(\frac{k-\ell}{2})}{\pi^4} \sin^2\left[\frac{(k+\ell)\pi}{2}\right] \sin^2\left[\frac{(k-\ell)\pi}{2}\right]$$

$$= \begin{cases} 0 ; & k,\ell \text{ even} \\ & k,\ell \text{ odd} \\ \dfrac{\Gamma^2(\frac{k+\ell}{2})\, \Gamma^2(\frac{k-\ell}{2})}{\pi^4} ; & k \text{ even, } \ell \text{ odd} \\ & k \text{ odd, } \ell \text{ even} \end{cases} \qquad (52)$$

Thus, using (49) and (52) in (17c), we get

$$R_{SxN}(\tau) = \frac{2}{\pi^4} \sum_{\substack{\ell=2 \\ \ell \text{ even}, \\ k \text{ odd}}}^{\infty} \sum_{k=1}^{\infty} \frac{2^k \Gamma^2\left(\frac{k+\ell}{2}\right) \Gamma^2\left(\frac{k-\ell}{2}\right)}{k!\, \rho_H^{\,k}} \rho_{\hat{n}}^{\,k}(\tau) \left[\sum_{i=0}^{\infty} \frac{\left(\frac{k+\ell}{2}\right)_i \left(\frac{k-\ell}{2}\right)_i}{i!\, \rho_H^{\,i}} \right]^2 \cos \ell\omega_s\tau$$

$$+ \frac{2\, R_m(\tau)}{\pi^4} \sum_{\substack{\ell=1 \\ \ell \text{ odd}, \\ k \text{ even}}}^{\infty} \sum_{k=2}^{\infty} \frac{2^k \Gamma^2\left(\frac{k+\ell}{2}\right) \Gamma^2\left(\frac{k-\ell}{2}\right)}{k!\, \rho_H^{\,k}} \rho_{\hat{n}}^{\,k}(\tau)$$

$$\times \left[\sum_{i=0}^{\infty} \frac{\left(\frac{k+\ell}{2}\right)_i \left(\frac{k-\ell}{2}\right)_i}{i!\, \rho_H^{\,i}} \right]^2 \cos \ell\omega_s\tau \qquad (53)$$

or letting $\ell = 2\ell'$, $k = 2k'+1$ in the first term and $\ell = 2\ell'+1$, $k = 2k'$ in the second term,

$$R_{SxN}(\tau) = \frac{2}{\pi^4} \sum_{\ell'=1}^{\infty} \sum_{k'=0}^{\infty} \frac{2^{2k'+1} \Gamma^2\left(k' + \ell' + \frac{1}{2}\right) \Gamma^2\left(k' - \ell' + \frac{1}{2}\right)}{(2k'+1)!\, \rho_H^{\,2k'+1}} \rho_{\hat{n}}^{\,2k'+1}(\tau)$$

$$\times \left[1 + \sum_{i=1}^{\infty} \frac{\left(k' + \ell' + \frac{1}{2}\right)_i \left(k' - \ell' + \frac{1}{2}\right)}{i!\, \rho_H^{\,i}} \right]^2 \cos 2\ell'\omega_s\tau$$

$$+ \frac{2\, R_m(\tau)}{\pi^4} \sum_{\ell'=0}^{\infty} \sum_{k'=1}^{\infty} \frac{2^{2k'} \Gamma^2\left(k' + \ell' + \frac{1}{2}\right) \Gamma^2\left(k' - \ell' - \frac{1}{2}\right)}{(2k')!\, \rho_H^{\,2k'}} \rho_{\hat{n}}^{\,2k'}(\tau)$$

$$\times \left[1 + \sum_{i=1}^{\infty} \frac{\left(k' + \ell' + \frac{1}{2}\right)_i \left(k' - \ell' - \frac{1}{2}\right)_i}{i!\, \rho_H^{\,i}} \right]^2 \cos (2\ell'+1)\omega_s\tau \qquad (54)$$

BENT-PIPE PREPROCESSOR OUTPUT SPECTRAL DENSITY

The spectral density at the preprocessor output is obtained by taking the Fourier transform of the output correlation function whose components are given in (38), (44), and (54). Thus,

$$S_y(f) = S_{SxS}(f) + S_{NxN}(f) + S_{SxN}(f) \qquad (55)$$

where
$$S_{SxS}(f) \triangleq \mathcal{F}\{R_{SxS}(\tau)\}$$
$$S_{NxN}(f) \triangleq \mathcal{F}\{R_{NxN}(\tau)\}$$
$$S_{SxN}(f) \triangleq \mathcal{F}\{R_{SxN}(\tau)\} \tag{56}$$

From (38), we immediately have that

$$S_{SxS}(f) = \frac{4}{\pi^2} \sum_{\ell'=0}^{\infty} \frac{1}{(2\ell'+1)^2} \left[1 + \sum_{i=1}^{\infty} \frac{(\ell'+\frac{1}{2})_i (-\ell'-\frac{1}{2})_i}{i!\,\rho_H^{\,i}}\right]^2$$
$$\times \left[S_m[f + (2\ell'+1) f_s] + S_m[f - (2\ell'+1) f_s]\right] \tag{57}$$

where
$$S_m(f) = \mathcal{F}\{R_m(\tau)\} = \int_{-\infty}^{\infty} R_m(\tau)\, e^{-j2\pi f\tau}\, d\tau \tag{58}$$

is the power spectrum of the input payload data modulation m(t). Letting ${}_{k'}S_{\hat{n}}(f)$ denote the 2k'-fold convolution of the noise spectral density $S_{\hat{n}}(f)$ at the input to the hard limiter, i.e.,

$${}_{k'}S_{\hat{n}}(f) \triangleq \int_{-\infty}^{\infty} \rho_{\hat{n}}^{2k'+1}(\tau)\, e^{-j2\pi f\tau}\, d\tau$$
$$= \underbrace{S_{\hat{n}}(f) * S_{\hat{n}}(f) * \cdots * S_{\hat{n}}(f)}_{\text{2k'-fold convolution}}$$

with
$$S_{\hat{n}}(f) \triangleq {}_0S_{\hat{n}}(f) = \int_{-\infty}^{\infty} \rho_{\hat{n}}(\tau)\, e^{-j2\pi f\tau}\, d\tau \tag{59}$$

then taking the Fourier transform of (44) gives

$$S_{NxN}(f) = \frac{1}{\pi^4} \sum_{k'=0}^{\infty} \frac{2^{2k'+1}\,\Gamma^4(k'+\frac{1}{2})}{(2k'+1)!\,\rho_H^{\,2k'+1}} \left[1 + \sum_{i=1}^{\infty} \frac{\left[(k'+\frac{1}{2})_i\right]^2}{i!\,\rho_H^{\,i}}\right]^2 {}_{k'}S_{\hat{n}}(f) \tag{60}$$

Finally, the signal x noise component spectral density is obtained by taking the Fourier transform of (54), with the result

$$S_{SxN}(f) = \frac{1}{\pi^4} \sum_{\ell'=1}^{\infty} \sum_{k'=0}^{\infty} \frac{2^{2k'+1}\, \Gamma^2(k'+\ell'+\frac{1}{2})\, \Gamma^2(k'-\ell'+\frac{1}{2})}{(2k+1)!\, \rho_H^{2k'+1}}$$

$$\times \left[1 + \sum_{i=1}^{\infty} \frac{(k'+\ell'+\frac{1}{2})_i\, (k'-\ell'+\frac{1}{2})_i}{i!\, \rho_H^{i}}\right]^2 \left[k', S_{\hat{n}}(f-2\ell' f_s) + k', S_{\hat{n}}(f+2\ell' f_s)\right]$$

$$+ \frac{1}{\pi^4} \sum_{\ell'=0}^{\infty} \sum_{k'=1}^{\infty} \frac{2^{2k'}\, \Gamma^2(k'+\ell'+\frac{1}{2})\, \Gamma^2(k'-\ell'-\frac{1}{2})}{(2k')!\, \rho_H^{2k'}}$$

$$\times \left[1 + \sum_{i=1}^{\infty} \frac{(k'+\ell'+\frac{1}{2})_i\, (k'-\ell'+\frac{1}{2})_i}{i!\, \rho_H^{i}}\right]^2$$

$$\times \int_{-\infty}^{\infty} S_m(f') \left[k', S_{\hat{n}}\left(f-(2\ell'+1) f_s - f'\right) + k', S_{\hat{n}}\left(f+(2\ell'+1) f_s - f'\right)\right] df' \qquad (61)$$

The sum of (58), (60), and (61) above thus provides the expression for the spectral density, $S_y(f)$, of the bent-pipe preprocessor device.

REFERENCES

1. NASA-JSC-EE7-76-435 Final Review, "Quick-Look System Design Evaluation Tests of 16 kbps Channel Ku-Band FM Mode-2," by J. Seyl and B. G. Smith.

2. Simon, M. K. "Tracking Performance of Unbalanced QPSK Demodulators," Axiomatix Report (to be published).

3. Simon, M. K. "Subcarrier Tracking Analysis for Three-Channel Orbiter Ku-Band Return Link," Axiomatix Report (to be published).

4. Davenport, W. B., Jr., and Root, W. L. An Introduction to the Theory of Random Signals and Noise. New York: McGraw-Hill Book Co., Inc., 1958.

5. Middleton, D. Statistical Communication Theory. New York: McGraw-Hill Book Co., Inc., 1960.

6. Price, R. "A Useful Theorem for Nonlinear Devices Having Gaussian Inputs," IRE Transactions on Information Theory, June 1958, pp. 69-72.

7. Gradshteyn, I. S., and Ryzhik, I. M. Table of Integrals, Series and Products. New York: Academic Press, 1965.